FACTORS GOVERNING SPONTANEOUS IGNITION OF COMBUSTIBLE DUSTS

Kulbhushan Arvind Joshi

A Dissertation

Submitted to the Faculty

of the

WORCESTER POLYTECHNIC INSTITUTE

in partial fulfillment of the requirements for the

Degree of Doctor of Philosophy

in

Fire Protection Engineering

May 2012

APPROVED:

Prof. Ali S. Rangwala – Major Advisor

Prof. Vasudevan Raghavan, Mechanical Engineering, IITM, Chennai, India – Co-advisor

Committee Members

Prof. Simon Evans, Mechanical and Aerospace Engineering, WPI

Prof. Yiannis A. Levendis, Mechanical and Industrial Engineering, Northeastern University, Boston, MA

Prof. Kathy Ann Notarianni, Head of Department, Fire Protection Engineering, WPI

Prof. Albert Simeoni, Fire Protection Engineering, WPI

TABLE OF CONTENTS

List of Figures

List of Tables

Nomenclature

C_p	Specific heat capacity (J/kg-K)
$\hat{e}_r$	Unit vector in radial direction
$\hat{e}_\omega$	Unit vector in tangential direction
E	Activation energy (kJ/mol)
$f(\alpha)$	Kinetic model reaction function
F	Ratio of y-coordinates of location of ignition to total height = h_m/h
$g(\alpha)$	Integral of kinetic model reaction function
H	Dust layer thickness or wedge height (m)
h	Non-dimensional dust layer thickness or wedge height
h_c	Convective heat transfer coefficient (W/m^2-K)
h_c^*	Non-dimensional convective heat transfer coefficient
h_m	Non-dimensional vertical distance where temperature is maximum (ignition location)
k	Thermal conductivity (W/m-K)
m	Mass (kg)
m_0	Initial mass (kg)
m_∞	Final mass (kg)

n	Reaction order
$p(\alpha)$	Exponential of integral of kinetic model reaction function
QA	Pre-exponential constant (J/kg-s)
r	Half dust layer thickness (m)
R	Universal gas constant, 8.314 (J/mol-K)
t	Time (s)
T	Dimensional temperature variable (K)
T_∞	Ambient temperature (K)
$T_{h/2}$	Temperature along the line of symmetry at half wedge height (K)
T_p	Temperature of the hot plate (K)
T_s	Temperature on the coal surface exposed to the ambient (K)
W	Wedge width (m)
w_o	Non-dimensional wedge width
x , y	Non-dimensional Cartesian co-ordinates
X, Y	Dimensional Cartesian co-ordinates
α	conversion degree
β	heating rate (K/s)
θ	Non-dimensional temperature variable

θ_∞ Non-dimensional ambient temperature

θ_p Non-dimensional hot surface temperature

θ_s Non-dimensional coal surface temperature

P Bulk density of coal dust (kg/m^3)

Abbreviations

PRB powder river basin coal

PSC Pittsburgh seam coal

TGA Thermo-gravimetric Analyzer

Acknowledgements

I would like thank both my advisor and co-advisor: Ali Rangwala and V. Raghavan for all the guidance and encouragement provided throughout the course of my research. Also, it has been wonderful to be a part of the department of fire protection engineering and to have known department head Kathy Notarianni. It was a great experience to learn fundamentals of fire science from Nicholas Dembsey and computational fluid dynamics from Gretar Tryggvason. The research simply would not have been achievable without the help of Fire Science Lab manager Randall Harris. The efforts of Sasha Strong, Catherine Fradette and Mary Racicot are commendable in handling the numerous types of official tasks efficiently. I would like to thank my committee members: Simon Evans, Yiannis Levendis and Albert Simeoni for their feedback and comments that helped in shaping the dissertation. My funding sourced from National Science Foundation allowed the research expenses. Expert opinions of Erdem Ural and Robert Zalosh guided the research in to the right direction.

My parents, Rashmi and Arvind Joshi and wife, Deepti Dutt provided the constant assurance and inspiration needed. I am thankful to my parents for their belief in me and to my wife for the support provided especially in the final year. My cousin Anish Karandikar was instrumental in linking me and Ali Rangwala together.

I am thankful to my fellow lab-mate, Scott Rockwell for all the help and advice; but mainly for the friendship. My graduate student office-mates: Hae-jun Park, Alberto Alvarez, Joel Sipe, Mihyun (Ester) Kim, Young-Geun, Jan Thomas, Majed Almejmaj, Brian Elias and Sreenivanasan Ranganathan made the academic life enjoyable.

Kulbhushan A. Joshi

Worcester Polytechnic Institute

Department of Fire Protection Engineering

100 Institute Road, Worcester MA 01609

E-mail: kulbhushan29@gmail.com

VITA

Doctorate of Philosophy, Worcester Polytechnic Institute, Worcester MA 2012
Department: Fire Protection Engineering
Committee: Prof. Ali S. Rangwala, Raghavan Vasudevan, Simon W. Evans, Yiannis A. Levendis, Kathy A. Notarianni and Albert Simeoni
Dissertation: *"Factors Governing Spontaneous Ignition of Combustible Dusts."*

Masters of Science, Northeastern University, Boston MA 2008
Department: Mechanical and Industrial Engineering, Concentration: Thermo-fluids
Advisor: Prof. Yiannis A. Levendis
Thesis: *"Study of Co-Combustion of Coal and Biomass."*

Bachelor of Engineering, Mumbai University, Mumbai, India 2006
Department: Mechanical Engineering

PUBLICATIONS

Refereed Publications (Journal):

1. K. A. Joshi, V. Raghavan and A. S. Rangwala, "An experimental study of coal dust ignition in wedge shaped hot plate configurations," *Combustion and Flame*, 159(1):376-384, 2012.
2. Y. A. Levendis, K. A. Joshi, R. Khatami and A. F. Sarofim, "Combustion behavior in air of single particles from three different coal ranks and from sugarcane bagasse," *Combustion and Flame*, 158(3):452 – 465, 2011.
3. R. Khatami, C. Stivers, K. A. Joshi, Y. A. Levendis and A. F. Sarofim, "Combustion behavior of single particles from three different coal ranks and from sugar cane bagasse in O_2/N_2 and O_2/CO_2 atmospheres," *Combustion and Flame*, 159(3):1253-1271, 2012.
4. M. Bragato, K. A. Joshi, J. B. Carlson, J. A.S. Tenorio and Y. A. Levendis, "Combustion of Coal, Bagasse and Blends thereof. Part I: Emissions from Batch Combustion of Fixed Beds of Fuels." *Fuel*, 96, 43-50, 2012.
5. M. Bragato, K. A. Joshi, J. B. Carlson, J. A.S. Tenorio and Y. A. Levendis, "Combustion of Coal, Bagasse and Blends thereof. Part II: Speciation of PAH Emissions." *Fuel*, 96, 51-58, 2012

Refereed Publications (Conferences):

1. K. A. Joshi, V. Raghavan and A. S. Ragnwala, "Influence of Confinement Geometry on Ignition Behavior of Dust Deposits," Proceedings of the Combustion Institute, accepted, 2012.
2. K. A. Joshi, A. S. Rangwala and V. Raghavan, "Spontaneous Ignition of Coal Dust Layers," 7th Asia-Pacific Conference on Combustion, Taiwan, 2009.

Non-refereed Publications:

Conferences

1. Y. A. Levendis and K. A. Joshi, "Combustion of Two Lignite Coals in O_2-N_2 and O_2-CO_2," 33rd International Technical Conference on Coal Utilization & Fuel Systems, Clearwater, Florida, June 2-6, 2008.
2. K. A. Joshi, V. Raghavan and A. S. Rangwala, "Spontaneous Ignition of Moist Coal," 6th U.S. National Technical Meeting of the Combustion Institute, Michigan, May 17-20 2009.
3. K. A. Joshi, V. Raghavan and A. S. Rangwala, "Effect of Weathering of Coal Dust on its Spontaneous Ignition," 7th U.S. National Technical Meeting of the Combustion Institute, Georgia, March 20-23 2011.
4. K. A. Joshi, V. Raghavan and A. S. Rangwala, "Effect of Weathering of Coal and Organic Dusts on their Spontaneous Ignition," 28th Annual International Pittsburgh Coal Conference, Pittsburgh, September 12-15 2011.
5. K. A. Joshi, V. Raghavan and A. S. Rangwala, "Modeling spontaneous ignition of coal dust trapped between two hot surfaces," Eastern States Section of Combustion Institute, Fall Technical Meeting, Connecticut, October 9-12 2011.

Posters

1. M. Bragato, K. A. Joshi, J. Carlson, J. A. S. Tenorio and Y. A. Levendis, "Emissions Generated during the Co-combustion of Coal and Bagasse Fuel Blends," 32nd International Symposium on Combustion, Montreal, Canada, August 3-8, 2008.
2. K. A. Joshi, V. Raghavan and A. S. Rangwala, "Effect of Geometry of Combustible Dust Deposit on its Hot Surface Ignition," National Fire Protection Association Conference & Expo, Boston, June 11-15, 2011.

Invited Speaker

1. "Factors governing spontaneous ignition of combustible dusts test", ASTM Committee E27 meeting, Tampa, Florida, November 15-17, 2011

Abstract

The problem of self-heating of combustible dusts accumulated on hot surfaces has caused several fires and dust explosions. The current test standards (ASTM E 2021, EN50281-2-1) used to ensure safe environment for a given dust, define a safe temperature of the flat hot surface for certain dust layer thickness. Since in these standards, measurement of temperature is taken along the centerline, they mainly represent a simplified scenario of one-dimensional heat transfer. A need to investigate behavior of spontaneous ignition in dust deposits in complex geometries forms the motivation of this work. The effect of hot surface geometry is experimentally studied by devising wedge-shaped configurations having angles of 60^o and 90^o. Results show that ignition always occurred around the top region in the case of 60^o wedge, and in the top and middle regions in the case of 90^o wedge. These trends are explained by investigating three parameters affecting the ignition behavior, namely, the heat transfer from the hot plate to the dust, the rate of heat transfer between different regions within the dust and the minimum volume of dust required to produce sufficient heat release. A mathematical method has been proposed to predict the ignition behavior of dust deposit subjected to any boundary conditions arising due to geometrical confinement. Further, numerical simulations have been carried out to simulate the conjugate heat transfer in the interface of dust surface and air. Both analyses, mathematical and numerical, compare well with the experimental data.

Furthermore, in the standard test method, ASTM E-2021, a metal ring is used to contain the sample dusts. It is observed from experimental and numerical simulations that the resultant temperature field is not one-dimensional as desired since the corner part ignites first due to heat transfer from both the bottom plate and the metal ring, which is at almost same temperature as that of bottom plate. Theories those describe the thermal ignition in these standard tests, use the assumption that the heat flow is unidirectional. Therefore, a better substitute to the metal

ring has been proposed as a ring made out of an insulating material (having low thermal conductivity). This makes the heat transfer to the dust layer phenomenally one-dimensional.

Another leg of the experiments have been carried out to investigate the effect of weathering of combustible dusts on their spontaneous ignition process. Two types of weathering methods, heat- and moisture-weathering are used. Sample preparation and weathering quantification methods follow the standard test procedure. Thermogravimetric analysis has been employed to understand the variation in weight loss of fresh, heat-weathered and moisture-weathered samples of coal and organic dusts. Preliminary results show that heat weathering increases the hazard level for organic (wheat) dust.

In summary, the current research work mainly involves modification of the standard test method such as ASTM E-2021 to include an insulated ring instead of a metal ring to ensure one-dimensional heat transfer and extending the test method to include wedge-shaped geometries. The spontaneous ignition of combustible dust in the new setups is investigated thoroughly. Furthermore, mathematical and numerical models have been proposed to simulate the experimental tests. Finally, the effect of two types of weathering processes on the characteristics of spontaneous ignition has been studied. In all the cases, results are thoroughly discussed with the explanation of the physics involved.

Chapter 1. INTRODUCTION

1.1 BACKGROUND

Property and life loss due to dust fires and explosions is a recurring problem in several industries which handle, store or produce combustible dusts. More than 200 incidents were reported between 1980 to 2005, which caused around 100 fatalities and more than 700 injuries [1]. A more recent report by Occupational Safety Hazard Association (OSHA) also brings forward similar concern with statistics indicating more than 400 explosible dust incidents over a period of 30 years from 1980 to 2010 [2]. The national emphasis program was started by OSHA in order to increase the awareness of dust explosion hazards and subsequently reduce the property damage and life loss. A combustible dust, as defined by NFPA 654 [3] , has a particle size less than 400 μm and poses fire or explosion hazard. Combustible dusts are classified into three broad categories: (1) metal dusts (e.g. Aluminum, Brass powders), (2) carbonaceous dusts (e.g. pulverized coal dusts used in coal-fired power plants) and (3) food, plastic, paper and other dusts (e.g. dusts found in printing press by-products, pharmaceutical industry). In this thesis, for simplicity sake, the word "dust" is used with an intended meaning to refer to a "combustible dust".

Accumulation of fugitive dusts in contact with hot electrical and mechanical parts can lead to spontaneous ignition that develops into hot spot and creates fire or explosion hazards. Such accumulations are usually unavoidable in industrial facilities with high levels of fugitive dusts. The only method for mitigating such hazards is to prescribe safe temperature to the equipment as discussed in the National Electric Code (NEC Class 2, Division 2 environment). A hot plate test to determine minimum hot-surface ignition temperature of a dust layer was recommended by the National Academy of Science (NAS) committee on Evaluation of Industrial Hazards [4] as well as by International Electrotechnical Commision (IEC) [5]. Today, the resulting standard test procedures - ASTM E-2021 [6] and EN 50281 [7] have been internationally accepted. The primary focus of the current study is to scientifically evaluate this testing methodology. It is

shown that with the advent of new materials, processing technologies, and automation the current test standard does not represent a worst case scenario and modifications to both the experimental setup as well as interpretation of the results are necessary.

1.2 OBJECTIVES

1) To re-examine the current test methodology (ASTM E-2021, EN 50281) used by industry to evaluate the hazard associated with spontaneous ignition of dust layer.
2) To investigate the ignition of dust in a realistic geometry (such as 2-D wedge using a wedge shaped hot plate constructed specifically for this study.
3) To predict the ignition behavior of a dust deposit in a wedge-shaped configuration using a validated mathematical model developed as a part of this study.
4) To explore the impact of the dust surface-air boundary condition on the ignition location using a computational model (FLUENT).
5) To provide a simple methodology to extract material properties relevant to the modeling of the ignition hazard of dust deposits, and examine the change in the hazard when these properties change due to natural processes such as moisture or temperature induced weathering.

Ultimately, the objectives are aligned to the broader impact of this study: to create a safer environment in industrial facilities that process, handle or produce combustible dusts by bridging the gap between fundamental scientific understanding of spontaneous ignition and testing methodologies used by industry to evaluate the hazard.

As a first step, the available literature related to spontaneous ignition of dust is reviewed. The industrial safety literature includes the current practices and standard tests used.

Industrial Safety Literature:

Industrial safety is regulated by codes and standards that specify the requirements of infrastructure and practices necessary to maintain safe environment. Fire and explosion safety is important to avoid business interruptions. The safe practices are recommended by government issued codes for example in United States of America, mainly National Fire Protection Association issued codes and standards are adopted as state requirements. ASTM International is known to standardize test procedures that can be then adopted anywhere in the world. This way the companies with global presence can comply with the local regulations as well as be consistent with in-house safety requirements. The current dust ignition mitigation strategies are discussed in following paragraphs:

1) Housekeeping

The basic idea of housekeeping is to avoid fugitive dust accumulation. Safe techniques are recommended based on the type of dust being handled [8]. Often it is noted from post-incident investigation reports that, the housekeeping is often limited to only easy to reach or visible areas. Hard to reach parts such as finned sections of machinery and out-of-reach areas such as top portions of ducts and casings are observed to accumulate dust commonly. Ideally, a perfect housekeeping practice should prevent any and all dust fires and explosion. In reality, housekeeping is not so efficient, and dust accumulation is unavoidable, especially in hard to reach areas in machineries. The results from this study are directly applicable to these situations since we examine what happens to the spontaneous ignition hazard when dust is trapped in wedges and hard to reach corners.

2) Inert environment and additives

In environments where the dust as a main product and needs to be transported around the facility, the handling systems are in general free from all ignition sources. Under special conditions, an inert atmosphere is created around the dust to avoid oxidation in the presence of oxygen using argon, carbon dioxide, helium, nitrogen, or flue gas [9]. The minimum safe concentration of oxygen in the atmosphere

to prevent ignition is determined by standard tests and sufficient inert gas quantity is used to achieve the oxygen concentration levels below that limit [10]. A study by Reddy et al. [11] reported the required concentrations of inert dust additives to avoid ignition.

3) Training

Chemical Safety Board (CSB) and Occupational Safety Hazard Association (OSHA) report about the importance of educating the workers in identifying and minimizing hazards. Trained people working in a dust hazard prone environment can have a close look at the operations in the facility and quickly recognize any unsafe conditions or practices, and take appropriate actions to report to or alert the co-workers about them, or, if possible, mitigate them. Serious concerns were raised about the current situation of training program contents for the fire inspectors, as in most states inspectors were not required to demonstrate knowledge of combustible dust hazard prevention [1]. The broader educational impact of the current study is to address this issue. Outcomes of the current study can be implemented in training modules for inspectors as well as workers. This was recently discussed in a presentation given by the author to ASTM committee E27 on hazard potential of chemicals [12].

4) Testing

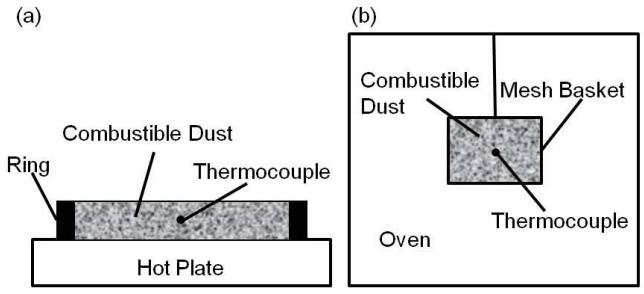

Figure1 Experimental set-up for standard tests: (a) layer ignition test and (b) oven test.

Standard tests developed by the National Academy of Sciences (NAS) Committee on Evaluation of Industrial Hazards and International Electrotechnical Commission (IEC) are used to determine the

minimum temperature of the surface with dust layer that would cause spontaneous ignition, as shown in Fig. 1(a). Similar standard test methods have been published by ASTM E 2021-06 and IEC 61241-2-1 [5, 13]. Both test methods utilize a dust layer contained in a metal ring with 10 cm internal diameter and 12.7 mm thickness placed on a heated plate having 20 cm diameter. The plate temperature is set at a pre-determined value for each test, and a thermocouple located along the centerline of the dust sample monitors the dust temperature as the plate heats it. The dust sample is exposed to the heated surface for a period of about 30 minutes unless there is a positive indication of ignition earlier. In general, ignition is said to have occurred if the thermocouple within the dust layer records a temperature 50 ºC more than the plate temperature. Tests are repeated with plate temperature incremented by 10 ºC from a no-ignition case and monitoring ignition every time until ignition occurs. The ignition temperature is then used for ranking the relative hazard of the dust.

Despite being a relatively short and easy test procedure and resembling actual hazardous conditions closer than the other test methods in terms of sample amount and configuration, the hot plate test is considered as an approximate screening method on the basis of 'go/ no go' criteria. This is because modeling ignition for other geometries most commonly found in an industrial environment is not possible solely from the ignition temperature estimated from hot plate test with a specific dust layer thickness. The minimum ignition temperature obtained from ASTM E 2021 also may not represent a worst case scenario, as other dust layer thicknesses and heating geometries can have lower ignition temperatures.

Another standard test method used to determine critical spontaneous ignition temperature by placing the bulk material in baskets inside a uniformly heated oven is shown in Fig. 1(b). Because of the uniform heating, usually the critical temperature determined by oven test is lower than that determined by hot plate test. This method is mainly used to classify transportation of hazardous substances [14, 15]. Both experimental methods, besides providing a screening tool can also be modeled using simple analytical equations to extract material properties related to spontaneous ignition conditions [16, 17]. Since, the experimental set-up of hot plate test represents real-life scenario more closely, the general test method is

internationally accepted as a way to determine minimum ignition temperature of dust layer. The current work also stresses on similar issue of representation of real-life conditions in the experimental test set-up. Therefore, oven tests are not discussed any further and the hot plate test method forms the starting point of the study.

This study shows that the metal ring used to contain the sample dust does not provide a one-dimensional heat flow from the hot surface to the coal dust. This is because of the high thermal conductivity of the metal ring creating a second hot surface and making the problem two-dimensional in nature. A simple solution of replacing the metal ring with an insulating ring is proposed. It is also shown that flat dust layers on hot surface do not represent complex hot surface geometries encountered in industrial environments.

Scientific Literature Review:

Theoretical work related to dust ignition:

There has been extensive work reporting several aspects of – what is called by different terms as - self-heating, spontaneous ignition, auto-ignition or thermal ignition and thermal explosion. All the terms refer to the same phenomenon of on-set of thermal runaway reactions whereby the heat generation exceeds heat loss and leads to sustained ignition. The first mathematical model governing the critical conditions of self-ignition phenomenon was proposed by Semenov [18]. The assumption of Semenov's theory was that the temperature within the reactive mixture is uniform i.e. the thermal conductivity approaches infinity and the Biot number is negligible. This model is applicable to stirred gases and liquids and can be extended to fluidized beds of reactive solid particulate matter, however, fails to analyze the ignition of a layer of reactive dust on a hot surface. This problem was first addressed by Frank-Kamenetskii in 1939 who considered temperature gradient in the mixture [19]. At the same time, the boundary of the reactant was assumed to be at the same temperature as that of its surroundings. In terms of the Biot number, this case is the other extreme of thermal ignition theory proposed by Semenov [18]. Here Biot number

approaches infinity. The most important contribution of the model was the dimensionless Frank-Kamenetskii parameter. A critical value of the Frank-Kamenetskii parameter represents conditions required for spontaneous ignition in terms of dust properties, boundary conditions and dust deposit geometry. If the value of the parameter calculated for a given case exceeds the critical value then ignition is expected. Critical values of the parameter were developed for several simple geometries such as a sphere, equi-dimensional cylinder, cube, infinite cylinder and infinite cube. Clemmow and Huffington [20] extend Frank-Kamenetskii thermal explosion theory to a reactive solid slab subjected to a constant heat flux on one side and at a constant temperature on the other. Properties of two materials: cordite and methyl nitrate were used to check the validity of the predictions. Calculations of induction periods preceding ignition were carried out by Gray and Harper [21]. Steady state and transient solutions were reported for adiabatic as well as thermally diffusive systems.

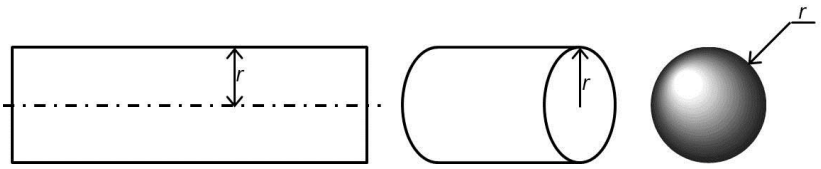

Figure2 Typical geometrical configurations of infinite slab, infinite cylinder and sphere solved in theoretical one-dimensional solutions.

Thomas and Bowes [22] developed a mathematical model to predict thermal ignition of a slab of solid reactive material of finite thickness subjected to constant high temperature on one face and Newtonian cooling boundary conditions on the other. This work forms the fundamental backbone of the current ASTM E-2021 test methodology. Various extensions to the theory developed by Thomas and Bowes are discussed in combustion literature [21, 23-26] with good reviews given by Gray and Lee [27], Merzhanov and Averson [28], and Bowes [29].

The study by Boddington et al. [30] generalized the critical criteria for runaway reactions in exothermic reactant mass subjected to heating conditions based on the reactant geometry. This was a significant

mathematical advancement as prior work by Frank-Kamenetskii [19] and Bowes and Thomas [22] was restricted to idealized geometries of the sphere, infinite cylinder and infinite slab as shown in Fig.2. Different geometries addressed by Boddington et al. include sphere, equi-cylinder, cube, regular tetrahedron and thin circular disk. This marked the beginning of studies involving variety of geometries and boundary conditions that were pursued in order to be able to model real-life scenarios.

Hardee et al. presented a technique to solve the heat conduction equation with generation term for a reactive solid using an approximate temperature profile method [31]. The idea originated from the engineering solution methodology proposed by von Karman [32] while solving momentum boundary layer problems using polynomial fits. Hardee et al. assumed a polynomial to represent the temperature distribution within the solid and the coefficients of the polynomial were solved using the relevant boundary conditions specific to the problem. The critical condition occurred when small perturbations in the boundary temperature caused large perturbations in the internal temperature. Specific geometries considered by Hardee et al. [31, 33] were a rectangular parallelepipied, a finite right cylinder, and a right cone. A comprehensive list of the published works, geometries considered and methods used in analysis is provided in Appendix A. The current study extends the mathematical model by Hardee et al. [31, 33] to a 2D wedge shaped geometry.

Experimental work related to dust ignition:

As with many classical combustion problems, the experimental work followed mathematical theories related to the topic and were performed for validation purposes. The first experimental study on layer ignition was performed by Bowes and Townshend [34] who for validation purposes addressed two types of test methods: hot plate and oven tests. The effect of change in dust layer thickness, packing density and particle size on ignition temperature was studied. It was shown that the ignition temperature increases with decrease in layer thickness. The experimental results were analyzed based on the thermal ignition theory by Thomas and Bowes [22] with good agreement.

Mirron and Lazzara [35] tested a wide variety of dusts including coal, oil shales, lycopodium spores, corn starch, grain and brass powder to determine minimum ignition temperature for dust layer of certain thickness on hot surface. Effects of the nature of the dust, layer thickness and particle size on the minimum hot-surface ignition temperature were discussed. Observations were made based on the structure of the dust particle, ignition pattern (e.g. softening, decomposition) and temperature rise during the ignition as a function of time (e.g. sharp rise in temperature in case of brass powder). Secondary factors such as heating rate, diameter to thickness ratio of the dust layer, affecting the minimum hot-surface ignition temperature of dust layers were addressed. The diameter-to-thickness ratios were varied from 3.3 to 15.6. Preliminary predictions were made regarding the tendency of a dust layer towards self-igniting based on the available literature and the obtained relationship between ignition temperature and layer thickness. ASTM E-2021 adopted the experimental setup and test procedure used by Miron and Lazzara in the standard.

The thermal ignition theory developed by Thomas and Bowes [22] was applied to understand self-heating of two types of coal dust samples and Sodium dithionite layers were used to commission the hot plate apparatus and validate the model predictions based on then available literature by Reddy et al. [11]. Five coal dust layer thicknesses - 5, 10, 15, 20 and 25 mm - were used to find ignition temperature as a function of layer thickness. The ignition temperature was reported to increase with decreasing dust layer thickness. Using the critical parameter and the relationship between the layer thickness and ignition temperature, ignition characteristics - activation energy (E kJ/mol) and pre-exponential constant (QA J/kg-s) of the dusts were extracted. Effect of mixing reactive dust with inert dusts on ignition behavior was also studied. Dolomite and Rock-dust dusts were used as inert dust additives. Increase in ignition temperature was observed with increase in proportion of the inert additive. About 65-70% by weight inert dust was required to completely avoid ignition. Lebecki et al. [36] compared thermal ignition of dust layer on a constant temperature hot surface to that under constant rate of heat generation conditions. Two coal dusts were used in the tests. The minimum ignition temperatures in case of constant rate of heat

generation method were reported to be lower than those determined by the constant hot-surface temperature method. Based on this observation, the constant temperature hot-surface basis of accepted by standard test methods used to determine safe surface temperature for dust accumulation without hazard was questioned. Further, it was recommended that the constant heat generation method which requires applying known heat flux across the surface of the heating plate would result in obtaining more reliable estimation of ignition hazard of the dust layer. Most recently, an experimental method was proposed by Park et al. [16] to estimate thermal and kinetic parameters of Pittsburgh seam coal using a standard test set-up of ASTM E-2021 hot surface ignition test. Thermal conductivity (k), activation energy (E) and product of heat of reaction and pre-exponential constant (QA) were the parameters governing spontaneous ignition which are determined in the study. Four dust layer thicknesses of 6.4 mm, 12.7 mm, 19.1 mm and 25.4 mm were tested to find the minimum hot-surface temperature leading to dust layer ignition. One-dimensional steady state heat transfer equation with zeroth order Arrhenius reaction rate term was applied to the system of an infinite slab of dust of given thickness subjected to constant high temperature at one face and Newtonian cooling at the other face. The standard hot plate test setup (ASTM E 2021 and EN 50281-2-1) rely on the assumption that the layer diameter D is large in relation to its thickness d. Typical values of $D/d > 5$ are recommended [29]. However, for thicker layers heat transport in the radial direction becomes significant. This problem has been recognized in literature [37-39].

The available literature on the experimental work related to spontaneous ignition has so far generated a comprehensive data-set related to critical ignition conditions in 1D geometries. Ignition behavior of dust under complex geometries has never been studied experimentally. This also implies that the theoretical variations in the geometry were never validated by constructing an experimental set-up to generate the same condition. To the best of the author's knowledge, the current study is one of the first to explore spontaneous ignition of a dust deposit in a 2D geometry of a wedge. As discussed earlier, this represents a real-life situation, where dust deposits are typically found to accumulate in wedges and cracks in industrial environments.

Computational work related to dust ignition:

Numerical work related to spontaneous ignition was predominantly published in the last two decades when computational ability of the computers increased tremendously. A numerical model was developed to predict spontaneous ignition of dust layers on hot surfaces by Kim and Hwang [40]. The model considered shrinking of the layer during pyrolysis. Shrinkage was based on reduction in particle diameter as an Arrhenius type function of temperature. The results obtained from the numerical model compared well with experimental work published previously. Effect of variation in parameters such as particle diameter, layer thickness was studied. Unsteady state modeling was also carried out to compare the time to ignition prediction and reasonable comparison was obtained with experimental results. Some discrepancies involved in the comparison between the model predictions and experimental data were attributed to complexities of transient heat transfer modes. With the advent of numerical work, traditional analytical models were re-tested. For example, the numerical work presented by Chen [41] claims that the Thomas' model [42] over-predicts time-to-ignition.

Numerical modeling was performed in the current study with the objective of gaining better understanding of the heat transfer taking place on the interface of dust surface and air. Numerical modeling cannot be used unless the properties of the dust are determined experimentally. It is difficult to achieve with the current experimental tools because accurate relationships of temperature dependent properties need to be obtained. Therefore, direct application of numerical modeling to predict ignition in the condensed phase is limited and is used as a tool to analyze gas phase conditions in most cases. Secondly, it is difficult to adapt a numerical model to existing engineering standards which rely on simple analytical expressions.

Overall, the literature review demonstrates that there is a disconnect between real life situations, industrial standard tests and scientific research. The broader objective of this study is to bridge this gap by demonstrating the use of a simple-engineering-mathematical model that can be easily implemented to

existing standards, thereby extending their applicability to analyze the hazard related with dust deposits in realistic situations such as 2D wedges and 3D corners.

1.3 Summary of Current Work

The effect of heat conduction, either one-dimensional (dust layer) or multidimensional (dust deposit), and the effect of heat generation by dust, on the ignition phenomenon should be understood clearly so as to prescribe safety measures to avoid dust ignition and explosions. To investigate the influence of these effects, experiments with two hot plates, configured at two different angles (90º and 60º) to form wedges, were carried out and the two-dimensional heat transfer and heat generation effects were envisaged. Three thermocouples, placed along the symmetry plane of the wedge cross-section at various heights, were used to record the transient temperature data. Results showed that ignition always occurs around the region surrounding the topmost thermocouple in the case of the 60º wedge, and in the regions surrounding both the topmost and the middle thermocouples, in the case of the 90º wedge. These trends were explained by investigating three parameters affecting the ignition behavior, namely, the heat transfer from the hot plate to the coal dust, subsequent chemical heat release and the rate of heat transfer between different regions within the coal dust. Further research on this line was conducted by developing a theoretical model with capability of predicting the location of ignition in an arbitrary geometry. The complex behavior on the interface between dust and air was studied by simulating the ignition condition using numerical modeling. Therefore, the three pronged study of the spontaneous ignition of dust layers and deposits provides useful tools and understanding of the phenomena necessary to design safe environments for dust processing and handling in industrial environments.

Finally, a study was conducted for envisaging the self-ignition behavior, taking into account the effects of weathering of combustible dusts. Weathering of coal and other cellulosic dusts occur due to the process of wetting and subsequent drying, or by subjecting them to a temperature higher than the ambient temperature for prolonged time periods [43]. Few studies available in literature are discussed in Section 4.1. The first type of weathering occurs in a wetted storage. The second type of weathering occurs when a

dust processing unit stores and maintains the dust deposit at an elevated temperature. As a result of weathering, the physical and thermal properties of the dust may change. Therefore, the weathered dust sample is expected to ignite at a different hot plate temperature as compared to that of a fresh sample, when tested in a standard test method (ASTM E 2021). In this study, three dust samples namely, wheat flour, Pittsburgh seam coal and Powder River Basin coal were tested. These dust samples are subjected to one or both types of weathering. Thermogravimetric analysis (TGA) and standard ignition tests were carried out with both fresh and weathered dust samples. Estimation of the activation energies and reactivity, and measurement of the minimum surface temperature for the onset of ignition have been carried out for all the cases. The implications of the observed results on industrial safety related to combustible dust layers were discussed. If weathering resulted in increase in hazard associated with the dust, then a prolonged hot surface test should be recommended in order to check if the safe limits of surface temperature are needed to be lowered.

1.4 ORGANIZATION

The chapters of the thesis align with the set objectives. The brief description of the chapter contents is provided as follows:

Chapter 1: The introductory chapter explains the goals set in this work and takes account of the relevant literature already available.

Chapter 2: Four issues related to the dust layer ignitions are addressed and can be listed as:

- Property estimation using dust layer ignition tests
- Improvements in the ring material for ASTM E-2021 test standard
- Mathematical model to predict critical ignition conditions
- Numerical simulation of dust layer ignition

Chapter 3: This chapter deals with two-dimensional wedge-shaped dust deposits formed between two hot surfaces and is divided into three parts:

- Experimental study of spontaneous ignition in wedge-shaped dust deposit geometry
- Mathematical method proposed to predict spontaneous ignition behavior of dust deposits in multi-dimensional geometrical configurations
- Numerical simulations performed to analyze complex behavior of the convective cooling currents set on the top of the dust layer

Chapter 4: This chapter addresses the issue of weathering of dusts and its effect on the minimum layer ignition temperature of the dust.

Chapter 5: The possible future work is discussed here.

Appendix: This section at the end provides reader with details such as programming codes, experimental repeatability, comparison of current versus previous mathematical models and literature review in chart form.

Chapter 2. SPONTANEOUS IGNITION OF COMBUSTIBLE DUST LAYERS (1-D GEOMETRY)

2.1 INTRODUCTION

The most common occurrence of dust accumulation is in the form of layers. Flat surfaces available in ducts, floors and above false ceilings in industrial facilities handling fine powders accumulate dust layers. If these surfaces or parts of them are at a sufficiently high temperature, the dust may undergo thermal ignition. This can further lead to smoldering or flaming fires and even provide ignition source to an explosive gas-air cloud. The experimental setup used by the industry to quantify the hazard posed by accumulation of dusts on hot surfaces is described by ASTM E-2021.

2.2 STANDARD TEST USED BY INDUSTRY

The National Academy of Sciences (NAS) Committee on Evaluation of Industrial Hazards recommended a hot surface test to determine minimum hot-surface ignition temperatures of dust layers. The International Electrotechnical Commission (IEC) has proposed a very similar test. Based on these two test reports and the work by the US Bureau of Mines [44], the ASTM standard E 2021 [6] and the European standard EN 50281-2-1(1999) [7] were proposed. These tests are based on determining a reference or minimum temperature of the solid surface necessary to cause ignition of a dust layer deposited over it. Common criteria for ignition in these hot surface tests are visible signs of combustion or glowing, or the temperature at a location within the dust layer rising to 50 ºC above the hot surface temperature [6]. The test procedure can be summarized as:

1. Pre-measured quantity of dust sample is introduced on a top surface of hot plate, which is at a preset constant temperature and confined by a metal ring.
2. A single thermocouple at the center of the ring monitors the temperature rise.
3. Due to oxidative reactions or decomposition reactions or the combination of two, ignition can take place. Ignition is said to have occurred either when the temperature at the center raises at

least 50°C above the constant hot plate temperature or when smoke, glow like evident combustion indicators are seen.

4. If no ignition occurs and the temperature reaches steady state, the test is repeated with higher temperature set for hot plate and fresh dust sample is used. The test standard recommends a 10°C difference between ignition and no-ignition hot plate temperatures.

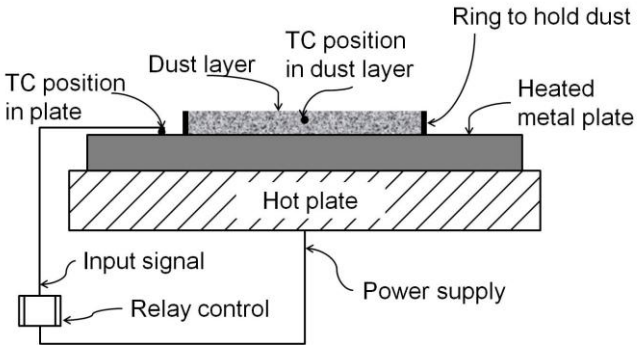

Figure3 Schematic of the ASTM E-2021 standard test method for hot surface ignition temperature of dust layers.

As shown in Fig. 3, ASTM E 2021 uses four inch (101.6 mm) diameter metal ring placed on eight inch (203.2 mm) diameter hot plate. The dust particle size is maintained lower than 75μm i.e. standard sieve number 200. The dust layer is recommended to be maintained at 12.7 mm. The minimum temperature for ignition is reported for a given dust layer thickness, as the layer thickness has strong influence on this critical value. An example of experimental results from the test procedure is shown in Table 1. The general observation is that as the layer thickness increases minimum ignition temperature decreases (as shown in Table 2).

Table 1. Representative data provided by ASTM E-2021 for verification of test apparatus using different dust samples and 12.7 mm dust layer thickness.

Dust Sample	Minimum Layer Ignition Temperature (°C)
Brass Powder	155-160
Pittsburgh Seam Coal	230-240
Lycopodium Spores	240-250

Table 2. Variation of ignition temperature with dust layer thickness is shown by ASTM E-2021 using Pittsburgh seam coal.

Dust Layer Thickness (mm)	Minimum Layer Ignition Temperature (°C)
6.4	300
9.4	260
12.7	240
25.4	210

2.3 1-D MATHEMATICAL MODEL

The flat plate test (ASTM E2021) can be modeled using the thermal ignition theory developed by Thomas and Bowes [22] for a slab subjected to constant high temperature on one side and convective cooling on the other. The governing steady state equation and boundary conditions for the problem in steady state (as shown in Fig. 4) can be written as:

$$-k\frac{d^2T}{dx^2}=\dot{q}''', \tag{1}$$

where heat generation term is defined using an Arhenius function as,

$$\dot{q}'''=\rho QAe^{(-E/RT)}, \tag{2}$$

and

$$\text{at } x=0, T=T_p, \tag{3}$$

$$\text{at } x=2r, -k\frac{dT}{dx}=h_c\left(T_s-T_\infty\right). \tag{4}$$

The governing equation and the boundary conditions can be written in non-dimensional form using the following approximation:

$$\text{For } \frac{E}{RT_p}>>1, \frac{E}{RT}\approx\frac{E}{RT_p}\left(1-\frac{T-T_p}{T_p}\right). \tag{5}$$

The non-dimensional variables can be expressed as,

$$\theta = \frac{E}{RT_p^2}(T - T_p) \tag{6}$$

and

$$z = \frac{x}{r}. \tag{7}$$

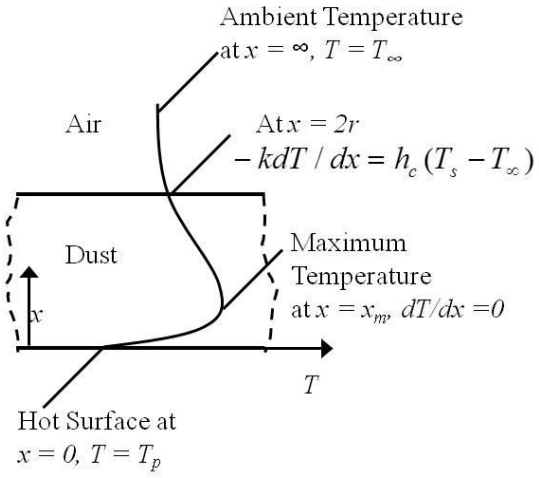

Figure4 Geometry of infinite slab of dust layer subjected to constant high temperature on one face and convective cooling on the other.

Two non-dimensional parameters can also be defined for the theory as,

$$\delta = \frac{QAEr^2\rho}{kRT_p^2} e^{(-E/RT_p)}, \tag{8}$$

known as Frank-Kamenetskii parameter and

$$Bi = hr/k, \tag{9}$$

known as Biot number.

The governing equation and the boundary conditions can now be written in non-dimensional form as,

$$\frac{d^2\theta}{dz^2} = -\delta e^{\theta} \tag{10}$$

and

$$\text{at, z = 0, } \theta = 0\,, \tag{11}$$

$$\text{at, z = 2, } -\frac{d\theta}{dz} = Bi(\theta_s - \theta_\infty). \tag{12}$$

The solution of Eq.(10) can be written as,

$$\theta = \theta_m - 2\ln\cosh\left(\sqrt{\frac{\delta e^{\theta_m}}{2}}(z - z_m)\right) \tag{13}$$

where, at $z = z_m$, $\frac{d\theta}{dz} = 0$.

θ_m and z_m are the non-dimensional maximum temperature and its location along the axis. If the maximum temperature occurs very close to the hot surface, it can be approximated that,

$$\text{at } z = 0, \ \frac{d\theta}{dz} = 0\,. \tag{14}$$

Then, the approximate solution for Frank-Kamenetskii parameter becomes,

$$\delta_c \approx \frac{1}{2}\left(\frac{Bi}{1+2Bi}\right)^2 (1.4 - \theta_\infty)\,. \tag{15}$$

The critical Frank-Kamenetskii parameter expressed in Eq. (15) represents conditions necessary for spontaneous ignition. If calculated value of δ exceeds the critical value, spontaneous ignition is expected in that case.

2.4 Experimental Study

In this study, a slightly modified ASTM E-2021 test setup [45] was used to analyze the problem of spontaneous ignition of dust layers. Three equidistant thermocouples were situated along the central axis of the ring instead of just one at the center of the ring in the standard test setup to monitor the temperature

within the dust layer. Also, the metal ring used to contain the dust was replaced by a ring made from insulating material. The details are discussed further in the chapter.

Test equipment includes a system for maintaining constant hot surface temperature, monitoring system for logging temperatures at various locations in the dust sample and a ring to contain the dust. A constant hot surface temperature was required on top of a 1 inch thick aluminum plate placed on top of an electric hot plate (ROPH -144). The constant hot surface temperature was maintained using electrical controller (CN 8592) - relay (SSRL240DC25) circuit, which gets an input temperature from a thermocouple adhered to the hot plate and matches it with desired temperature. All the thermocouple data was collected using USB-TC data acquisition system which can log data from up to eight channels at a frequency of 1 Hz.

Thermocouples were situated at desired locations and the hot plate was allowed to heat-up. Once the pre-set temperature was reached, data acquisition system was turned on. A pre-measured quantity of the dust sample was then introduced in the ring and leveled to have a uniform layer thickness. The temperature at all locations within the dust layer was observed for increase in temperature. The condition of the dust sample was also observed for signs of ignition. The test was ended by switching the hot plate power off when either spontaneous ignition occurred or a steady state was reached i.e. temperature of the dust was consistently below the hot surface temperature at any time. Since the initial tests were started at a considerably low temperature values of hot surface temperature (150°C for half inch layer thickness), if test resulted in no-ignition repeatedly then next set of tests was carried out at 10°C higher value of pre-set hot surface temperature.

Pittsburgh seam coal (average particle size 32 μm and pulverized to pass through mesh size of 75 μm) was used as the combustible dust sample. Dust layer thickness values of 6.35 mm (1/4”), 12.7 mm (1/2”), 25.4 mm (1 inch), 50.8 mm (2 inches) and 76.2 mm (3 inches) were tested. The minimum ignition temperatures obtained are plotted in Fig. 5 along with data available from literature [16]. The curve

represents critical ignition conditions above which lie conditions leading to ignition and no-ignition zone below.

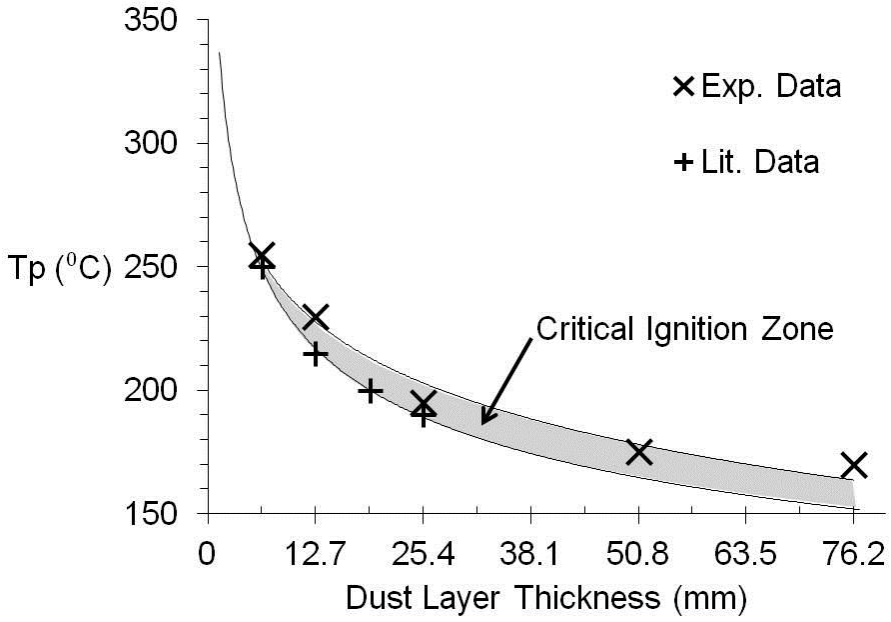

Figure5 Minimum layer ignition temperature plotted for several dust layer thickness values.

The current work is focused on two main issues. First, the fact that such test set-up can be used to extract properties of dust such as thermal conductivity, one-step Arrhenius reaction rate activation energy and pre-exponential constant is highlighted. Literature available on this practice is ample and well documented by Park et al. [16]. The second part discusses a possible amendment in the standard test procedure, where the metal ring can be replaced by an insulating material ring. The two issues are discussed in the following sub-sections.

2.4.1 PROPERTY ESTIMATION USING ASTM E-2021

The flat plate tests were conducted at several dust layer thickness values from 6.35 mm to 76.2 mm as shown in Fig. 5. This data can be represented using the critical Frank-Kamenetskii parameter from Eq. (8).

Taking logarithm of Eq. (8),

$$\ln\left(\delta_c T_p^2 / r^2\right) = -\frac{E}{RT_p} + \ln\left(\frac{E\rho QA}{Rk}\right). \qquad (16)$$

The terms in the linear Eq. (16) can be plotted as $\ln\left(\delta_c T_p^2 / r^2\right)$ against $1/T_p$, the slope of which gives the activation energy (E) and intercept gives pre-exponential constant in product form (QA).

The non-dimensional ambient temperature θ_∞ is required to calculate δ_c using Eq. (15) and is expressed as,

$$\theta_\infty = \frac{E}{RT_p^2}(T_\infty - T_p). \qquad (17)$$

Therefore, it is clear from Eq. (17) that an iteration exercise is required to converge the value of the activation energy, as θ_∞ is a function of the activation energy (E). Once the value of activation energy converges, the value of QA can be obtained by the intercept value from Eq. (16).

2.4.2 Improvements in Test Apparatus

The temporal variations of temperatures at four locations in a 25.4 mm thick coal dust layer subjected to a hot surface temperature (T_p) of 190°C are shown in Fig. 6. Two thermocouples are located 45 mm away from the center of the ring at 6.35 mm and 12.7 mm heights from the hot plate. The third thermocouple is located at the center of the ring at 12.7 mm height from the hot plate. The last thermocouple is located 25.4 mm from center and 12.7 mm from the hot surface. The black solid horizontal line in Fig. 6 represents the set hot surface temperature of 190°C.

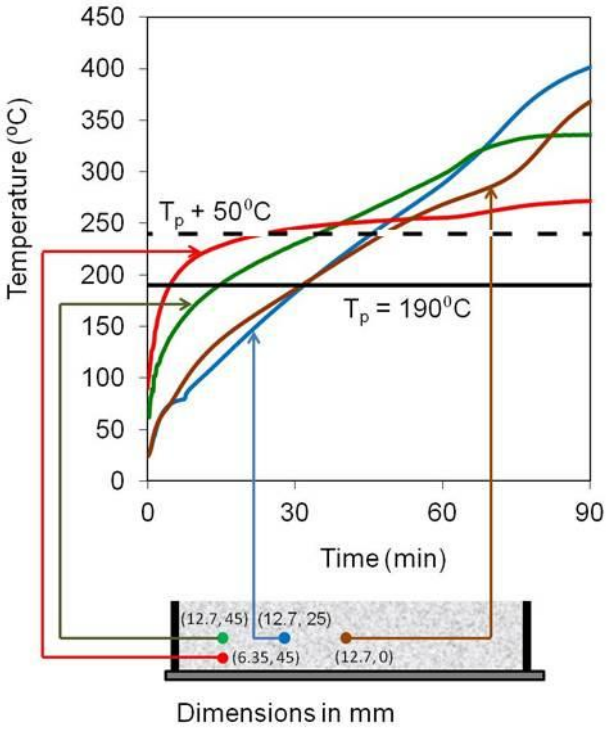

Figure6 Time histories of temperature at four locations in one inch dust layer subjected to hot surface temperature of 190°C. The four locations of thermocouples are displayed in a schematic of the set-up at the bottom of the graph along with their (vertical and radial) co-ordinates adjacent to each.

The ASTM E 2021 standard describes the occurrence of ignition as the point in time at which the thermocouple located at the center of the dust layer, i.e., half way from hot surface at the axis, indicates a temperature 50°C above that of the hot surface. This is depicted by the horizontal dashed line in Fig. 6. The test shows that the thermocouple located at the corner (red line) is the first to ignite followed by the thermocouple above it (green line). Both thermocouples are not along the axis of symmetry but rather closer to the metal ring. The time difference between the instance of first ignition occurring at the location near the ring and the hot plate (red dot in Fig. 6), and the same occurring midway from the hot plate near at the axis (brown dot in Fig. 6), is significantly large (~25 min). Even for the ring diameter to dust layer thickness ratio of 8:1, the corner ignition problem persisted, as seen in Fig.7, when stainless steel ring was used. This is contrary to the general rule of maintaining aspect ratio above 4 or 5 to avoid corner ignition

in such tests [29]. The standard test sets the minimum safe temperature based upon the temperature at the center. Clearly, the center line temperature is not the best representation of the worst case scenario.

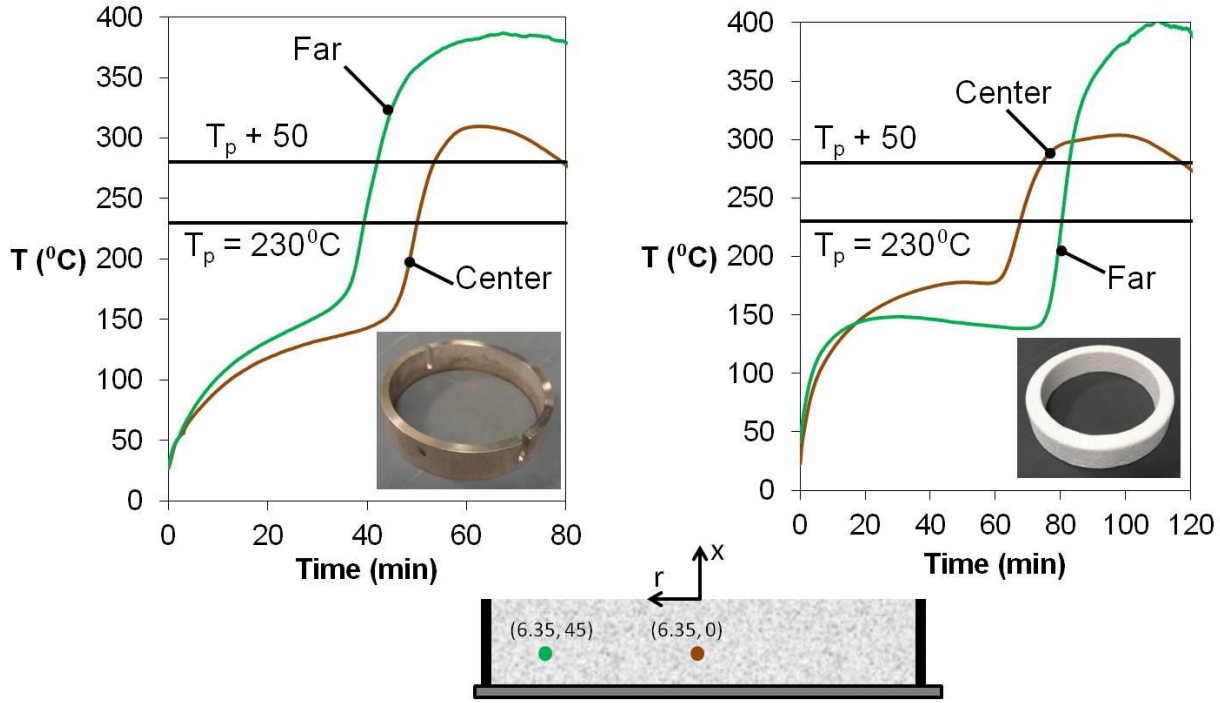

Figure7 Comparison of ignition tests done using metal ring (left) and insulating ring (right) for half inch thick dust layer of Pittsburgh Seam coal.

The dust layer set-up is expected to be a practical representation of infinite slab geometry, where the only dimension required to define the geometry is the thickness of the dust layer. Because of the high thermal conductivity of steel (~16 W/m-K), a sudden discontinuity in temperature distribution is experienced by the dust layer in contact with the inner surface of the ring. Therefore, a ring material which imitates the dust inside and "tricks" the dust into believing it is an infinite slab would be more appropriate.

Thermally insulating materials were considered to construct ring. As a first trial, Kaowool insulating fiber board (thermal conductivity = 0.06 W/m-K, heat capacity = 1088.6 J/kg-K and bulk density = 200 kg/m^3) was used. The physical strength of the fiber board demanded cutting thick walls (25.4 to 50.8 mm) for the ring. The resulting large surface area in contact with the hot plate created similar problems as the metal ring. Therefore, a stronger insulating ring material having thermal conductivity of about 0.09 W/m-K and

carrying the commercial name KVS® 124 was tested as an alternative with a ring wall thickness limited to 12.7 mm. The thermal conductivity of the Pittsburgh Seam coal dust is of the same order and varies from 0.1 to 0.2 W/m-K depending on its composition. The results of the ignition tests with the insulating ring are shown in Fig. 7(b). The thermocouple at the center (brown dot in Fig 7(b)) reached temperature 50^0C above the set hot plate temperature of 230^0C. This proves that the change in the ring material allowed the desired one-dimensional heat transfer and the dust layer behaved like an infinite slab at least until the on-set of ignition.

Even though the minimum ignition temperature in both the cases remained same, there are few factors that make the insulating ring a more favorable option as discussed below:

- Time to ignition: Corner ignition in case of the use of metal ring also leads to an early ignition compared to the insulating material ring (by about 33 minutes in case of 12.7 mm Pittsburgh seam coal dust layer). This clearly misleads the user of the data derived from metal ring. If determination of ignition time is the prime motivation of such test, then the metal ring would definitely generate erroneous results.
- Estimation of properties: In addition to the early ignition that takes place near the inner surface of the ring, the time history of the temperature rise at the center of the metal ring indicates an early ignition as compared to the insulating ring. The high temperature zone developed in the corner, therefore, seems to be influencing the temperature distribution along the center line. Obviously, the temperature distribution in the dust along the center line would not represent a one-dimensional heat transfer from the hot plate to the ambient air on the top. The method to extract kinetic parameters of the dust involves application of one-dimensional energy conservation equation. In the case of metal ring, such mathematical exercise could lead to erroneous results.
- Test accuracy: The minimum ignition temperature, in case of Pittsburgh seam coal, remained same for both cases of metal and insulating ring material. But the corner ignition can occur at a

lower temperature for a reactive material. In that case, an excessively safe temperature limit may be imposed on the industry.

2.5 NUMERICAL ANALYSIS

2.5.1 INTEGRAL METHOD

The problem of thermal ignition of infinite slab on hot surface exposed to convective cooling was originally solved by Thomas and Bowes [22]. They extended the theory of thermal ignition of a slab of reactive material [42] to a configuration where one face of the slab was held at the constant high temperature and other face exposed to cooler surroundings. However, a different solution approach is used in this study by using an approximate temperature profile method. A polynomial is assumed to closely represent the temperature distribution along the dust layer and the coefficients of the polynomial are determined by using the physical boundary and additional conditions [31]. The mathematical analysis and results are presented in the following sections.

2.5.1.1 Mathematical Model

One-dimensional steady state energy conservation equation is written as,

$$k\frac{d^2T}{dY^2}+\rho QAe^{-E/RT}=0. \qquad (18)$$

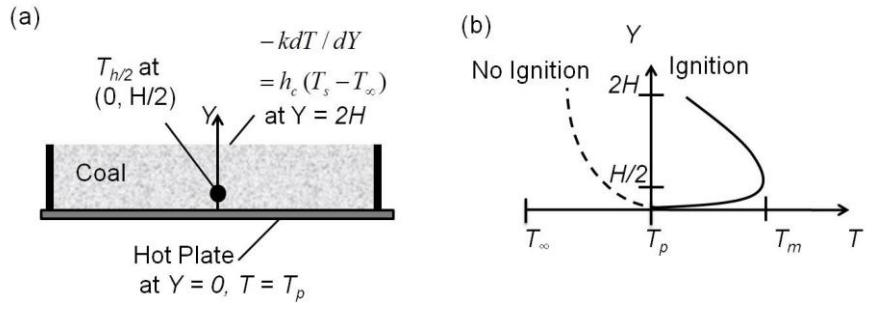

Figure8 (a) One-dimensional coordinate system and boundary conditions for flat plate geometry and (b) representative temperature profiles along the y-axis.

Two necessary boundary conditions for this second-order problem are shown in Fig. 8(a) and listed as,

$$Y = 0,\ T = T_p \text{ and} \tag{19}$$

$$Y = 2H, -k\frac{dT}{dY} = h_c(T_s - T_\infty). \tag{20}$$

The steady-state energy conservation equation is re-written in non-dimensional form using

$$\theta = \frac{RT}{E},\ h_c^* = \frac{h_c}{\left(\frac{\rho QAkR}{E}\right)^{1/2}},\ y = \left(\frac{\rho QAR}{kE}\right)^{1/2} Y \text{ and } h = \left(\frac{\rho QAR}{kE}\right)^{1/2} H,$$

as:

$$\frac{d^2\theta}{dy^2} = -e^{1/\theta}. \tag{21}$$

The boundary conditions in non-dimensional form (Eq. (19) and Eq. (20)) can be written as:

$$y = 0,\ \theta = \theta_p, \tag{22}$$

and

$$y = 2h, -\frac{d\theta}{dy} = h_c^*(\theta_s - \theta_\infty). \tag{23}$$

As mentioned before, a cubic polynomial is assumed to represent the temperature variation along *y*-axis as,

$$\theta = A + By + Cy^2 + Dy^3. \tag{24}$$

At the critical ignition condition, a certain temperature, $\theta_{h/2}$, prevails at 1/4th of the layer thickness, as shown in Fig. 8(a), and given (in non-dimensional form) as,

$$y = h/2,\ \theta = \theta_{h/2}. \tag{25}$$

At a certain height, $y = h_m$, there exists the maximum temperature value, which represents the location of ignition. It is expressed (in non-dimensional form) using zero slope condition at the maxima as,

$$\text{at } y = h_m, \frac{d\theta}{dy} = 0 . \qquad (26)$$

The four unknown constants (A, B, C and D) in Eq. (24) can be determined by solving four simultaneous equations obtained using Eq. (22) and Eq. (23) and two more conditions described by Eq. (25) and Eq. (26), if values of h_m, $\theta_{h/2}$ and θ_s are known.

The four coefficients of the polynomial in Eq. (24) can be solved as,

$$\begin{aligned} A &= \theta_p \\ B &= \frac{h_c^*(\theta_s - \theta_\infty)(2f^2 - f) + e^{-1/\theta_{h/2}} 4Hf(f-1)}{(1-f)(1-2(1+f))} \\ C &= \frac{h_c^*(\theta_s - \theta_\infty) + e^{-1/\theta_{h/2}} 4H(1-f^2)}{4H(1-f)(1-2(1+f))} \\ D &= \frac{h_c^*(\theta_s - \theta_\infty) + e^{-1/\theta_{h/2}} 2H(1-f)}{6H^2(1-f)(2(1+f)-1)} \end{aligned} \quad , \qquad (27)$$

where f is the ratio of $h_m/2h$.

A non-linear expression for $\theta_{h/2}$ is obtained by applying the condition given in Eq. (25) to Eq. (24) as,

$$\begin{aligned} \theta_{h/2} = \theta_p &+ \frac{h_c^*(\theta_s - \theta_\infty)(2f^2 - f)}{(1-f)(1-2(1+f))} fH + \frac{e^{-1/\theta_{h/2}} 4Hf(f-1)}{(1-f)(1-2(1+f))} fH + \\ &\frac{h_c^*(\theta_s - \theta_\infty)}{4H(1-f)(1-2(1+f))} f^2H^2 + \frac{e^{-1/\theta_{h/2}} 4H(1-f^2)}{4H(1-f)(1-2(1+f))} f^2H^2 + . \\ &\frac{h_c^*(\theta_s - \theta_\infty)}{6H^2(1-f)(2(1+f)-1)} f^3H^3 + \frac{e^{-1/\theta_{h/2}} 2H(1-f)}{6H^2(1-f)(2(1+f)-1)} f^3H^3 \end{aligned} \qquad (28)$$

To solve $\theta_{h/2}$, the following approximations are invoked; it is noted that at critical ignition conditions, a small increase in plate temperature θ_p results in large increase in the maximum temperature and therefore in the value of $\theta_{h/2}$, as shown in Fig. 8(b). Also, there is only a small increase in the value of θ_s. Therefore, it can be assumed that,

$$\frac{d\theta_p}{d\theta_{h/2}} = \frac{d\theta_s}{d\theta_{h/2}} = 0 . \qquad (29)$$

Taking derivative of Eq. (28) with respect to $\theta_{h/2}$, and invoking the approximations given in Eq. (29), a quadratic expression for $\theta_{h/2}$ is obtained:

$$\theta_{h/2}^2 - \theta_{h/2} + \theta_p + \frac{\frac{h_c^*(\theta_s - \theta_\infty)(2f^2 - f)}{(1-f)(1-2(1+f))} fH + \frac{h_c^*(\theta_s - \theta_\infty)}{4H(1-f)(1-2(1+f))} f^2H^2 + = 0 . \qquad (30)}{\frac{h_c^*(\theta_s - \theta_\infty)}{6H^2(1-f)(2(1+f)-1)} f^3H^3}$$

A quadratic equation in terms of $\theta_{h/2}$ is obtained as shown in Eq. (30). The negative root of the quadratic is chosen to adhere to the physically attainable temperature in both, one and two dimensional cases.

The expression of $\theta_{h/2}$ needs values of θ_s and f (*i.e.* $h_m/2h$). The value of θ_s is determined using the critical condition defined by Hardee et al. The critical value of expression is obtained as,

$$\frac{L^2}{\theta_{h/2}^2 e^{1/\theta_{h/2}}} = \frac{3(2f+1)}{f^2(9-2f)} , \qquad (31)$$

for a very large layer thickness value (the maximum layer thickness of 101.6 mm is used) by assuming $\theta_s \approx \theta_\infty$ to be equal to 3.8. Then, for the cases of other thickness values, the value of θ_s is obtained by seeking the critical value as f is incremented from 0 to 1. The computational code (MATLAB®) used to perform calculations is provided in Appendix C.

2.5.1.2 Results and Discussion

For the flat plate case having a coal layer thickness of 25.4 mm, the temperature profile along *Y*-axis is shown in Fig. 9. From this profile, the ignition location is estimated as 18% of the total height from the hot plate. This compares reasonably well against the experimental result, where bottom thermocouple, located at 25% of total height from the plate, records the maximum temperature (note that experimental

data is only available at 3 points). Since, experimental results follow the ignition criteria, set at 50°C above the plate temperature, than the mathematical model; direct comparison of temperature profiles is not presented.

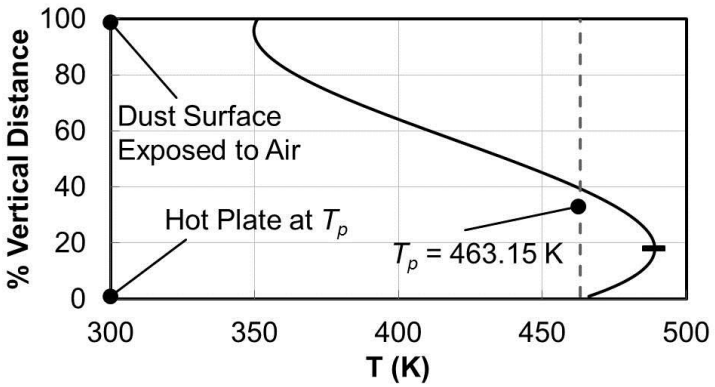

Figure9 Mathematically predicted temperature profiles along Y-axis for flat plate case.

The mathematical model can predict critical ignition conditions for different layer thicknesses, which is characterized by the plate temperature at which ignition occurs. Figure 10 shows the minimum hot plate temperature which caused ignition in various layer thickness cases. The mathematical prediction is in good agreement with the present experimental results as well as against those reported in literature [22]. Since, there is already a theoretical solution available in literature; the comparison only verifies the current mathematical method. The comparison of the two method approaches is presented in Appendix B. The maximum deviation between the present model prediction and the experimental data is around 3.3% for the highest thickness. The deviation between both mathematical models and the experimental data at increased layer thicknesses is probably due to decreasing aspect ratio (from 16:1 to 2:1) of ring diameter (101. 6 mm) to the layer thickness (from 6.35 mm to 50.8 mm) in the experiments. Lower than 4:1 aspect ratio of ring diameter to layer thickness may impart some inaccuracies to the model results [29] as shown in Section 2.5.2.3.

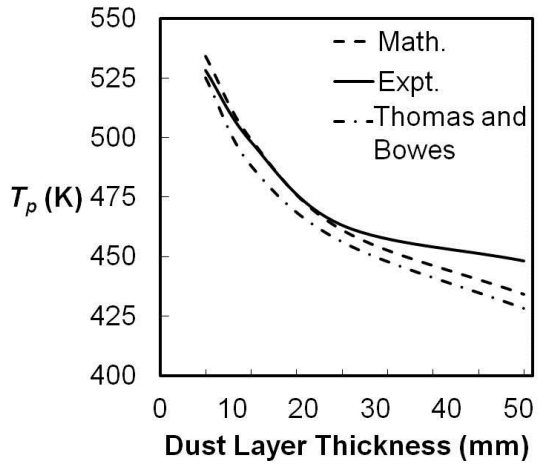

Figure10 Variation of minimum hot plate temperature that causes ignition of coal layers having different thicknesses deposited over a flat plate.

2.5.2 COMPUTATIONAL MODEL

2.5.2.1 Set-up for the Model

Combustible dust deposited on a flat hot plate with insulating or metal ring boundaries is shown in Fig. 11. Dust layer thickness of 25.4 mm is considered in the case of flat plate geometry.

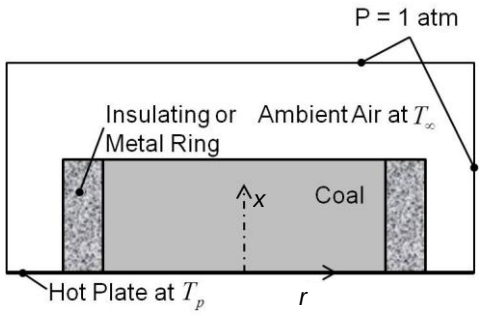

Figure11 Coordinate system and boundary conditions for flat plate configuration; hot plate shown by thick line.

The equation governing the flat plate problem (Fig. 11) for solving the temperature T as a function of cylindrical space co-ordinates (x, y) and time (t) can be represented by a partial differential equation given as:

$$\rho C_p \frac{\partial T}{\partial t} = \frac{\partial}{\partial x}\left(k\frac{\partial T}{\partial x}\right) + \frac{1}{r}\frac{\partial}{\partial r}\left(rk\frac{\partial T}{\partial r}\right) + \rho QAe^{-E/RT} \cdot \qquad (32)$$

An axi-symmetric model (Fig. 11), build on FLUENT, a commercial code, has been employed for solving Eq. (32).

The boundary conditions are set as constant temperature at the hot surface (T_p) along the entire base line which represents the hot plate and pressure based condition (pressure inlet condition in FLUENT) at the extended boundaries. The top surface of the coal dust layer will be then subjected to a coupled convection-conduction boundary condition. The thermo-physical properties of Pittsburgh seam coal are used. The source term (last term in the RHS of Eq. (32)) is calculated using a zeroth order Arrhenius type rate equation. The parameters such as the activation energy (E = 88.1 kJ/mol) and the pre-exponential constant (QA = 1.8 e+12 W/kg) are taken from Park *et al.* [16]. The value of heat capacity and thermal conductivity are assumed to be constants (1300 J/kg-K and 0.2 W/m-K, respectively). The bulk density is measured during experimental work (580 kg/m^3). The ambient air is assumed to be at a constant temperature of 295 K. The insulation material properties (Fig. 11) are taken to be that of KVS-124 (thermal conductivity = 0.09 W/m-K, heat capacity = 1088.6 J/kg-K and bulk density = 288.3 kg/m^3). Numerical results obtained for 25.4 mm dust layer thickness case are validated against experimental data.

2.5.2.2 Validation

The flat plate experiments were conducted in the previous work, for thickness value of 25.4 mm. Three thermocouples were situated along the center line (y-axis in Fig. 11) to monitor the temperature of the dust throughout the experiment at 6.35 mm, 12.7 mm and 19.05 mm heights from the hot plate. The experimental results were proved repeatable with consistent data obtained from four tests as described in section 2.2. The ignition location is defined as the point along y-axis that reaches temperature 50 K above the plate temperature. The ignition location is seen to be at the thermocouple closest to the hot plate from experimental data shown for flat plate in Fig. 12(a). The numerical temperature profile captures the

ignition location and the temperature variation observed experimentally. The ignition location is situated in the region at about 25% of total dust layer thickness from the hot plate according to the experimental data. The numerical results indicate the ignition location to be at 32% of the total thickness. The experimental data is limited to maximum resolution of 25% and therefore considered in valid agreement with the numerical results. Also, the thermocouple farthest from the hot surface showed maximum deviation from the numerical value. This can be attributed to the complex nature of heat transfer in the zone above ignition location which was not captured in the simplistic numerical simulation.

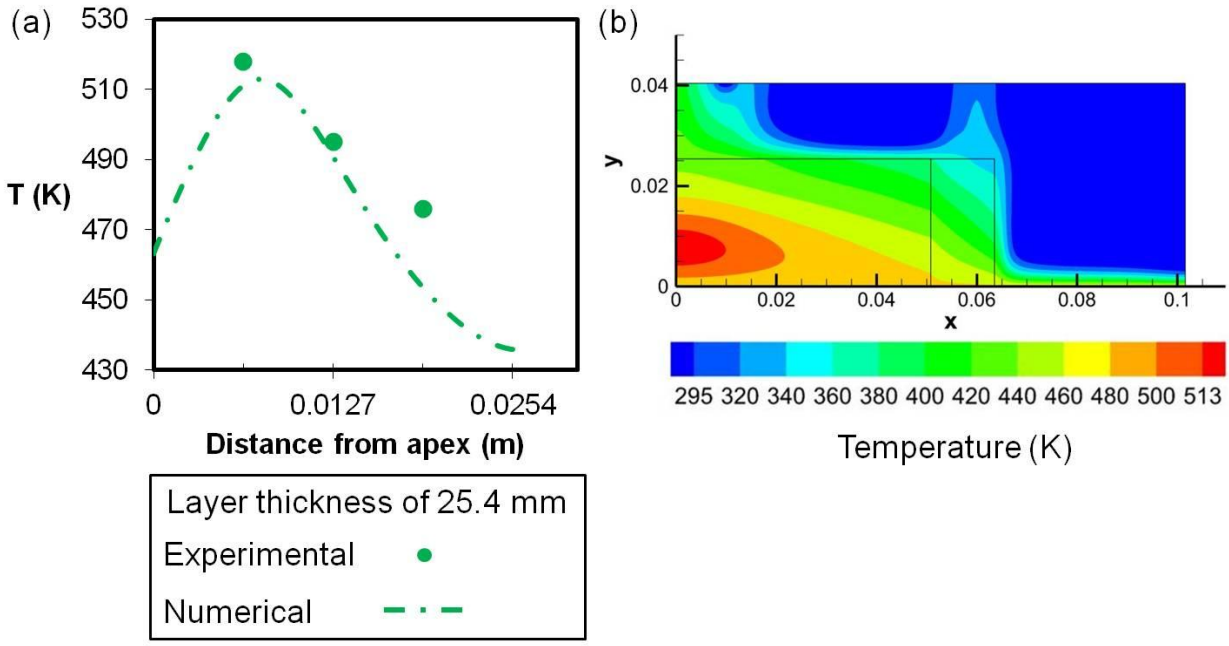

Figure12 (a) Numerical and experimental data of temperature against distance from hot plate is presented for flat plate where the layer thickness is 25.4 mm. (b) Temperature contour at the time of ignition.

2.5.2.3 Ring Material

The discussion from Section 2.4.2, about the ring material used in the standard test to contain the dust, is continued here. The two materials under consideration are 1) stainless steel and 2) KVS® 124 (insulation). The properties of both the materials were used to simulate the spontaneous ignition by constructing two cases. The temperature contours at the time of ignition are shown in Fig.13. Clearly, the

insulation helped in generating a much closer temperature gradient in the dust to one-dimensional heat transfer, as shown in Fig. 13(a). The metal ring, on the other hand, created a hot spot away from the central axis, as shown in Fig. 13(b). The results from the simulation matched with the experimental observation of corner ignition in case of use of metal ring. Therefore, the corner ignition problem is originated from the presence of multiple hot surfaces that the dust is subjected to. The possibility of oxygen diffusion playing any significant role in the process is hence eliminated.

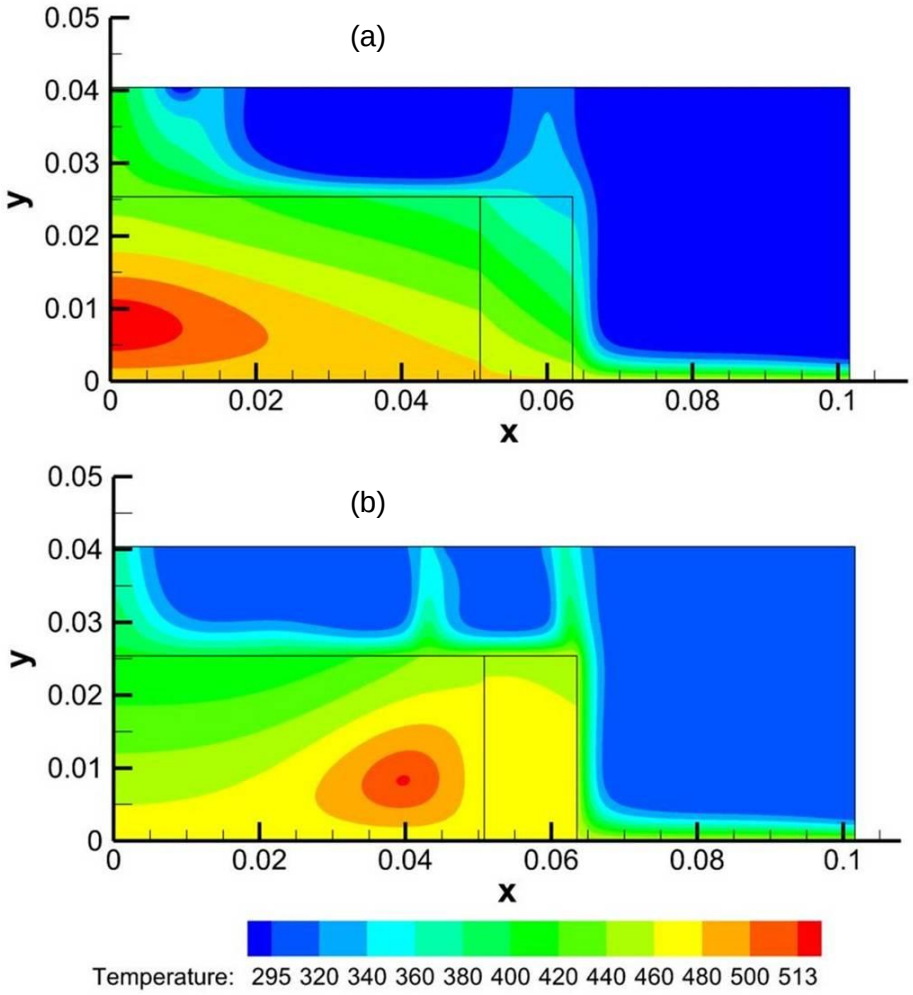

Figure13 Temperature contours at the time of ignition are shown for one inch thick Pittsburgh seam coal dust layer on hot plate at constant temperature of 463 K and contained by (a) KVS 124 (insulation) and (b) stainless steel rings.

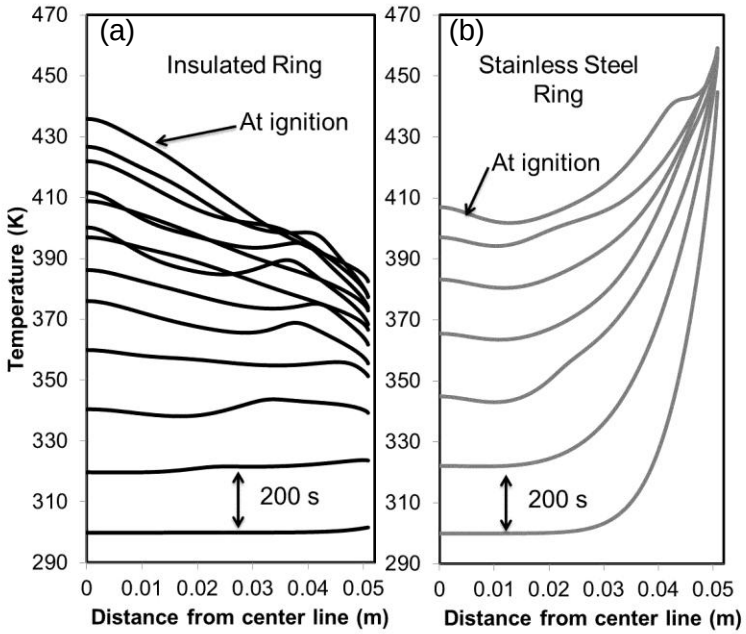

Figure14 Temperature variation along the coal surface exposed to air is shown from the center line to the inner end of dust containing ring in flat plate cases of (a) insulated ring and (b) stainless steel ring. Lowest temperatures indicated by curve at time of 200 s f from the start and each next curve representing 200 s increase in time until the last curve showing ignition conditions.

The transient analysis of the temperature distribution on the interface between coal layer and air provided further understanding of the effect the ring material has on the spontaneous ignition process. The highly conductive stainless steel ring temperature equals the hot plate, within the first 200 seconds of the simulation, as shown in Fig. 14(b). The dust closer to the ring is then subjected to heat fluxes from the ring as well as from the hot plate. Whereas, the high thermal inertia of the insulating material allowed almost simultaneous temperature rise with the dust during the initial 600 seconds of the simulation, as shown in Fig. 14(a). After 600 seconds, the heat generation along the central axis became dominant and led to generation of hot spot along the central axis, as shown in Fig. 13(a).

2.6 CONCLUSION

The standard test method aimed at determination of minimum hot surface temperature at which a dust layer of certain thickness would go under spontaneous ignition is considered. The method to extract kinetic parameters from experimental results is reviewed. A problem of multi-dimensional heat transfer, where one-dimensional heat transfer is desired, caused by the use of metal ring to contain dust on hot plate is identified. A suitable solution of replacing metal ring with an insulating material is suggested and proved to work satisfactorily.

An integral solution method is developed to predict the ignition location for a given dust layer thickness. The solution procedure will be again used in the two dimensional wedge cases in next chapter. The mathematical model is seen to accurately predict the minimum plate temperature required for causing ignition for different dust layer thickness cases. Further a validated computational model is presented to simulate spontaneous ignition in one dimensional combustible dust layer configurations.

Chapter 3. SPONTANEOUS IGNITION OF COMBUSTIBLE DUSTS DEPOSITS (2-D GEOMETRY)

3.1 INTRODUCTION

In most industrial accidents, dust layer ignition usually initiates in corners and wedges where the dust is trapped. In addition, dust accumulation on a level surface can be easily cleaned, but the dust deposits in corners and grooves are typically left behind. The current test standards cannot address these issues where dusts accumulate in complex geometries. This is because modeling ignition for other geometries found in industrial environments is not possible solely from the measured ignition temperature at a specific dust layer thickness. Studies discussed in Section 1.3 have shown that the ignition temperature is highly geometry dependent, and is therefore not a quantifiable parameter to analyze the risk associated with all dust layers. The purpose of this study is to analyze the ignition behavior of a dust deposit trapped in a wedge shaped configuration having hot surfaces.

This problem is addressed using three methodologies: lab-scale experimental study, mathematical modeling and numerical simulations. The experimental setup consists of two hot surfaces kept at desired inclination between which a dust layer is trapped. Temperature measurements at various locations provided useful information about the heat generation and heat flux inside the dust during the process of spontaneous ignition. The mathematical model follows a simple approach to determine the ignition behavior in any wedge-shaped multi-dimensional dust deposit with convective boundary conditions. The numerical simulations run are comprehensive as they include conjugate heat transfer processes. This validated numerical model has been used to predict the ignition behavior in complex geometries and understand the heat loss phenomena at dust layer – air interface. All three aspects of this research are discussed in the following sections.

3.2 EXPERIMENTAL STUDY

In order to represent real life scenarios, it is first necessary to define them. Two such scenarios are dust deposits between vents, room corners and so on, which represent two surfaces oriented in right-angles, and gaps between cracks, motor fins and so on which represent surfaces oriented in acute angles. Therefore, experiments with two hot plates configured to form wedges of two angles (90º and 60º) have been carried out and the two-dimensional heat transfer effects are envisaged. The two-dimensional nature of the system was necessary to maintain simplicity of the analysis and repeatability of the experiments.

3.2.1 EXPERIMENTAL TEST SET-UP

The experimental setup comprised of two stainless steel plates that were used as hot surfaces attached to each other to form a wedge like geometry as shown in Fig. 15. The angle of the wedge was adjusted by using a stainless steel base-plate (shaded light gray) which allowed the plates to be adjusted to an acute angle of 60º and a right angle of 90º. Each plate was attached to an electrically heated plate, ROPH-144, Omega engineering, with thermally conductive cement (Omegabond 700), to provide uniform temperature distribution all along the plate. The perimeter wall was also wrapped by a 5 mm thick insulating material (ceramic paper 390 manufactured by Cotronic Co.) to minimize the heat loss to the environment. The temperature of the plates was measured by a Type-K surface temperature thermocouple, CO1-K, Omega engineering, kept 35 mm inside from the plate edge. Furthermore, experiments with a flat hot plate, which follows the standard test case and also equivalent to a 180º wedge, were conducted using a setup similar to that reported by Park *et al.* [16]. This setup is comprised of a circular disc shaped hot plate (203 mm diameter) and uses stainless steel rings of different thicknesses to contain the coal dust layer.

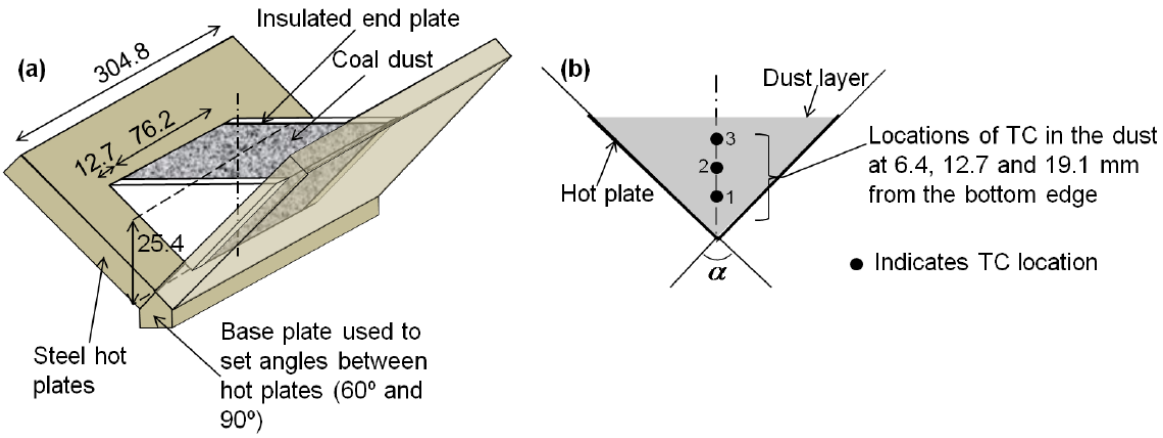

Figure 15 (a) Wedge shaped hot plate experimental setup (isometric view). (b) Cross-section of wedge along the plane of symmetry. All dimensions are in mm.

A temperature controller, CN 8592, Omega engineering, and solid state relay, SSRL240DC25, Omega engineering, were used to control as well as maintain the hot surface temperature at a steady constant value throughout any given test. Temperatures on the stainless steel wedge, set at 250^{o}C, showed very good uniformity. Temperatures were measured at 12 uniformly spaced locations on the hot surface, 6 points each and on two lines normal to each other. Except one point at which temperature was 249^{o}C, all other thermocouples indicated 250 ^{o}C. The thermocouples for both surface and dust layer temperature have an error of ±1.1 ^{o}C and the temperature controller, CN8592, has an error range of ±1 ^{o}C prescribed by the manufacturer. NI data acquisition unit has shown ±1 ^{o}C temperature fluctuations throughout the tests. The inherent uncertainty of the test apparatus is within an acceptable range, since tests were conducted with either 5 ^{o}C or 10^{o}C resolution with respect to the layer ignition temperature. All tests were performed in a fume hood where the ambient temperature was maintained at 22^{o}C.

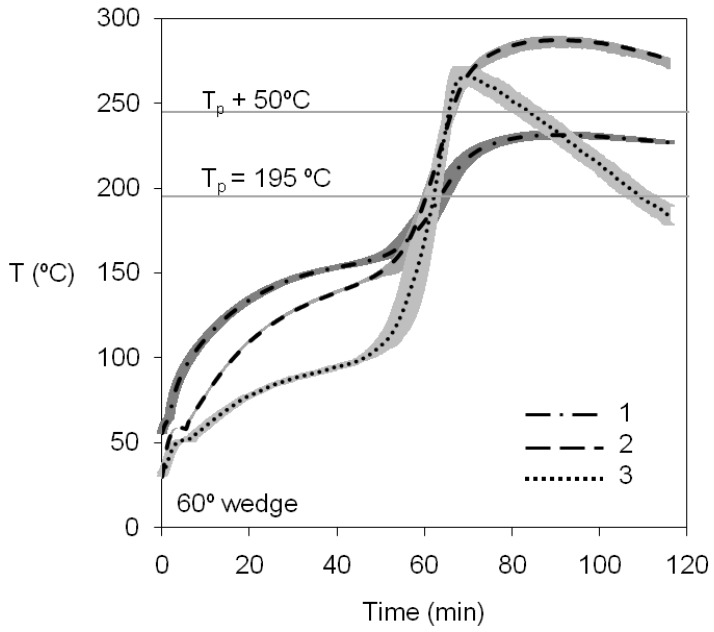

Figure16 Average temperature variation with time, obtained from four tests in 90º wedge with the plate temperature at 195 ºC; grey bands indicate the deviations in the measured values from different tests. Horizontal grey lines indicate hot plates temperature (T_p) and the temperature 50 ºC more than T_p.

All tests were performed using Pittsburgh seam coal dust provided by CONSOL energy laboratory and reported to have an average particle size of 32 µm. The measured average bulk density was 580kg/m^3. Other physical and chemical properties of the dust are reported in Park *et al.* [16]. The experimental procedure comprised of turning the hot plate on and using the temperature controller to set the desired temperature of the wedge. This typically took about 45 to 60 minutes. Once the temperature of the wedge shaped hot plate was stabilized, three type-K thermocouples with bead size of 0.38 mm were mounted along the centerline of the wedge at 6.4, 12.7 and 19.1 mm from the base (shown in Fig. 15 and labeled as 1, 2, and 3). These thermocouples allowed monitoring of the temperature of the coal dust in the wedge as a function of time. The wedge was then gently filled with a pre-measured amount of coal dust and the surface of the layer was evenly leveled with a flat iron ruler. In all the experiments, the wedge is packed with a coal dust layer 25.4 mm thick (measured from the apex of the wedge) and 73.5 mm wide (in the direction perpendicular to the paper). The ends of the dust layer were blocked by 12.7 mm (½")

thick insulations (Kaowool®) triangular piece as shown in Fig.15. Tests were run until either the layer temperature reached a steady state for no less than 60 minutes or clear thermal runaway was observed. If thermal runaway did not occur at the pre-set plate temperature (T_p), it was increased by 10^{o}C until thermal runaway was observed. Once ignition was observed, the resolution between ignition and no ignition cases was fine tuned to within 5ºC. Fresh coal samples were used for each test. To ensure repeatability in the temperatures recorded by the 3 thermocouples, each ignition experiment was then repeated at least four times. Figure 16 shows average temperatures recorded by three thermocouples for 90º wedge with the plate temperature set at 195ºC. Deviations in transient temperature variations obtained from four different tests are represented by gray bands. It can be noted that the tests are consistent and produce temperature variations within ±7 ºC. Test data from four tests for both wedge angles is shown in Appendix D. Table 3 reports the average ignition times. Since the onset of ignition is not instantaneous, the ignition time is calculated by taking the average of the time instants where the temporal variation of temperature changes its slope before and after the rapid rise as shown in Fig. 17.

Table 3: Ignition time data in minutes

T_p	60º Wedge	T_p	90º Wedge	
	TC3		TC2	TC3
190 ºC	59	195 ºC	64	62
210 ºC	38	215 ºC	46	43
235 ºC	29	240 ºC	34	32

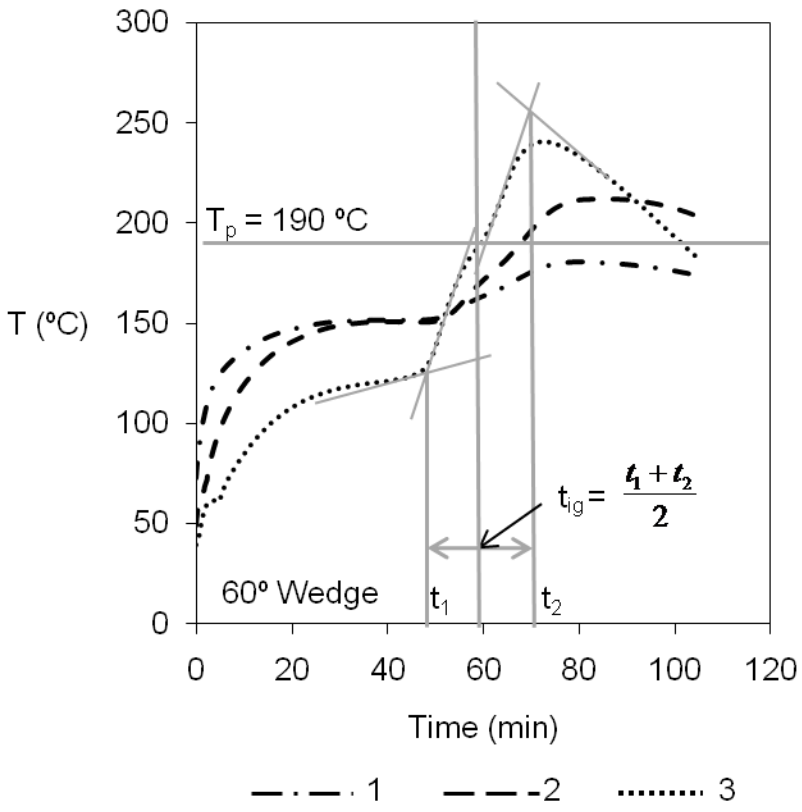

Figure17 Ignition time determined by taking the average of the time instants where the transient temperature curve changes its slope before and after a rapid rise.

3.2.2 RESULTS AND DISCUSSION

The temperatures recorded by the three thermocouples for the wedge shaped hot plates are shown in Fig. 18. Figure 18 (a) shows the no-ignition scenario for 60º wedge, where the plates are maintained at 185 ºC. When the temperature of the plates is increased by 5ºC to 190 ºC, the coal in the 60º wedge ignites and the *first ignition* is recorded by the top thermocouple. Only the top region ignites for this case, indicated by the temperature profile of the top thermocouple, which records a temperature 50 ºC more than the hot plate temperature of 190 ºC (Fig. 18c). For the 90º wedge, ignition occurs at 195 ºC, which is 5 ºC higher than the 60º case (Fig. 18d). This is because the rate of heat transfer from the hot plate to the symmetry plane is lower in the 90º wedge than in the 60º wedge. Unlike the acute-angle case, both top and middle

thermocouples record rapid temperature rise indicating that both regions ignite almost simultaneously (around 60 minutes), as shown by the enlarged inset in Fig. 18d. The slopes of the temperature profiles before the onset of ignition are also different for the two wedges. For the 60º wedge, the temperature plateaus before the onset of ignition (Fig. 18c), while for the right-angled wedge, the temperatures continuously and gradually increase before the onset of ignition (Fig. 18d). The difference in ignition behavior between the two geometries and their implication to hazardous dust build up in industrial settings is discussed in the following sections.

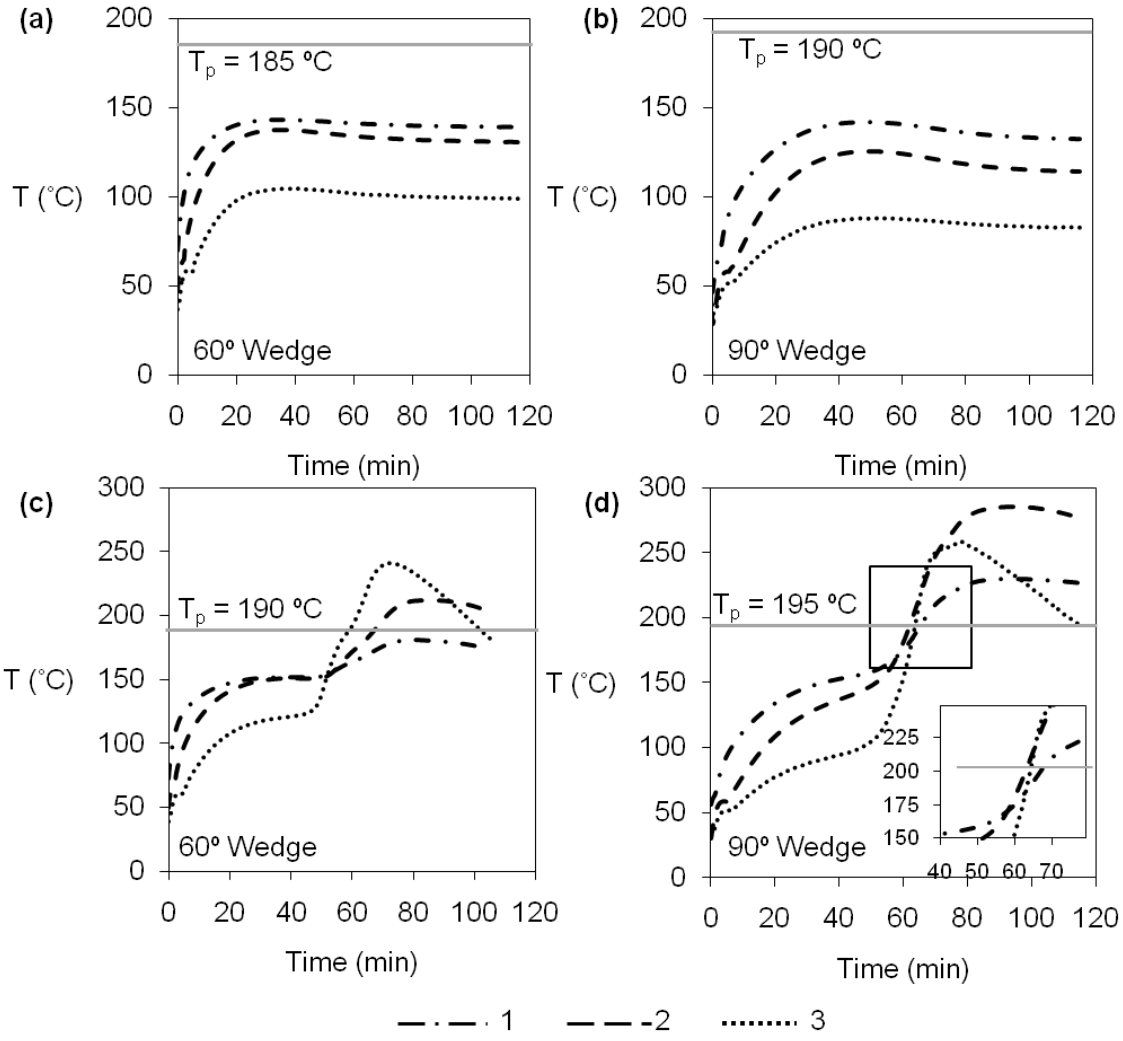

Figure18 Temporal variation of temperature recorded at three locations; bottom (6.4 mm from the wedge apex), middle (12.7 mm from the apex) and top (19.1 mm from the apex) for (a, c) 60º wedge and (b, d) 90º wedge; temperature of the hot plates 185 ºC (a), 190 ºC (b, c) and 195 ºC (d).

Identification of Controlling Processes

There are three processes which control the ignition behavior in a wedge, namely, the heat transfer from the hot plate to the coal dust, the subsequent chemical heat release, and the heat transfer between different regions within the coal dust. Eq. (33) shows the general energy balance for spontaneous ignition [22], which can be applied to the wedge geometry in a cylindrical coordinate system (*r*-*ω*) depicted in Fig. 19. The second term in the RHS of Eq. (34) represents the heat flux from the hot-plate to any point within the coal dust layer acting along a normal *n* perpendicular to the plate (shown by 1′-1, 2′-2, and 3′-3 in Fig. 19). The heat flux from one region to another within the coal layer can be investigated in the radial direction (first term in RHS of Eq. (34)).

$$\nabla.\vec{q} + \rho QA\exp\left(\frac{-E}{R_u T}\right) = \rho C_p \frac{\partial T}{\partial t}, \tag{33}$$

where,

$$\vec{q} = k\frac{\partial T}{\partial r}\hat{e}_r + k\frac{\partial T}{r\partial \omega}\hat{e}_\omega . \tag{34}$$

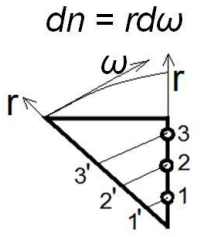

Figure 19 Cylindrical (r-*ω*) coordinate system for a half-wedge configuration; n is the dimensional angular distance.

In Eq. (33) and (34), *QA* and *E* are the pre-exponential factor and the activation energy, *k*, ρ, and C_p, represent the thermal conductivity, density and specific heat of the coal dust, respectively, and $\hat{e}_r$ and $\hat{e}_\omega$

represent the unit vectors in r and ω directions, respectively. The heat flux in ω -direction can be written as,

$$k\frac{\partial T}{r\partial \omega} = k\frac{\partial T}{\partial n} \tag{35}$$

The second term in Eq. (33) represents the chemical heat released per unit volume. Consistent with previous studies [11, 16, 22, 34], it is assumed that reactant consumption is negligible and the order of the reaction is zero. During all the tests, the coal dust is packed in the wedge using a mass equal to the volume of packing multiplied by its bulk density, so that the packed density and the bulk density are almost the same. As a result, the permeability in the packed dust layer is expected to be very small and it can be assumed that oxygen transport into the coal dust is negligible until the onset of ignition. It is possible that a post-ignition scenario that leads to a smoldering process, oxygen diffusion would come in to play [46]. However, this part of the problem is not analyzed. In addition, experiments performed by Bowes and Thoams [47] showed the influence of reduced oxygen concentration in the surrounding atmosphere had little effect on the spontaneous ignition phenomenon.

The three processes controlling the ignition behavior are studied using a scaling type analysis using experimentally measured temperatures fitted into algebraic equations formed by the three terms in the left hand side of the governing Eq. (33). The temporal variations thus obtained are then used to qualitatively analyze the strengths of the three processes at any time instant. The algebraic equations for the three terms are given as follows:

(a) Heat flux from the hot plate to a thermocouple location is calculated based on the difference in temperature between the two divided by the horizontal distance between them (n-n′). This is given as follows:

$$k\frac{\partial T}{\partial n} = k\frac{T_p - T_n}{n - n'}\left(W/m^2\right);\ n = 1, 2, 3\ldots \tag{36}$$

(b) The heat transfer per unit area, between the lowermost to middle, and middle to top regions, are calculated based on the second term in Eq. (34) as follows:

$$\dot{q}''_{[n-(n+1)]} = k\frac{\partial T}{\partial r} = k\frac{T_n - T_{n+1}}{r_n - r_{n+1}}\left(\frac{W}{m^2}\right);\ n = 1,\ 2,\ 3 \tag{37}$$

where a positive value of $\dot{q}''_{[n-(n+1)]}$ denotes heat transfer in the upward direction.

(c) The third term in Eq.(33) represents the volumetric source term given by:

$$\dot{q}'''_i = \rho QA\exp\left(\frac{-E}{R_u T_i(t)}\right)\left(\frac{W}{m^3}\right);\ i = 1,\ 2,\ 3 \tag{38}$$

The heat generation is calculated in W/m^3 based on the temperature measured by the thermocouple at any time instant. To summarize, Eq. (36) and (37) represent the heat flux from the hot plate to a point and the heat dissipation between adjacent layers respectively. The heat release is determined per unit volume and is given by Eq. (38).

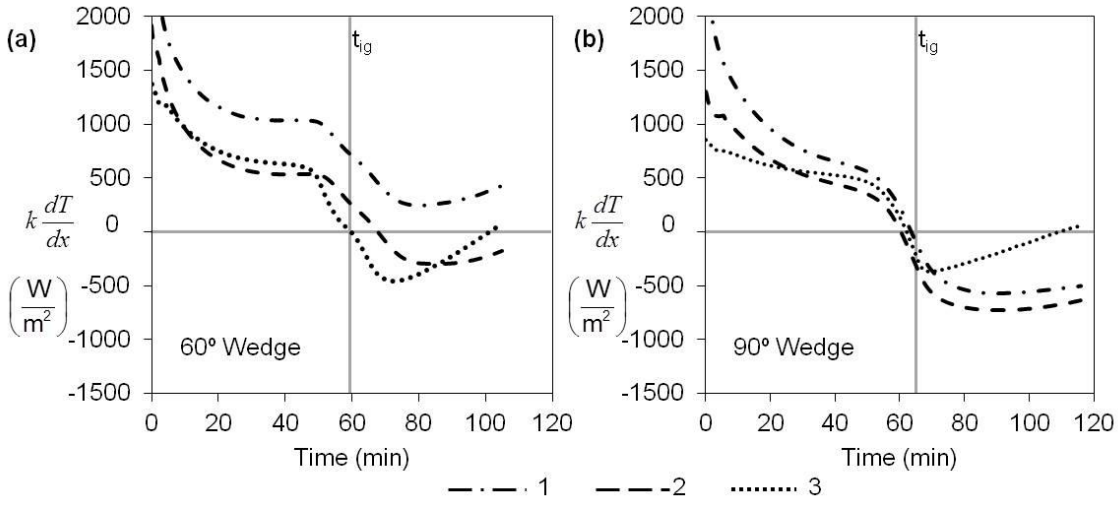

Figure 20 Temporal variations of the temperature gradients normal to the hot plate in the direction of a normal vector connecting the hot plate and a thermocouple for (a) 60º wedge (hot plates maintained at 190˚C) and (b) 90º wedge (hot plates maintained at 195ºC), for all the three thermocouples.

Relative Strengths of the Controlling Processes

The heat fluxes from the hot plate to all the thermocouples, evaluated by Eq. (36), are shown in Fig. 20, for 60º wedge (Fig. 20a) and 90º wedge (Fig. 20b). The vertical gray lines shown in Fig. 20 represent the onset of ignition or the ignition time (reported in Table 3). It is observed that just prior to ignition the heat flux received by the lowermost thermocouple is the highest irrespective of the wedge angle, due to its closeness to the hot plate. Correspondingly this thermocouple records the maximum temperature for both the wedges prior to ignition (Fig. 18). However, the lowermost thermocouple does not record ignition, which can be explained by analyzing the rate of heat release and heat dissipation.

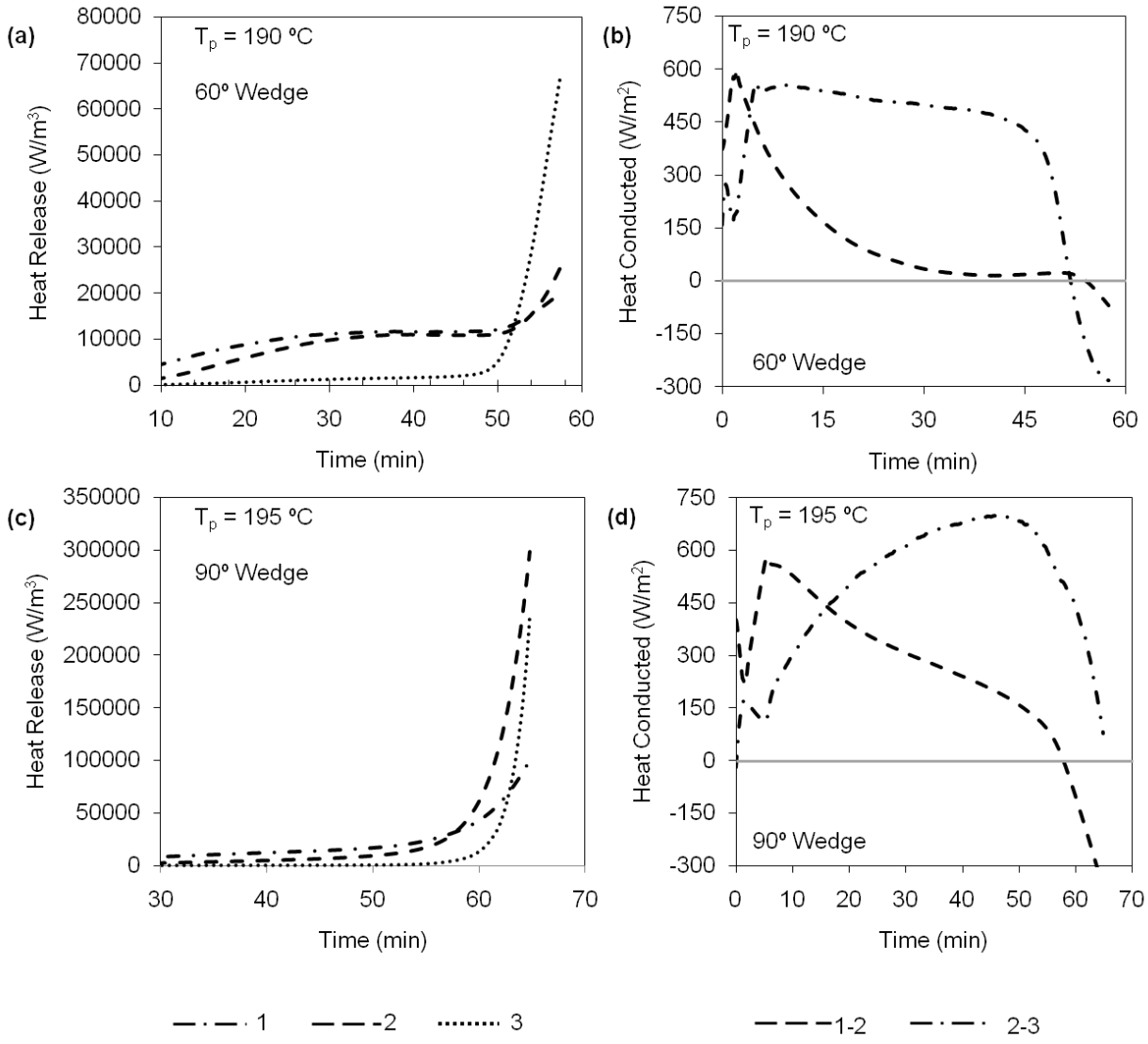

Figure21 Temporal variations of heat release (a, c) in the volume surrounding each thermocouple and heat conducted between regions 1 - 2 and between 2 – 3 (b, d), for 60º (a, b) and 90º (c, d) wedges, until ignition.

Figure 21 shows temporal variation of heat release at any thermocouple position and the heat fluxes between points 1-2 and 2-3 calculated using the appropriate temperatures recorded by the thermocouples 1, 2, and 3. Only the time before ignition, which is important for the analysis, is considered. The trends of variations of these quantities would give an idea of their qualitative relative strengths at each point and at each time instant. This is analyzed for each wedge angle.

60º Wedge

In spite of recording the highest temperature before ignition (around 59 min), Fig. 21a shows that the heat generated in the lowermost layer is the lowest, mainly due to the continuous heat dissipation from this layer to the middle layer as shown in Fig. 21b. Both the top and middle layers receive similar amounts of heat from the hot plate (Fig. 20a). However, the reason the top region always ignites first is due to the continuous positive heat transfer from the middle to top as shown by Fig. 21b (2-3). As a result, the temperature (Fig. 18c) and thus, the heat generation (Fig. 21a) in the top region, starts to increase around 48 minutes and eventually causes the top thermocouple to reach the ignition criterion.

90º Wedge

For the 90º wedge, the overall heat release rates in all the regions are significantly higher compared to the 60° wedge (Fig. 21 a and c) even though the hot plate temperatures are not significantly different between the two wedges. Both middle and top regions ignite (Fig. 18d) almost simultaneously (around 64 and 62 minutes, respectively). The heat release recorded by thermocouple 2 is also the maximum (Fig. 21c). The continuous positive heat transfer from the middle to top region (Fig. 21d) does not affect the heat release scenario in the middle region, rather it helps the top region to record sufficient heat release (Fig. 21c) to cause ignition. Therefore, due to monotonically increasing heat release in the middle region, that region reaches the ignition criterion and also favors the top region to reach the ignition criterion by providing good amount of heat flux.

The ignition behavior observed in the two wedge angle cases provides significant insight to hazardous conditions that can develop due to dust deposits trapped in corners. It is observed that in acute angle wedges the top layer ignites and as the angle increases, the ignition zone moves to inner layers. The results show that dust build up in acute angled wedges pose increased level of hazardous conditions since the high-temperature top layer can ignite flammable material in its vicinity.

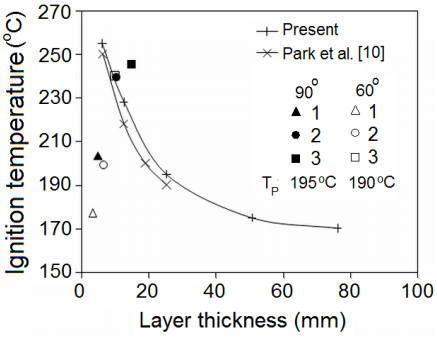

Figure22 Present experimental data of flat plate ignition studies (+) along with the data from a similar study by Park et al. (x), and the temperature of thermocouples 1, 2 and 3 recorded at the time of ignition for both 60º and 90º wedges.

Safety in Industrial Environments Exposed to Dust Layers

The ASTM standard E 2021 and the European standard EN 50281-2-1(1999) are current test methodologies used in practice to estimate the minimum ignition temperature of fugitive dust layers. The minimum ignition temperature obtained from these tests represents the minimum temperature of a flat hot plate at which a dust layer ignites. These tests are phenomenally one-dimensional in nature. The mathematical model of this test has an explicit solution first developed by Thomas and Bowes [22]. Since there is no influence of geometry, for the flat plate case, all three regions (lowermost, middle and upper) of a dust layer reach ignition conditions in this case. This has been confirmed with experimental data reported by Park et al. [16] for the same type of coal dust (Pittsburg Seam Coal). Experiments using the standard test apparatus (flat plate equivalent to a 180º wedge) were also performed and showed that the minimum ignition temperature decreases nonlinearly with layer thickness as shown in Fig. 22, consistent with the theoretical work by Thomas and Bowes [22] as well as experimental data of Park et al. [16]. The curve in Fig. 22 delineates the no-ignition zone against the regions where a combination of plate temperature and layer thickness can sustain ignition.

At the onset of ignition, the net dissipative heat flux and volumetric heat generation can be coupled to form an effective length scale, which represents an effective thermal diffusion length scale, such that heat dissipation is balanced by the heat generation. This length scale can be used to determine

the feasibility of ignition and for the standard test with flat dust layer heated at one end, it is equal to the thickness of the layer itself. The heat transfer processes in the case of a wedge is two dimensional in nature and hence difficult to resolve using a simple analytical model as in the case of a flat plate. However, an approximate thermal diffusion length scale similar to that in the flat plate case can be determined based on the distance of the thermocouple location from the hot plate, as shown in Fig. 19. That is, the distance between any thermocouple and the hot plate, as indicated in Fig. 19, will be equivalent to a coal layer thickness on a flat horizontal hot plate. Therefore corresponding to that thickness, a suitable ignition temperature, as given by the curve in Fig. 22, would be needed to initiate ignition at that layer. Several other combinations such as the ratio of volume to surface area of spheres, cylinders or trapezoidal shapes in the regions surrounding each thermocouple would also provide similar qualitative results.

Table 4. Temperatures of the thermocouples at the time of ignition for both wedges

Thermocouple	Temperature ºC	
	60º wedge	90º wedge
1	177	203
2	199	240
3	240	245

Also shown in Fig. 22 is the temperatures recorded by all the three thermocouples at the time of ignition for both the wedges (reported in Table 4). It should be noted that the lowermost and middle thermocouples in the 60º wedge and the lowermost thermocouple in the 90º wedge fall in the no-ignition region when plotted against the effective length scale discussed above. The top thermocouple in the 60º wedge, and the middle and the top thermocouples in the 90º wedge reach the ignition region because of their increased effective lengths from the hot plate. The effective length scale can be determined by only using the geometric factors for different configurations, since this is based on the distance of a particular

location from the hot plate. Since standard flat hot plate experimental data is available for most hazardous dusts, the approach presented in Fig. 22 can be useful in determining the ignition behavior of dust collected in several geometrical configurations.

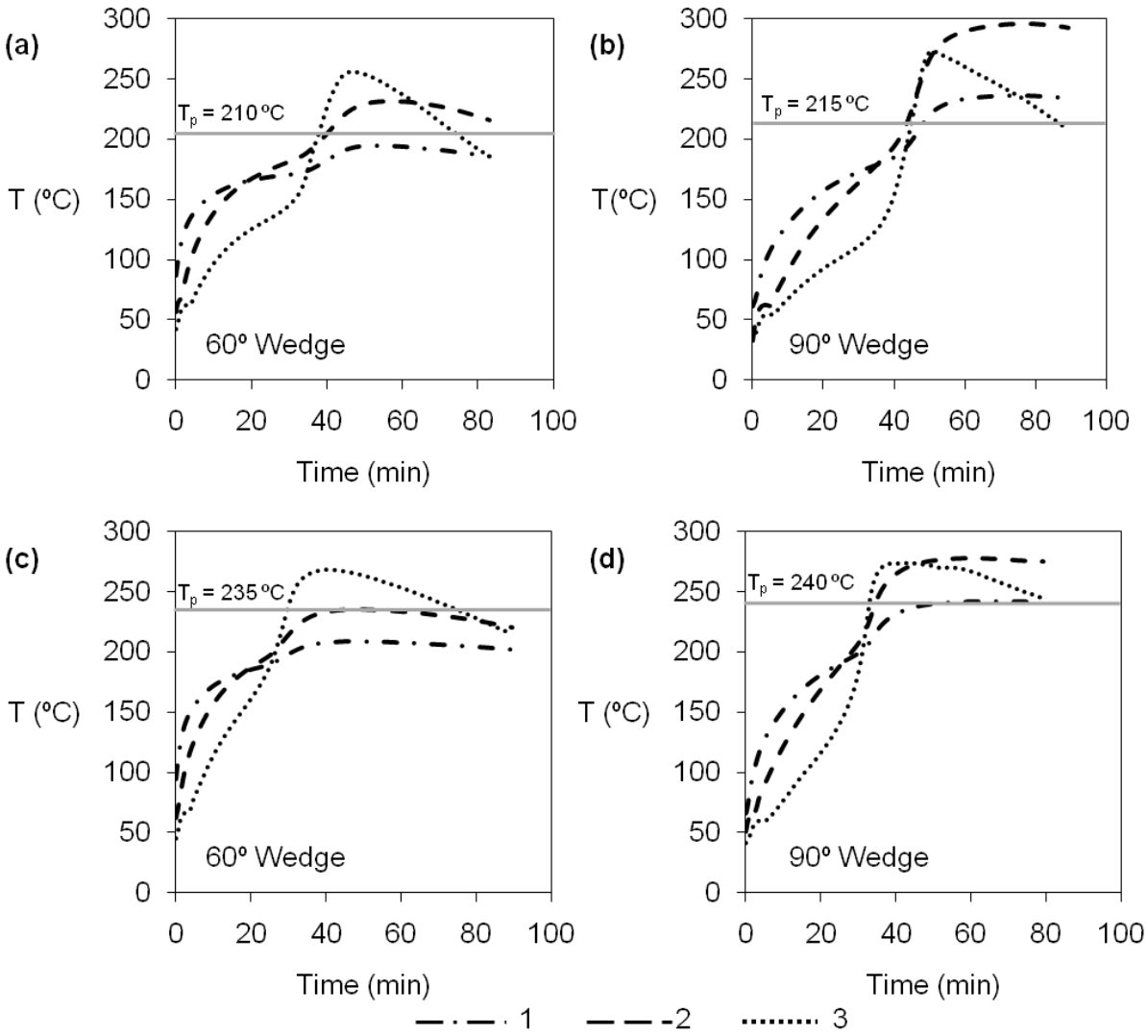

Figure23 Time histories of temperatures recorded by three thermocouples inside the dust layer when the hot plates are maintained at 20 ºC above the minimum ignition temperature (a, b) and at 45 ºC above the minimum ignition temperature (c, d) for 60 º wedge (a, c) and 90º wedge (b, d).

Ignition at Elevated Plate Temperatures

The influence of the controlling processes of heat transfer and energy generation on ignition characteristics of coal dust in a 60º and 90º wedges are further analyzed by increasing the temperature of the hot plates above the minimum ignition temperature (hot plates are maintained at 20 ºC and 45 ºC above the corresponding minimum ignition temperatures). The hot plate temperatures for 60º wedge are 210 ºC (Fig. 23a) and 235 ºC (Fig. 23c) and for the 90º wedge, the temperatures are 215 ºC (Fig. 23b) and 240 ºC (Fig. 23d). As the hot plate temperature is increased, the onset of ignition is seen to occur at an earlier time instant (Table 3), due to the increased availability of the amount of heat. Figure 23 shows that in both wedge geometries, temperature recorded by the top thermocouple decreases after the rapid increase. It is observed that this decrease in the temperature coincides with formation of cracks on the top surface, which facilitates the diffusion of cold ambient air into the top region. The cracks seem to influence the top region alone and the temperatures recorded by the middle and bottom do not decrease, instead reach steady values as shown in Fig. 23.

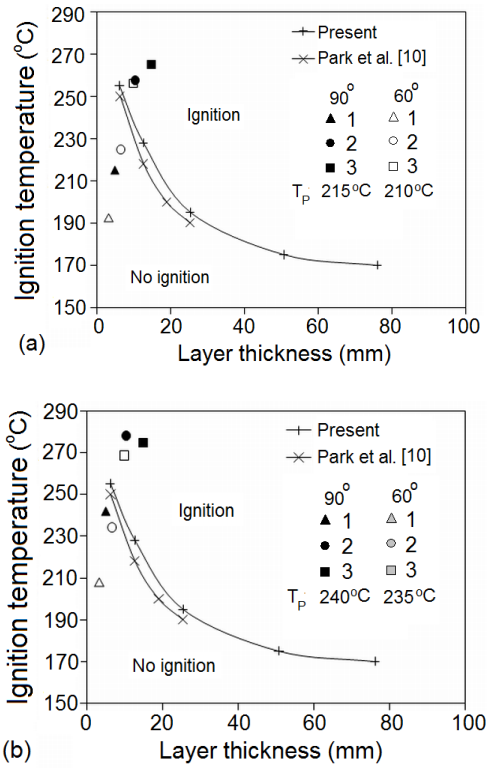

Figure 24 Present experimental data of flat plate ignition studies (+) along with the data from a similar study by Park et al. (x), and the temperature of thermocouples 1, 2 and 3 recorded at the time of ignition for both 60º and 90º wedges when the hot plate is at higher temperature than the corresponding minimum ignition temperature.

Figure 24 shows the temperatures recorded by the thermocouples in both the wedges at the time of ignition, along with the flat plate ignition temperature data. The minimum ignition temperature vs. layer thickness curve delineates the data for the cases with hot plate temperature higher than the corresponding minimum ignition temperatures of both wedges. Clearly, top and middle thermocouples in the 90º wedge record ignition at the hot plate temperature of 215ºC (Fig. 24a) and only the top thermocouple records ignition for the 60º wedge at the hot plate temperature of 210ºC. The same trend is observed in Fig. 24b, where the corresponding hot plate temperatures are 240ºC and 235ºC, respectively, for 90º and 60º wedges.

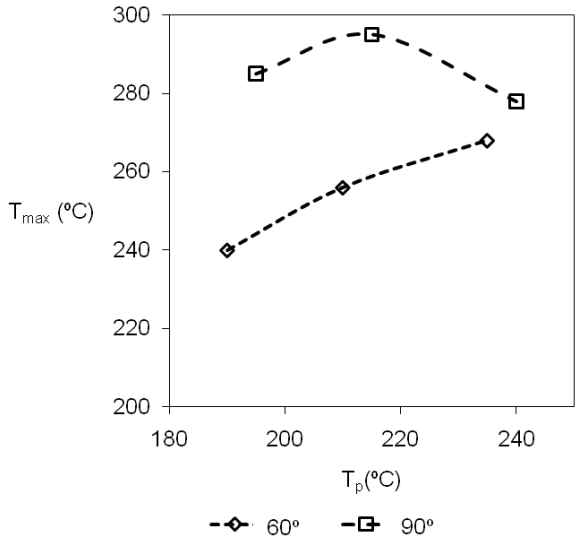

Figure 25 Maximum temperature reached inside the domain as a function of hot plate/base temperatures for 60º and 90º wedges.

The maximum temperatures for three different plate temperatures conducted in this study are plotted in Fig. 25. The peak temperatures recorded in the 60º wedge are always lower than the 90º wedge. For the 60º wedge the peak temperature increases as plate temperature is increased. This is mainly due to an enhancement in heat generation with an increase in the hot plate temperature. For the 90º wedge, when the hot plate temperature is 45 ºC more than the minimum ignition temperature, the maximum temperature recorded is only around 280 ºC, that is, 10 ºC less than the maximum temperature recorded in the case where the base temperature is 20 ºC above the minimum ignition temperature. The highest hot plate temperature developed large quantities of smoke and opened the coal dust surface at ignition leading to cooler temperatures.

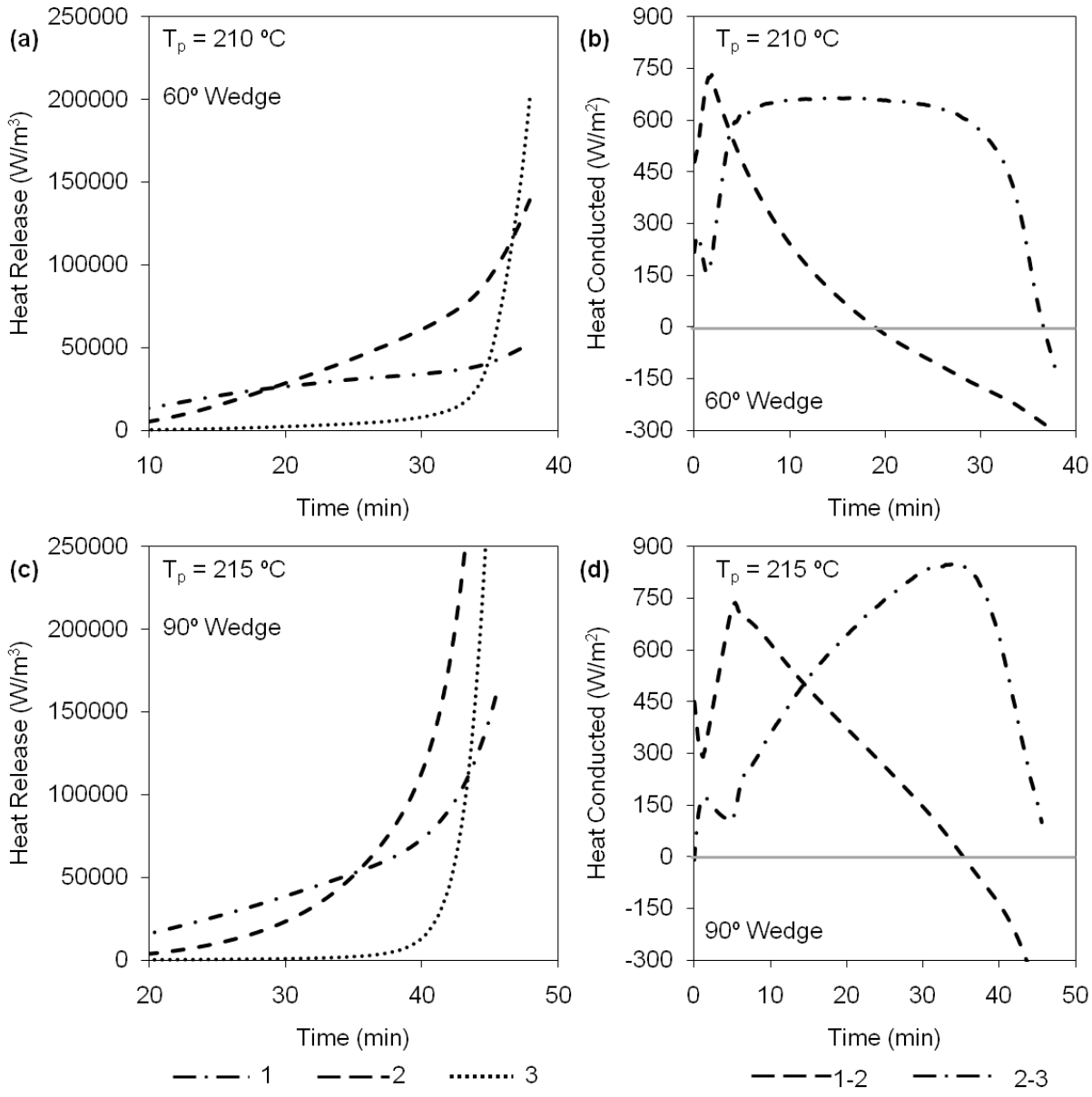

Figure26 Temporal variation of heat release (a, c) and heat conducted (b, d), until ignition, in 60º (a, b) and 90º (c, d) wedges, when hot plates are maintained at 20 ºC more than minimum ignition temperature.

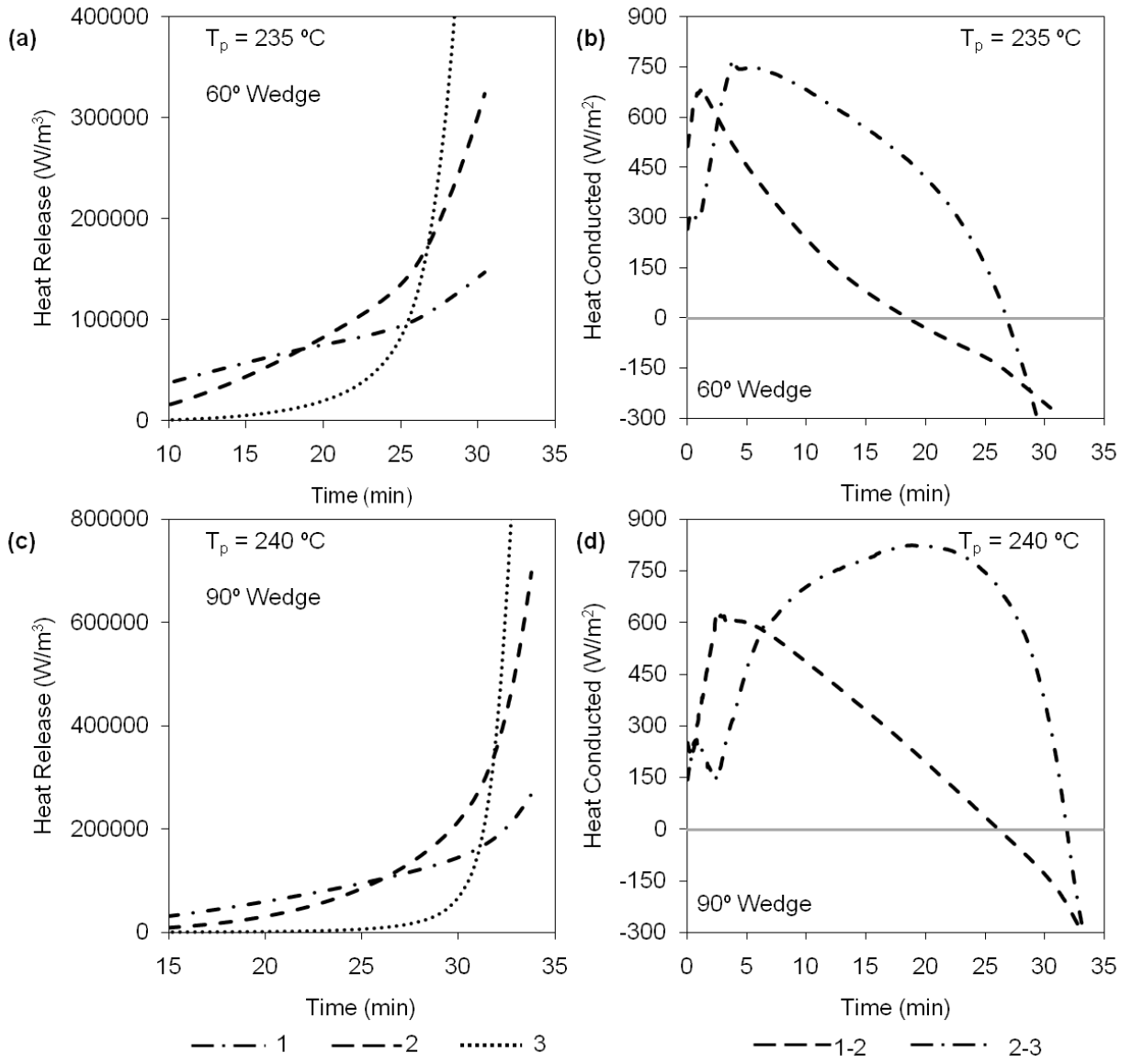

Figure 27 Temporal variation of heat release (a, c) and heat conducted (b, d), until ignition, in 60º (a, b) and 90º (c, d) wedges, when hot plates are maintained at 45 ºC more than minimum ignition temperature.

Similar to Fig. 21, variations of heat released in a given region and heat conducted from one region to another is shown in Figs. 26 and 27, for cases where the plate temperatures are maintained at 20°C and 45°C, above the corresponding minimum ignition temperatures, respectively. The trends in the variations of these quantities for 60º wedge (Fig. 26 a, b) and 90º wedge (Fig. 26 c, d) are similar to their respective cases in Fig. 21. However, the amount of heat release has significantly increased in both

wedges at higher plate temperature although the heat dissipation has not altered significantly. This explains the increase in the maximum temperature in the domain for both wedges. At still higher plate temperatures (45 ºC above minimum ignition plate temperature) the trends in the variations of these quantities for 60º wedge (Fig. 27 a, b) and 90º wedge (Fig. 27 c, d) are different than the earlier cases presented in Fig. 21 and 26, especially for 90º wedge case. The heat release in the top region increases significantly equalling that obtained in the middle region (Fig. 27c). This is due to the increased rate of heat dissipation from middle to top region (Fig. 27d). Therefore, at elevated temperatures heat generated is efficiently dissipated between regions resulting in a reduction in the maximum temperature in the case of the 90º wedge.

3.3 NUMERICAL ANALYSIS

3.3.1 INTEGRAL METHOD

3.3.1.1 Introduction

The phenomenon of spontaneous ignition is dependent on the physical and chemical properties, the condition of the exposed dust surface, the geometry and the temperature of hot surfaces holding the dust. The critical conditions such as minimum temperature at which ignition occurs and the ignition location change with the dust holding geometry [31, 42]. From the experimental results reported in section 3.2.2, the onset of ignition was reported to occur near the exposed dust surface in case of the 60° wedge and close to the middle region in case of the 90° wedge. The flat plate case (regarded as 180° wedge) exhibited ignition in its lower region, closer to the hot surface. These observations show that the ignition location moves downwards as the wedge angle increases. As explained in Section 3.2, the scaling-type analysis espoused the reasons for this behavior using an energy balance around the thermocouple locations that were placed at three different locations in the 60º and 90º wedges. The objective of the current work is to develop a mathematical model which can predict this behavior. Further a parametric study allowing all wedge angles (10º to 150º) is also presented.

3.3.1.2 Mathematical Model

The mathematical model is based on using a polynomial expression to represent the temperature profile originating from the classical work by von Kármán [32]. The schematic of the coordinate systems along with the boundary conditions and typical temperature profiles are shown in Fig. 28. The order of the polynomials representing the approximate temperature profile is chosen based on a prior study reported by Hardee *et al.* [31, 33] where a solution for ignition of a solid shaped as a slab [31] and cone [33] exposed to uniform temperature conditions on all sides was obtained. The boundary conditions of the current problem (shown in Fig. 28(a)) are significantly different which cause additional complications

which are resolved later. For a plate temperature less than the critical temperature, the temperature in the dust along the central line is less than the plate temperature as shown in Fig. 28(b), by the dotted line (no ignition case). For a plate at or slightly above critical temperature, the temperature of the dust increases from the plate temperature, reaches a maximum at some location along the central line and then decreases towards the surface (Fig. 28(b), ignition). For wedge cases, the wedge angle influences this ignition location as indicated in Fig. 28(b).

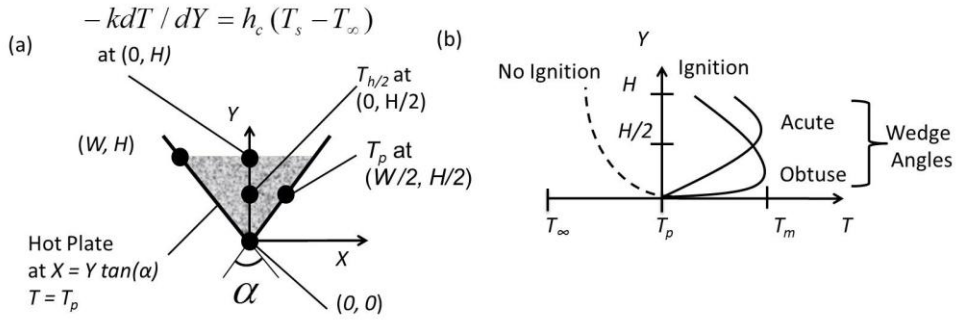

Figure 28 (a) Two-dimensional coordinate system and boundary conditions for wedge geometry and (b) representative temperature profiles along the y-axis.

The heat conduction equation with non-linear source term in two-dimensional Cartesian coordinate system is expressed as,

$$k\left(\frac{d^2T}{dX^2}+\frac{d^2T}{dY^2}\right)+\rho QAe^{-E/RT}=0 \qquad (39)$$

with boundary conditions (Fig. 28a), $X = Y\frac{W}{H}$, $T = T_p$ and at $X = 0, \frac{dT}{dX} = 0.$

Ignition occurs at some point 'm' along the *Y*-axis, where maximum temperature occurs; therefore, at $X = 0,\ Y = H_m,\ \frac{dT}{dY} = 0$, and on the exposed surface, convective cooling boundary condition is applied as, at $\mathrm{X} = 0, Y = H, -k\frac{dT}{dY} = h_c\left(T_s - T_\infty\right)$.

Non-dimensionalizing the energy equation using,

$$\theta = \frac{RT}{E},\ \ h_c^* = \frac{h_c}{\left(\frac{\rho QAkR}{E}\right)^{1/2}}$$

$$x = \left(\frac{\rho QAR}{kE}\right)^{1/2} X \text{ and } w_o = \left(\frac{\rho QAR}{kE}\right)^{1/2} W,$$

$$y = \left(\frac{\rho QAR}{kE}\right)^{1/2} Y \text{ and } h = \left(\frac{\rho QAR}{kE}\right)^{1/2} H,$$

gives,

$$\frac{d^2\theta}{dx^2} + \frac{d^2\theta}{dy^2} = -e^{1/\theta}. \tag{40}$$

Similarly, the non-dimensional boundary conditions are listed as,

$$at\ x = y\frac{w_o}{h}, \theta = \theta_p, \tag{41}$$

and on the surface, convective cooling boundary condition is applied as,

$$at\ x = 0, y = h, \frac{d\theta}{dy} = h_c^*\left(\theta_s - \theta_\infty\right) \tag{42}$$

Another boundary condition is obtained by considering temperature $T_{h/2}$ to exist at half wedge height (as shown in Fig. 28b) as,

$$x = 0\,,\, y = h/2,\, \theta = \theta_{h/2} \tag{43}$$

A 2D temperature profile is assumed with x and y as independent variables given as,

$$\begin{aligned}\theta - \theta_s\left(\frac{y}{h}\right) - \theta_p\left(1 - \frac{y}{h}\right) = {} & A_w(x^2\frac{h^2}{w_o^2} - y^2)(y^2 - h^2)\frac{w_o^2}{h^2} + \\ & B_w(x^2\frac{h^2}{w_o^2} - y^2)(y^3 - h^3)\frac{w_o^2}{h^2} + \\ & C_w(x^3\frac{h^3}{w_o^3} - y^3)(y^2 - h^2)\frac{w_o^3}{h^3}\end{aligned} \tag{44}$$

The right hand side of Eq. (44) is a polynomial in x and y of fifth order as proposed by Hardee *et al.* [33]. The left hand side of Eq. (44) is modified to incorporate the asymmetric nature of boundary conditions at the lower and upper bounds of the domain along y-axis. A_w, B_w and C_w are constants that need to be determined. Three simultaneous equations are obtained to solve for A_w, B_w and C_w by applying Eq. (41) at $y = h/2$ and $x = w_o/2$, Eq. (43) and substituting θ from Eq. (44) in Eq. (42) as,

$$\begin{bmatrix} \left(1.5h^2 + \frac{1}{2}w_o^{\,2}\right) & \left(1.75h^3 - 0.25hw_o^{\,2}\right) & \left(2.25h^2w_o - 0.75w_o^{\,3}\right) \\ \left(1.5h^2 + w_o^{\,2}\right) & \left(1.75h^3 + 0.5hw_o^{\,2}\right) & \left(-0.5w_o^{\,3}\right) \\ \left(2hw_o^{\,2}\right) & \left(3h^2w_o^{\,2}\right) & \left(2hw_o^{\,3}\right) \end{bmatrix} \begin{bmatrix} A_w \\ B_w \\ C_w \end{bmatrix} = \begin{bmatrix} e^{(-1/\theta_p)} \\ e^{(-1/\theta_{h/2})} \\ h_c^*(\theta_s - \theta_\infty) + \theta_s/h - \theta_p/h \end{bmatrix} \tag{45}$$

Solutions for A_w, B_w and C_w are obtained from Eq. (45) in terms of two unknowns: $\theta_{h/2}$ and θ_s. A value of θ_s is assumed for the first iteration to be equal to θ_∞. Expressions of A_w, B_w and C_w are substituted in Eq. (44) and an expression for $\theta_{h/2}$ is derived using Eq. (43). Now the expression for $\theta_{h/2}$ is simplified to a quadratic equation by using the approximation (See Section 2.3 for details),

$$\frac{d\theta_p}{d\theta_{h/2}} = \frac{d\theta_s}{d\theta_{h/2}} = 0 \tag{46}$$

Subsequently θ_s is calculated using the solution profile, and if this value differs from the assumed θ_s by more than a tolerance of 0.0001, the calculations are repeated using an updated value of θ_s as shown in Fig. 29. The number of iterations required to achieve required convergence decreased as the wedge angle increased. This is because the surface temperature also decreased as the wedge angle increased and led to fewer iterations needed for convergence. The computational code used for calculations is provided in Appendix F. The location of ignition is defined as the point where maximum temperature occurs along the Y-axis.

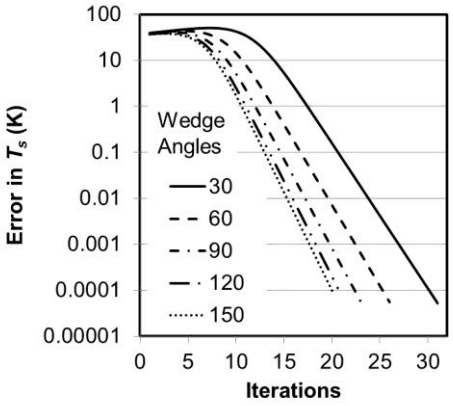

Figure29 Error in surface temperature calculation is shown as a function of number of iterations.

The approach used in the mathematical analysis can be extended to other geometries and boundary conditions as well. The model requires that the physical properties (k, ρ) and chemical parameters for source term representation (E, QA) are known. Therefore, the model proves to be a comprehensive tool which can be adapted to standards such as the ASTM standard E 2021 [13] and the European standard EN 50281-2-1(1999) [7] which are current test methodologies used in practice to estimate the minimum ignition temperature of fugitive dust layers.

3.3.1.3 Results and Discussion

For the wedge cases, the temperature profiles along the symmetry line (*Y*-axis) are shown in Fig. 30; wedge angles are indicated over the respective curves. As the wedge angle decreases from 150^o to 30^o, the ignition location (indicated by maximum temperature) moves from the wedge apex, as indicated by the vertical lines towards the surface, similar to what is observed experimentally. The maximum temperature in the profile significantly increases due to lesser dissipation in *X*-directions for acute angled wedges.

Furthermore, the dissipation in *Y*-direction also increases with increasing exposed surface area available. The iteratively obtained surface temperature also decreases as shown in Fig. 31. The downward shift of ignition location, increase in the surface area with wedge angle and decrease in the surface temperature are all coupled and depend on the overall geometry. It can be noted that, the surface temperature reduces even below the plate temperature for wedge angles 90^o or greater.

Figure 32 consolidates the mathematically calculated ignition location for wedge cases having wedge angle in the range of 10^o to 150^o .The experimental data (for 2 wedge angles of 60^o and 90^o) is shown with error bars to indicate that the thermocouple is representative of a region rather than a point in the layer.

It should be noted here that the mathematical predictions for the wedge cases have been restricted to the wedge angle of 150^o. This is due to the fact that beyond this angle transition from two-dimensional to one-dimensional configuration occurs and the predictions for ignition location flatten-off and also maximum temperature decreases significantly. The assumed polynomial temperature profile is no longer accurate.

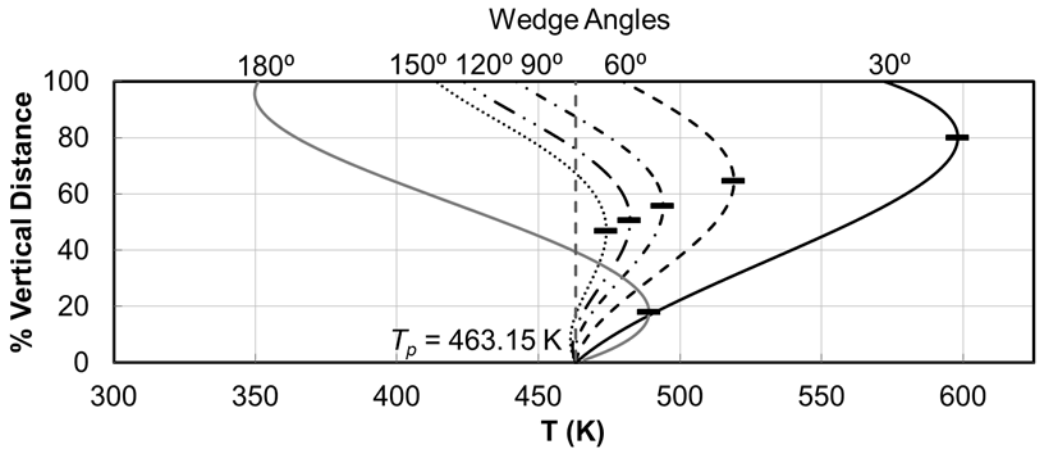

Figure30 Mathematically predicted temperature profiles along Y-axis for wedge and flat plate cases.

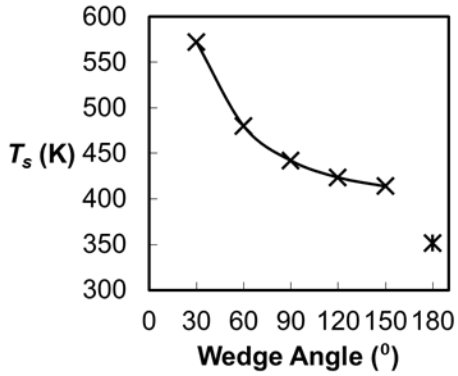

Figure31 Variation of surface temperature Ts (K) as a function of wedge angle.

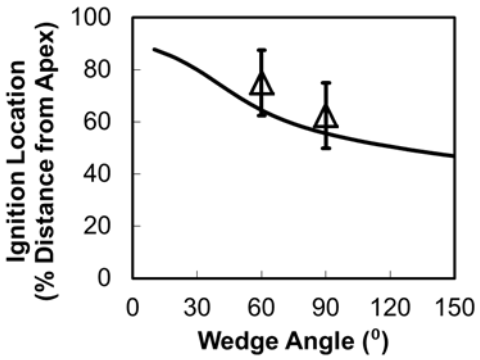

Figure32 Variation of predicted ignition location as a function of wedge angle, along with experimental data (symbols). Layer thickness (H) = 25.4 mm.

3.3.2 COMPUTATIONAL MODEL

This numerical study used Computational Fluid Dynamics (CFD) to solve the energy conservation equation for predicting the onset of ignition in a combustible dust layer deposited over hot surfaces of several geometrical shapes. Commercially available CFD packages, FLUENT® and GAMBIT®, were used to carry out conjugate numerical calculations of unsteady equations. The simulations of ignition of coal dust layers trapped between two hot plates those form the shape of a wedge having different angles and thickness values are carried out. These cases are solved in two-dimensional Cartesian coordinates (x, y).

3.3.2.1 Set-up for the Model Cases

Coal dust deposited between two hot surfaces formed as a wedge is shown in Fig. 33. The maximum height from the apex of the wedge to the top of the dust layer in a wedge is set as 25.4 mm. The angle formed by wedge is varied as 60^0, 90^0, 120^0 and 150^0. The coordinate system and the boundary conditions for both geometries are shown in Fig. 33.

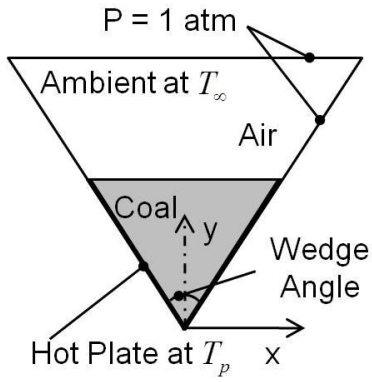

Figure33 The coordinate systems and boundary conditions for wedge shaped configuration; hot plate shown by thicker lines.

The unsteady state equation governing two-dimensional heat transfer problem for solving the temperature (T) as a function of Cartesian space co-ordinates (x, y) and time (t) can be represented by a partial differential equation,

$$\rho C_p \frac{\partial T}{\partial t} = \frac{\partial}{\partial x}\left(k \frac{\partial T}{\partial x}\right) + \frac{\partial}{\partial y}\left(k \frac{\partial T}{\partial y}\right) + \rho Q A e^{-E/RT} . \qquad (47)$$

Two-dimensional model with symmetry condition along y-axis has been applied for FLUENT simulation of Eq. (47). The boundary conditions are set as constant temperature at the hot surfaces (T_p) and pressure based condition (pressure inlet condition in FLUENT) at the extended boundaries. The top surface of the coal dust layer will be then subjected to a coupled convection-conduction boundary condition. The thermo-physical properties of Pittsburgh seam coal are used. The source term (last term in the RHS of Eq. (47)) is calculated using a zeroth order Arrhenius type rate equation. The parameters such as the activation energy (E = 88.1 kJ/mol) and the pre-exponential constant (QA = 1.8 e+12 W/kg) are taken from Park *et al.* [16]. The value of heat capacity and thermal conductivity are assumed to be constants (1300 J/kg-K and 0.2 W/m-K, respectively). The bulk density is measured during experimental work (580 kg/m^3). The ambient air is assumed to be at a constant temperature of 295 K.

The numerical results obtained for flat plate case with dust layer height 25.4 mm as well as 60^0 and 90^0 wedge cases with maximum dust layer height of 25.4 mm, are validated against the experimental data [48].

3.3.2.2 Validation

In the wedge experiments [48], temperatures have been reported at three locations along the vertical *y* axis same as in case of the flat plate, in both the wedges. The onset of ignition is said to occur when a thermocouple records a value of 50 K higher than the set hot plate temperature. In the experiments, the region/location of ignition is observed to be closer to the top surface of the coal dust (75% of the total height measured from apex) in case of the 60^0 wedge. On the other hand, in case of the 90^0 wedge, the location of ignition is observed to be in between the middle and top regions (50% to 75% of the total height from the apex). Numerical simulations predict the same trend as shown in Fig. 34. It is clear from Fig. 34 that the experimental data point at ignition (temperature at a point being 50 K more than that of the hot plate temperature) is well predicted by the numerical model for both the cases, even though there are some discrepancies in the overall profile.

The discrepancy is due to the fact that the thermo-physical values change with temperature, which becomes rapid near to ignition time, especially due to rapid heat conduction from the ignition zone to the bottom layer that is not ignited. Therefore the temperatures measured by the thermocouples at the time instant where one of the thermocouple reads the ignition temperature, would be different than those predicted by the model using constant k and C_p values. However, since predicting the region of onset of ignition alone is the primary motive of the numerical model, it can be concluded that the regions or the locations of ignition temperature are predicted quite well by this simplified model itself. Further, the temperature contours shown in Fig. 35 clearly shows the cooler apex regions and heat transferred by flow induced by natural convection in the extended domain. Streamlines in the fluid zone of air are shown at the point of ignition. These streamline represent the movement of hot air away from the coal surface, carrying the heat lost by coal. As the wedge angle increases, multi-cellular vortices are seen in the air domain. The vortices are transient in nature and therefore, the heat loss at the surface is considered in terms of convective heat transfer coefficient and surface temperature in the following section.

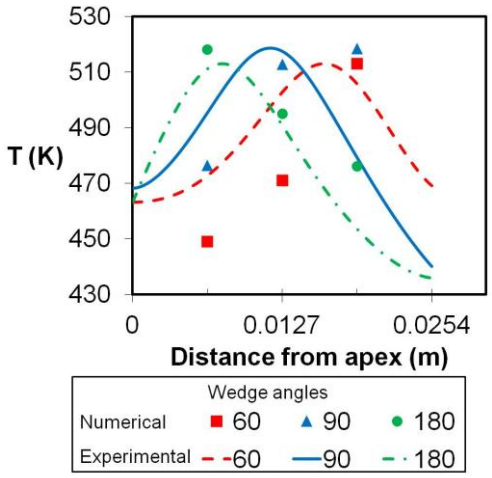

Figure34 Numerical and experimental data of temperature against distance from apex is presented for wedge angles 60^0 and 90^0 and flat plate as 180^0. The layer thickness is 25.4 mm in all cases.

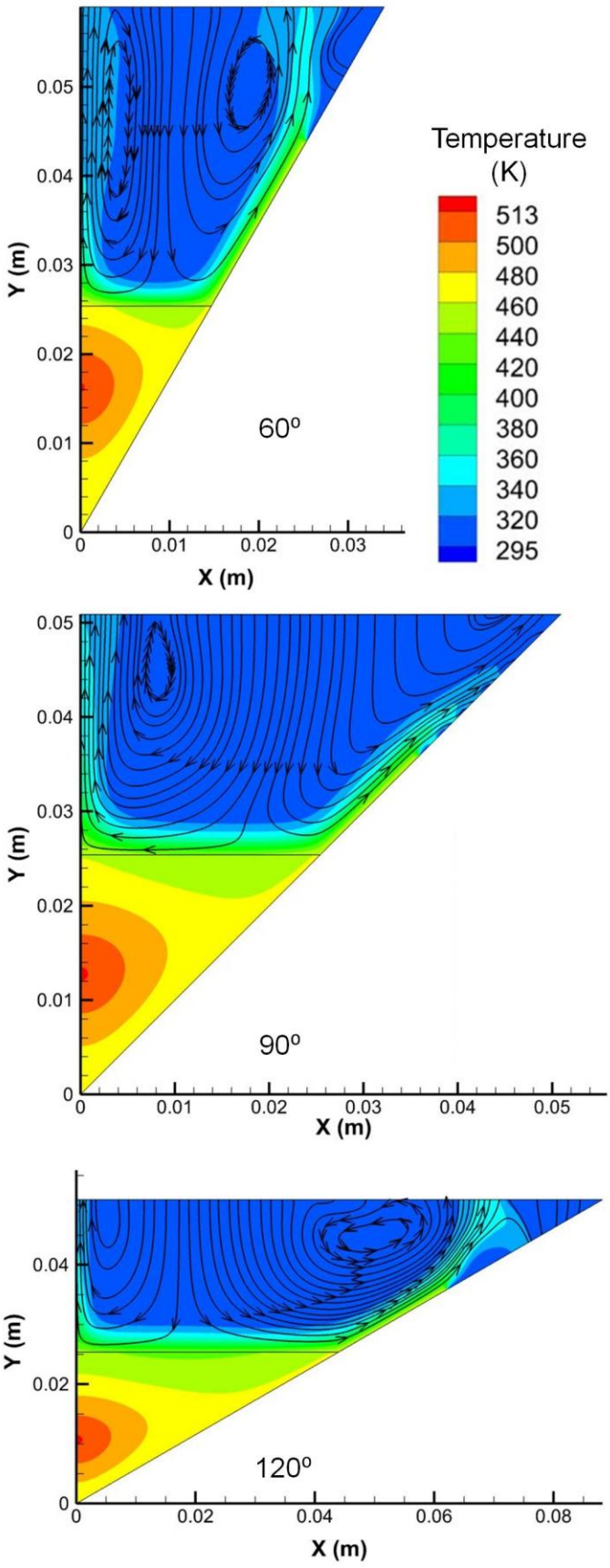
Temperature
(K)
513
500
480
460
440
420
400
380
360
340
320
295
60º
90º
120º
Y (m)
X (m)
0
0.01
0.02
0.03
0.04
0.05
0.06
0.08

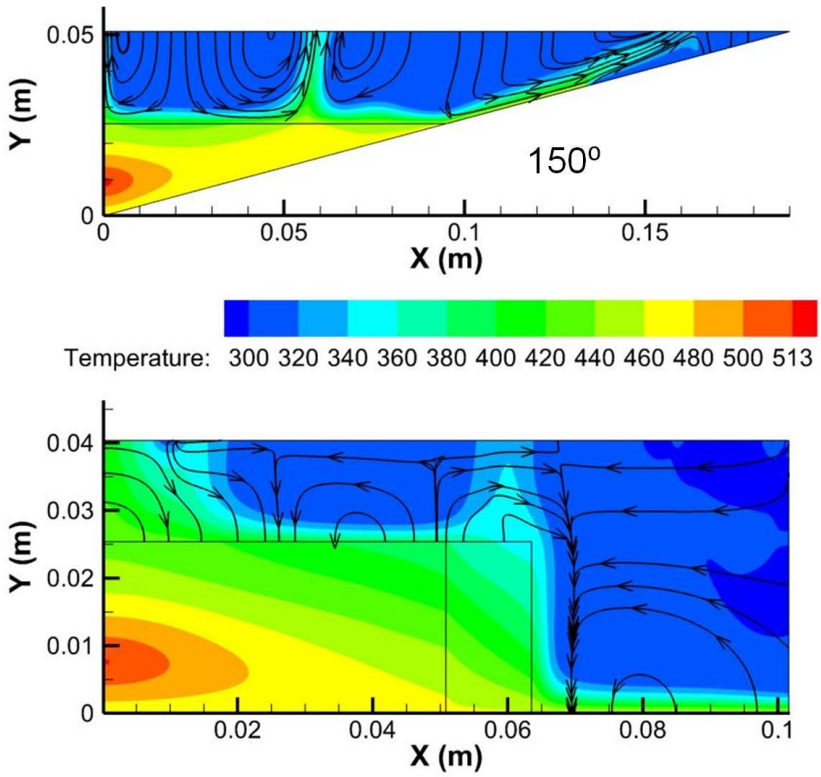

Figure35 Temperature contours at onset of ignition of wedge angles 60^0, 90^0, 120^0, 150^0 and flat plate with layer thickness 25.4 mm.

Temperature profiles at the time of ignition are plotted in Fig. 36. These show the shift in position of the maximum temperature towards the apex as the wedge angle increases. This position of maximum temperature is also regarded as ignition location. Change in ignition location as percentage of total maximum dust layer thickness is plotted against wedge angle in Fig. 37. The observed trend corresponds with the experimental observation that the ignition location shifts towards apex as the wedge angle is increased.

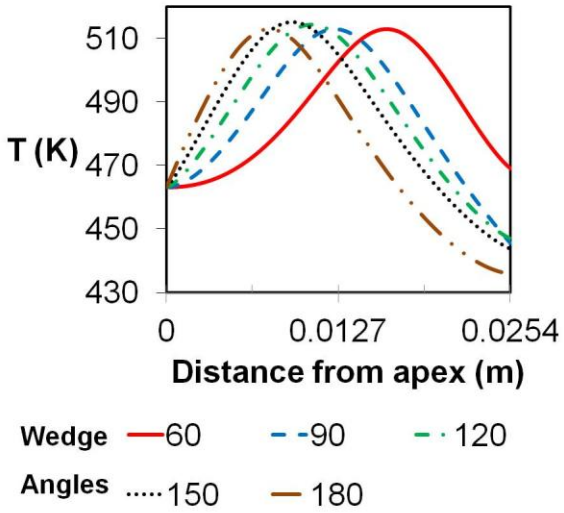

Figure 36 Temperature profiles along the center line shown for wedge angles of 60^0 to 150^0 and the flat plate case as 180^0. Maximum layer thickness in all cases is 25.4 mm.

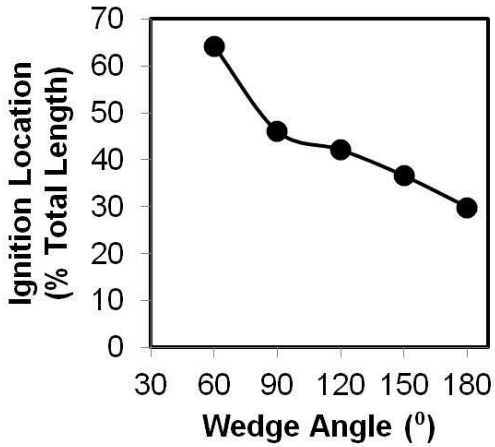

Figure 37 Change in ignition location as a function of wedge angle is shown for wedge angle range of 60^0 to 150^0 and the flat plate case shown as 180^0.

3.3.2.3 Coal-Air Surface Heat Transfer

Heat loss from the coal surface exposed to ambient air is given special attention in this section. The fact that the area of surface exposed to air increases with wedge angle makes it important aspect of the comprehensive study. The flat plat case is considered as a special case where the area of hot surface and surface exposed to air are equal. The extended domain including the complete length of the hot surface and air above the dust deposit is considered in the numerical simulation to accurately represent the experimental conditions. The variation in convective heat transfer coefficient and surface temperature

averaged over the coal surface at every time instant are plotted as a function of normalized time, for all the geometrical configurations from the beginning till the point of ignition (Fig. 38). Amongst the four wedge angles, the surface temperature of the smallest wedge angle, 60°, is seen in Fig. 38(a) to be the highest throughout the process leading to ignition. The average surface temperature decreases when the wedge angle is increased from 60°. However, the average surface temperature recorded for angles greater than 60°, except the case of flat plate, are almost same. It is seen that in case of flat plate, the surface temperature is lowest and separated by a significant margin than the other wedge cases. These trends are explained below.

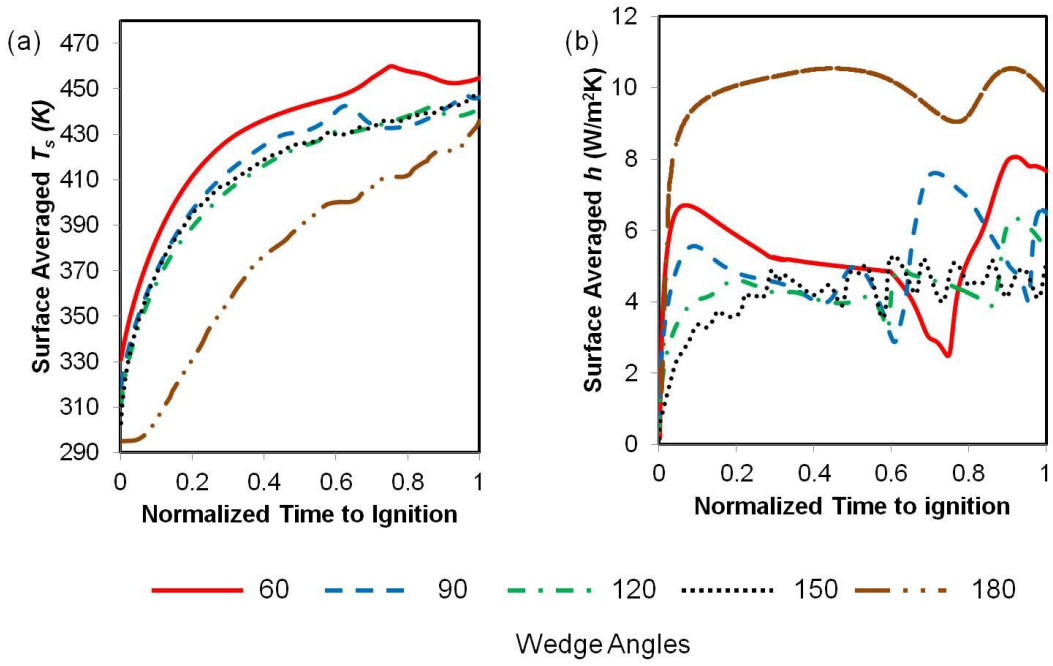

Figure 38 (a) Average surface temperature and (b) Average convective heat transfer coefficient are plotted as a function of normalized time from beginning (0) to ignition (1) for four wedge angles – 60°, 90°, 120° and 150° as well as for flat plate case (180°).

Another factor in the heat loss relationship is convective heat transfer coefficient (h). Figure 38 (b) shows that the initial trend of reduction in *h* as the wedge angle increases is disrupted by near ignition conditions. The initial period, up to normalized time to ignition of 0.3, shows that the smallest angle of 60° exhibited highest *h* value. The exactly reversed variation in 90° wedge as compared to 60° wedge at

normalized time to ignition from 0.6 to 0.8 signifies the separate consideration given to temporal variation of convective heat transfer coefficient. The change in geometrical configuration of the dust deposit and the confinement imparts transient variation in *h*. The initial high value of h and high surface temperature in case of 60° wedge sets the trend for inverse relationship between exposed surface area and the two parameters considered – *h* and T_s. A complete reversal of such trend is noted in case of flat plate geometry, where convective heat transfer is higher than any wedge case while surface temperature is lowest. The one dimensional system in case of flat plate makes the flat plate a particular case where heat loss from the exposed coal area is governed by the convective heat transfer coefficient. The different geometrical configuration of the confinement boundaries is also responsible for the change.

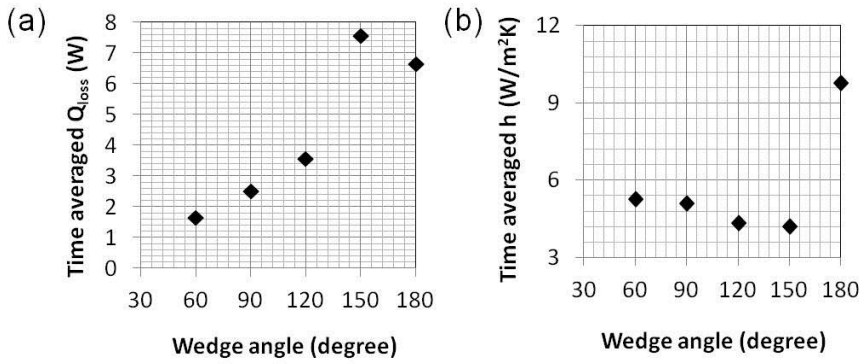

Figure39 Time averaged values of average surface heat transfer coefficient and heat loss from the surface

Time averaged values of the heat transfer coefficient averaged over the surface-area at each time instant as shown in Fig. 38(b), as well as the time averaged net heat loss from the coal surface are shown for all the cases in Fig.39. It is clear that for the cases other than the flat plate case, there is a slight decreasing trend in the time averaged heat transfer coefficient values with increasing wedge angle. The time averaged heat loss from the surface shows an increasing trend due to significant increase in the exposed area with wedge angle. The increasing trend in the heat loss with wedge angle forms the primary

reason for downward shift in the ignition location. The average surface temperature variation is dictated by the combined effects of ignition location and heat loss value.

3.4 CLOSURE

In the experimental work, the ignition behavior of bituminous coal dust deposited in 60º and 90º wedge shaped hot plates was studied. Interestingly, the dust around the apex of the wedge, which receives the maximum heat flux from the hot plates, never ignites. Instead, tests show that the top layer of coal dust records ignition in the case of 60º wedge and both the top and the middle regions record ignition in the case of 90º wedge. This unique behavior is examined by three parameters affecting the ignition, namely, the heat transfer from the hot plate to the coal dust, the subsequent chemical heat release and the heat transfer between different points within the coal dust. A thermal diffusion length scale is used to illustrate that the minimum ignition temperature increases as this length decreases. The influence of wedge geometry is also examined using this concept.

An increase in the hot plate temperature beyond the minimum ignition temperature affects the ignition characteristics (occurrence of ignition at an earlier time and higher value of maximum temperature within the coal dust) but the same trend of ignition location is maintained. The ignition behavior observed in the two wedge angle cases provides significant insight to hazardous conditions that can develop due to dust deposits trapped in corners. The results show that dust build up in acute angled wedges pose increased level of hazardous conditions since the high-temperature top layer can ignite flammable material in its vicinity.

First, in numerical analysis, ignition behavior of combustible coal dust deposited on surfaces having different configurations is studied using simplified mathematical model. Integral solution method is used for predicting ignition location for a given configuration of a wedge (two-dimensional). The results have

been validated with experimental data. It is systematically shown that as the wedge angle increases, the ignition location moves towards the apex of the wedge.

Second, a numerical model is developed based on FLUENT® and is validated using experimental data by comparing the locations of the ignition for two wedge cases. The validated model is further used to predict 120^0 and 150^0 wedges in addition to 60^o and 90^o wedges. The ignition location shifts down as the wedge angle increases. The reduction in heat loss and increase in heat generation are the causes for such trends. The convective heat transfer coefficient is calculated at the coal dust surface exposed to the ambient and it is seen to decrease as the ignition location moves closer to the hot surface.

Chapter 4. WEATHERING OF COMBUSTIBLE DUSTS

4.1 INTRODUCTION

Industrial process safety design depends on the physical, chemical, and thermodynamic properties of the substances handled by the facility. When the substance is a fine particulate solid matter, or solid dust, the facility should be designed for dust explosion protection to avoid layer ignition of dust deposited over hot surfaces. This safety design procedure becomes challenging if the properties of the dust change due to weathering. Weathering is generally a natural process that occurs independent of human activities. It can take place in stockpiles, in-seam, refuse dumps and ponds, abandoned mines, sample storage in air or in inert atmosphere [43]. All types of dusts undergo weathering as soon as they come into contact with the atmosphere. As a result, the thermal and physical properties of the dust are affected. This can prove harmful for the intended processing or storage facility [49]. Weathering is caused by temperature gradients due to seasonal changes and/or due to moisture absorption/desorption effects. For example, seasonal temperature changes can cause decomposition of the relatively unstable oxygen complexes in coal. Effect of long term storage (over 12 months) on wood-chips was tested by Casal *et al*. [50], where both physical and chemical properties changed within three months causing decrease in volatiles contents. Other than natural causes, the drying process used commonly in industry can also cause weathering because of the heat sources present intended for moisture removal. These are important considerations because it enables recognition and assessment of fire hazards. In order to avoid these hazards, prevention based safety is employed by drying in inert atmosphere, eliminating formation of explosive mixtures or rigorous exclusion of all possible ignition sources [51]. There are established standard tests to check these safety parameters [6, 52-54].

Hot surfaces produced due to frictional, electrical or some other heat source are one of the most prominent ignition sources observed in industries. Combustible dust settled on a sufficiently hot surface can be spontaneously ignited. Numerous case histories demonstrating such chain of events are found in

literature [55]. The National Academy of Sciences (NAS) Committee on Evaluation of Industrial Hazards has recommended a hot surface test to determine minimum hot-surface ignition temperatures of dust layers. The International Electrotechnical Commission (IEC) has proposed a very similar test. Based on these two test reports and the work by the US Bureau of Mines [44], the ASTM standard E 2021 [6] and the European standard EN 50281-2-1(1999) [7] were proposed. These tests are based on determining a reference or minimum temperature of the solid surface necessary to cause ignition of a dust layer deposited over it. Common criteria for ignition in these hot surface tests are visible signs of combustion or glowing, or the temperature at a location within the dust layer rising to 50 ºC above the hot surface temperature [6]. The safety measures espoused by such test standards consider fresh dust samples, in general.

Prior researches studying the influence of weathering on ignition characteristics have predominantly focused on flammable liquids with a good review provided by Wu *et al.* [56]. Research related to weathering of dusts has been limited to weathering of coal types using Fourier Transform Infra Red spectroscopy (FTIR) [43, 57]. FTIR technique involves study of the changes in spectrum of specific bands such as aliphatic C-H, -COOH. In order to decide which of these bands would be ideal to monitor weathering, the operator needs special expertise in the field of organic chemistry. In addition, FTIR may not be applicable to all types of dusts. Therefore, there is a need for a simple yet scientifically sound test procedure, which can be readily adopted to test weathering on any type of combustible dust. The objective of this study is to propose such a methodology which can be readily applied to existing test standards such as the hot plate test or ASTM E 2021 [6].

In this study, three dust samples namely, wheat flour, Pittsburgh Seam Coal (PSC) and Powder River Basin (PRB) coal, are tested. These dust samples are subjected to two types of weathering; first is by the process of wetting and subsequent drying of dust samples (moisture weathering), and second is by subjecting the samples to a temperature higher than the ambient temperature for prolonged time periods (heat weathering). Thermogravimetric analysis (TGA) and standard ignition tests (ASTM E 2021) are

carried out with both fresh and weathered dust samples. The minimum or critical surface temperature for the onset of ignition have been recorded for all the cases. Activation energies and reactivity of the dusts are estimated using the TGA results, for all the cases, by using a simplified theory available in literature. It is shown that for wheat flour the kinetic parameters are significantly altered due to weathering and as a result its critical plate temperature for ignition is reduced. With this result, further tests to determine changes in other safety aspects [6, 52-54] of the weathered dust sample can be recommended. An economical screening test method to quantify the effects of weathering of dusts is thus proposed.

4.2 TYPES OF WEATHERING IN SOLID FUELS

There is no standard method reported in literature related to weathering of dusts. Therefore, a methodology to simulate the weathering process of a dust sample in a controlled laboratory environment is first established. The heat weathering of dust is achieved by heating a 6 mm (quarter inch) thick layer of the dust on an aluminum pan placed on a hot plate maintained at a constant high temperature for 12 hours. The lower of the two temperatures, 70 ºC less than the minimum ignition temperature of one-inch thick layer of fresh dust sample, or 160 ºC, is chosen as the constant high temperature for heat weathering. This is based on the factor of safety used in European standard EN 50281 and NFPA 654 Section 9.7 Edition 2006 [3, 7]. The 6 mm thickness of layer ensured safety of such pro-longed procedure as ignition would require very high surface temperatures. Both organic (wheat flour) and coal dust samples (PSC and PRB) have been heat weathered.

Moisture weathering is carried out on only coal dust samples by mixing 25% water (by mass) with the coal dust and drying it for 4 hours by forming a 6 mm (quarter inch) thick layer on a hot surface maintained at a constant temperature of 90°C. In each case, the weight of the sample is noted before and after heating period to make sure that the loss in weight corresponds to the weight of the added moisture content only. In both heat and moisture weathering processes, the dust layer thickness which was

subjected to constant hot plate temperatures, is kept as 6 mm taking into account the least possible ignitable layer thickness [48].

4.3 Experimental Procedure

4.3.1 Thermo-Gravimetric Analysis

The weight loss of a dust sample due to thermal degradation is recorded using a TGA (Q50 - TA Instruments) by subjecting it to an oxidizing atmosphere of hot air, at different heating rates. Temperature, furnace and weight of the TGA are calibrated according to the manufacturer's recommendation. The furnace is continuously purged with a flow of atmospheric air at 60 mL/min to sweep the exhaust gases from the reaction zone. This mitigates chances of secondary reactions such as thermal cracking, re-polymerization and re-condensation. Experiments are performed at three different heating rates such as 5, 10 and 20 K/minutes, where the temperature is increased from ambient to 1073 K. The sample is spread evenly in the platinum pan to ensure uniform heat transfer and the sample weight is maintained less than 50 mg. The sample temperature and the preset linear temperature rise show negligible difference. To check the repeatability, each experimental run is performed at least three times.

4.3.2 Hot Plate Tests

The experimental setup closely follows the standard ASTM E 2021 hot surface test. A stainless steel ring 25.4 mm in height and 50.8 mm radius is used to contain the dust layer. Two slots are located at diametrically opposite points on the circumference of the metal ring to accommodate thermocouple wires. A K-type thermocouple with bead diameter of 0.38 mm, is placed at the center of the dust layer. Further details of the experimental setup and procedures of the dust layer are given in Park *et al*. [16]. Each test is repeated three times and consistent ignition temperatures are obtained for all tests.

4.4 RESULTS AND DISCUSSION

4.4.1 RESULTS FROM HOT PLATE TESTS

As mentioned earlier, the ASTM E-2021 standard test procedure is followed to determine the minimum hot plate surface temperature required to ignite (critical temperature) the weathered as well as fresh samples of wheat and coal dust layers having uniform thickness of 12.7 mm. The test criteria is set to check and observe the onset of ignition at the given plate temperature.

For both coal samples (PSC and PRB), irrespective of the weathering process, the critical temperatures (503 K and 488 K, respectively) remain almost the same corresponding to those of the fresh coal samples. This indicates that both types of weathering have negligible influence on the coal reactivity and on the onset of ignition.

On the other hand, in case of wheat flour, there is a 10 K difference in the critical temperature of ignition between the fresh and weathered samples as shown in Fig. 40 – critical temperature of heat weathered sample is 563 K and that of fresh sample is 573 K. This indicates that the weathering process has increased the reactivity of the organic dust. These trends are further analyzed using TGA, where the reactivity of all types of dusts are evaluated.

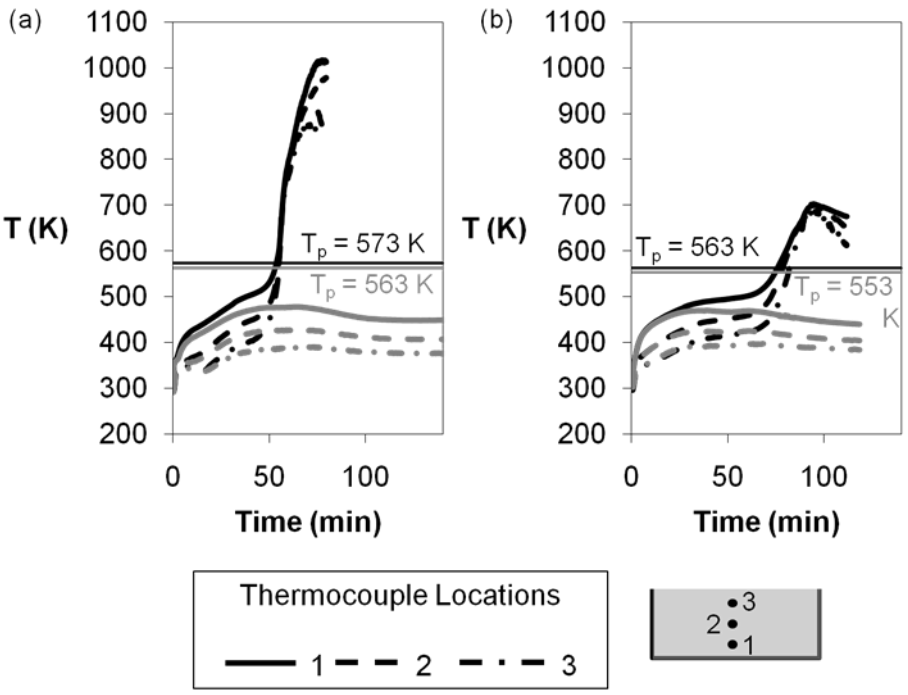

Figure 40 Temperatures recorded by three thermocouples inside wheat flour dust at heights (1) 4 mm, (2) 7 mm and (3) 10 mm are shown as a function of time for (a) fresh sample and (b) heat weathered sample. The black lines show ignition cases, whereas the grey lines show the no-ignition cases. T_p represents the temperature of the plate

4.4.2 RESULTS FROM THERMO-GRAVIMETRIC ANALYSIS

Thermal degradation of the dust samples gradually occurs as the temperature gradually increases inside the small scale furnace of the thermo-gravimetric analyzer. In case of wheat flour and powder river basin coal, four phases of degradation are observed, as shown by the horizontal lines in Figs. 41 and 42. These phases mainly correspond to moisture release, release of volatiles in stages and combustion of fixed carbon as indicated by visible change in the slope of weight loss curve. It is evident from the Fig. 41 that the volatile release is almost instantaneous for the wheat flour and occurs around 550 K for both fresh and heat weathered samples. The volatile content in wheat flour is around 55% and its fixed carbon or char content is around 30%. It has the least ash (Table 5). For powder river basin coal (PRB), which contains about 33% volatile matter and 35% fixed carbon [58], it is evident from the Fig. 42 that the release of volatile occurs in two stages. In its second stage, the volatile release is accompanied by the char oxidation such that the char oxidation is not distinctly observed as in the case of wheat flour. Therefore, in this

study the phases are marked as per the TGA data, tracking the points where the slope of the weight-loss curve changes with temperature. The start and end of these phases vary because of weathering and the percent weight loss during each phase is shown in Table 5. It is also clear from Table 5 that fresh Pittsburgh seam coal (PSC) shows a gradual weight loss from 97% to 12%, without showing any significant change of slope in its weight-loss curve even though it typically contains about 33% volatile matter and 50% fixed carbon [58]. Therefore, phase-wise investigations of the reactivity of the dust are carried out for wheat flour, PRB dusts, while single phase is considered for PSC dusts.

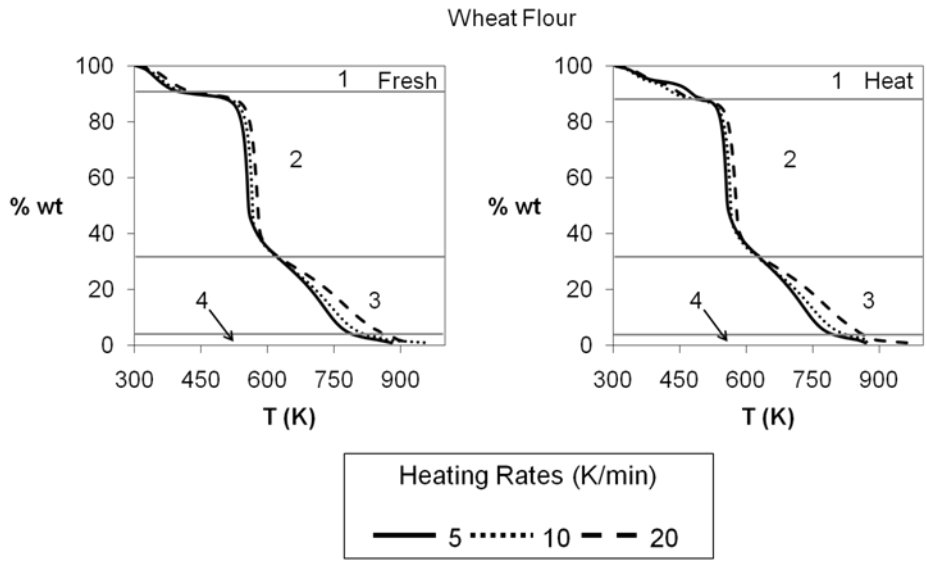

Figure41 TGA data of fresh and heat weathered samples of wheat flour at heating rates of 5, 10 and 20 K/min.

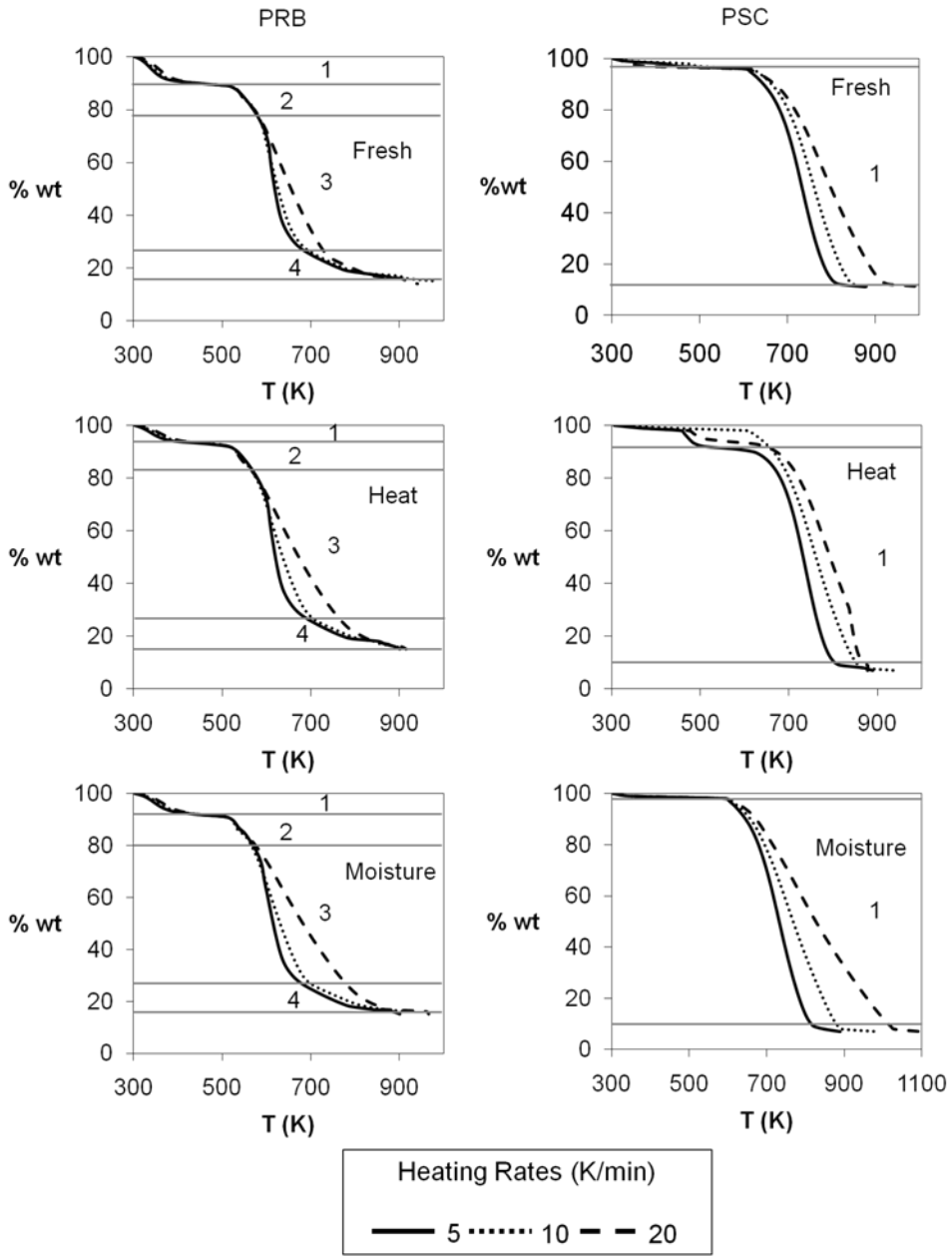

Figure 42 Thermogravimetric analysis data shows thermal degradation of fresh, heat weathered and moisture treated samples of powder river basin coal and Pittsburgh Seam coal at heating rates of 5, 10 and 20 K/min.

Table 5 Percent weight loss in each phase of degradation and percentage ash contents (by weight) of wheat flour, powder river basin coal and Pittsburgh seam coal.

Dust Sample	Treatment	Phases				% Ash
		1	**2**	**3**	**4**	
Wheat Flour	Fresh	9	59	28	4	0
	Heat	12	56	28	4	0
Powder River Basin Coal	Fresh	10	12	51	11	16
	Heat	6	11	56	11	16
	Moisture	8	12	53	11	16
		Phases				
		1		**2**		
Pittsburgh Seam Coal	Fresh	3		85		12
	Heat	8		82		10
	Moisture	2		88		10

4.4.3 THEORETICAL ANALYSIS TO EVALUATE KINETIC PARAMETERS

To arrive at the kinetics parameters, a theoretical analysis is carried out as reported in literature [59]. A parameter called the conversion degree, α, is defined for the subsequent analysis of each phase of the process. If m is the mass of the sample at any time instant, that is, at any temperature within that phase,

then that instantaneous mass can be normalized by using the initial mass, m_0, and the final mass, m_f, within that phase as shown in Figs. 41 and 42, as given in Eq. (48).

$$\alpha = \frac{m_0 - m}{m_0 - m_f} \tag{48}$$

For the last phase, the final mass, m_f, corresponds to that of the ash (Table 5). The parameter α varies between 0, indicating no mass loss, to 1, indicating end of the phase. The rate of heterogeneous solid-state reactions is described using Arrhenius type rate equation as:

$$\frac{d\alpha}{dt} = Ae^{-E_a/RT} f(\alpha) \tag{49}$$

As the heating rate is maintained constant for each test, the explicit temporal dependence in Eq. (49) can be eliminated by introducing the quantity $\beta = dT/dt$:

$$\frac{d\alpha}{dT} = \frac{A}{\beta} e^{-E_a/RT} f(\alpha) \tag{50}$$

It can be rewritten as,

$$\frac{d\alpha}{f(\alpha)} = \frac{A}{\beta} e^{-E_a/RT} dT \tag{51}$$

Equation (51) is integrated from initial conditions $(\alpha = \alpha_1, T = T_1)$ to the final condition within a phase $(\alpha = \alpha_2, T = T_2)$ to get,

$$\int_{\alpha_1}^{\alpha_2} \frac{d\alpha}{f(\alpha)} = \frac{A}{\beta} \int_{T_1}^{T_2} e^{-E_a/RT} dT \tag{52}$$

and say, $\int_{\alpha_1}^{\alpha_2} \frac{d\alpha}{f(\alpha)} = g(\alpha)$ and $\int_{T_1}^{T_2} e^{-E_a/RT} dT = p(T)$.

New variable $x = E_a / RT$ is introduced, which on differentiation with respect to *T* gives, $\frac{dx}{dT} = -\frac{E_a}{RT^2}$

i.e. $dT = \frac{RT^2}{E_a} dx = \frac{E_a}{R} \frac{dx}{x^2}$. Therefore, $p(x) = \frac{E_a}{R} \int_{x_1}^{x_2} \frac{e^{-x}}{x^2} dx$. On substitution of functions *g(α)* and *p(x)* in Eq. (52), following equation is obtained,

$$g(\alpha) = \frac{AE_a}{R\beta} p(x) \tag{53}$$

The Kissinger-Akahira-Sunose approximation method [60] is used for making the following simplification:

$$\int_{x_1}^{x_2} \frac{e^{-x}}{x^2} dx \approx \frac{e^{-x}}{x^2} \tag{54}$$

Equation (54) is substituted in Eq.(53) to get,

$$g(\alpha) = \frac{AE_a}{R\beta} \frac{e^{-E_a / RT}}{\left(\frac{E_a}{RT}\right)^2}$$

and re-arranged in the form,

$$\frac{\beta}{\mathrm{T}^2} = \frac{AE_a}{R} \frac{1}{g(\alpha)} e^{(-E_a / RT)}.$$

Then, by taking logarithm of both sides, a linear equation is obtained:

$$\ln\left(\frac{\beta}{T^2}\right) = \ln\left(\frac{AR}{E_a}\right) - \ln(g(\alpha)) - \frac{E_a}{R}\left(\frac{1}{T}\right) \tag{55}$$

The linear equation and its terms in can be written as follows:

$$y = ax + b, \tag{56}$$

where, $y = \ln\left(\frac{\beta}{T^2}\right)$, $a = \left(-\frac{E_a}{R \cdot 1000}\right)$, $x = \frac{1000}{T}$ and $b = \left(\ln\left(\frac{AR}{E_a}\right) - \ln(g(\alpha))\right)$.

The function $g(\alpha)$ is determined by assuming $f(\alpha)$ to have a classical nth order reaction form, given by, $f(\alpha) = (1-\alpha)^n$ [61]. Then,

$$g(\alpha) = \int_0^{\alpha} \frac{d\alpha}{f(\alpha)} = \frac{(1-\alpha)^{1-n}}{n-1} \tag{57}$$

The apparent activation energy (E_a) and pre-exponential factor (A) are obtained by plotting $\ln\left(\frac{\beta}{T^2}\right)$ against $\frac{1000}{T}$. Three data points are obtained by the three heating rates (5, 10 and 20 K/min) and at each phase of conversion, the slope and intercept is calculated. This gives the average values of the activation energy (E_a) and pre-exponential factor (A), respectively, for that phase. To evaluate the Arhenius type source term which contributes to the ignition source, the following equation is used.

$$\text{Reactivity} = Ae^{\left(-E_a / RT_{avg}\right)} \tag{58}$$

The reactivity term is evaluated using the values of pre-exponential constant and activation energy at each degree of conversion in each phase as a function of average temperature (T_{avg}). The average temperature (T_{avg}) arises due to three values of temperature attained for each conversion degree (α), as three heating rates are employed. The effective pre-exponential constant and activation energy values applicable to an entire phase are then determined by a linear equation generated by taking natural logarithm of both sides of Eq. (58), and using the data in each phase. The linear equation is given by,

$$\ln(\text{Reactivity}) = \ln(A) - \frac{E_a}{R}\frac{1}{T_{avg}} \qquad (59)$$

Table 6. Sample calculations of activation energy (Ea) and pre-exponential constant (A) and reactivity shown for the first phase of fresh wheat flour sample.

% Weight	*A*	T_{avg}	E_a	*A*	Reactivity
100	0.00	305.62	144.09	2.91E+23	6.85E-02
99	0.11	328.21	83.57	4.86E+11	2.43E-02
98	0.22	339.33	69.91	1.21E+09	2.09E-02
97	0.33	347.95	63.80	7.66E+07	2.03E-02
96	0.44	355.69	60.30	1.49E+07	2.09E-02
95	0.56	363.37	57.83	4.61E+06	2.24E-02
94	0.67	371.57	56.35	2.13E+06	2.56E-02
93	0.78	380.92	55.86	1.46E+06	3.21E-02
92	0.89	392.05	54.63	9.13E+05	4.81E-02
91	1.00	408.50	56.73	--	--

For example, for phase 1 (shown in Table 6), the slope of the line, $-E_a/R$, is equal to -2604.2, so that the value of E_a is 21651.5 J/mol. Similarly, the intercept of the line is equal to ln(A), has a value of 3.46, which gives the value of *A* as 31.8 s^{-1}. This way reactivity of each phase of thermal conversion can be defined by a set of kinetic parameters (E_a, A). and its characteristic temperature range. Values of Pittsburgh seam coal reactivity (E_a, A) are reported in Table 7.

Table 7. Pre-exponential constant (A, 1/s), activation energy (E, kJ/mol) and reactivity (1/s) of Pittsburgh seam coal.

Dust Treatment	Pre-exponential Constant (*A*) (1/s)	Activation Energy (E_a) (kJ/mol)	Reactivity (1/s)
Fresh	38935.6	101.1	0.0083
Heat	3090.2	73.6	0.0039
Moisture	1150.3	84.9	0.0029

4.4.4 REACTIVITY OF FRESH AND WEATHERED DUST SAMPLES

Thermogravimetric data of Pittsburgh seam coal shows no change in slope at the end of the pyrolysis or at the beginning of the char oxidation process. Therefore, only a single phase conversion is considered starting from 92% - 98% and ending at 10% - 12% of its initial weight (Table 5). Both the activation energy and pre-exponential constant of the heat weathered and moisture weathered coal remains such that their resulting reactivity values are lower than the fresh sample. This shows that the weathering does not elevate the ignition related risk.

At the same time, Pittsburgh coal dust is used as a standard dust to check whether the kinetics parameters determined using the present theory match the values in the prior work available in literature (Table 7). The activation energy obtained from the present theory, which is in the range of 73.6 to 101.1 kJ/mol, is well within the range reported by Park *et. al.* [16] (65.4 to 115.9 kJ/mol). A large range of variation in pre-exponential constant is reported in Park *et al.* [16] (from 706 s^{-1} to 5.4e+06 s^{-1}). The present theory is able to predict the value of *A* well within this range as well (1150 s^{-1} to 3.9e+04 s^{-1}).

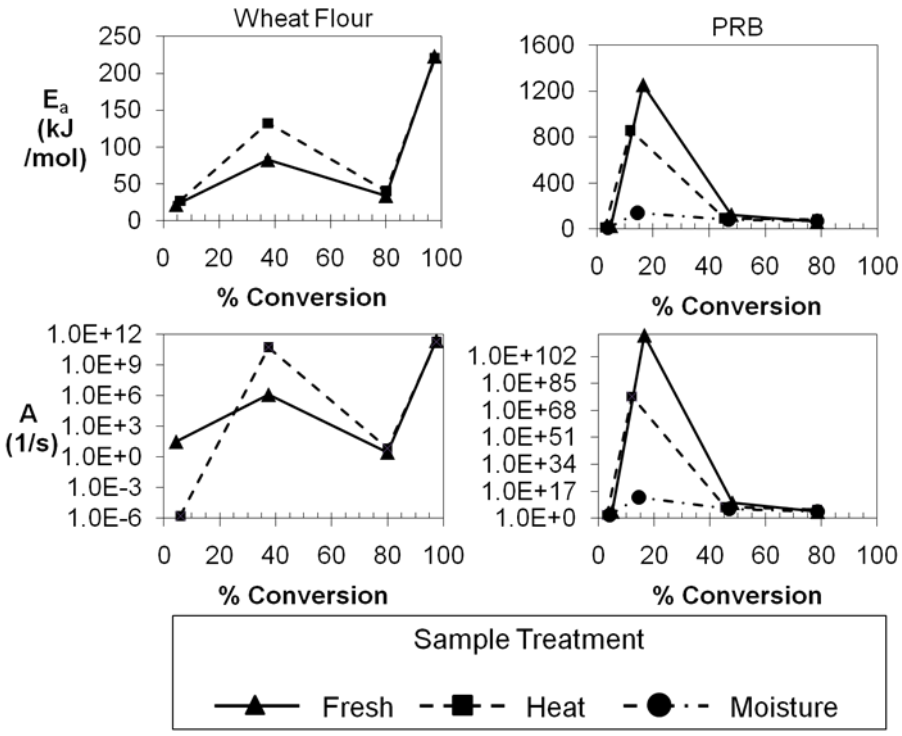

Figure 43 Activation energy (Ea) and pre-exponential factor (A) for each phase of degradation of fresh and heat weathered samples of wheat flour and fresh, heat and moisture weathered powder river basin coal is plotted against percentage conversion

Figure 43 shows the E_a and A values for the four stages of mass loss curve for fresh and heat weathered wheat flour samples. Especially during the phase 2, where major mass loss occurs (Fig. 41), it is clear that the values of the kinetic parameters are modified favorably for heat weathered samples (Fig. 43). This eventually translates to higher reactivity as shown in Fig. 44, for phase two. In this phase the sample is heated to a temperature in the range 550 K to 600 K. Since in this range, the reactivity of heat weathered wheat flour is around 76% higher than that of the fresh sample, this clearly explains the cause for observing a lower critical temperature of ignition for the weathered sample. At phase 3, which occurs at much higher temperature than the critical ignition temperature, the reactivity of weathered wheat flour sample is lower compared to that of the fresh sample.

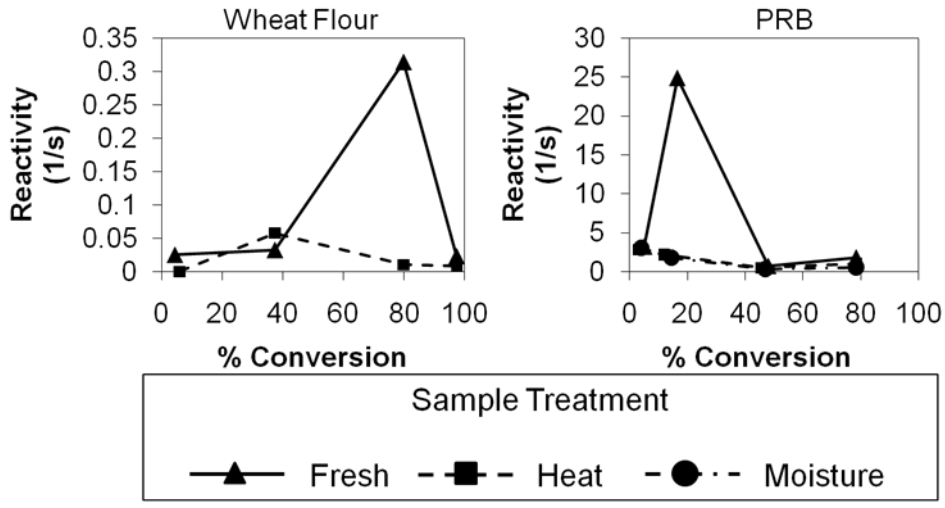

Figure 44 Reactivity (Eq. (58)) calculated as a function of temperature for fresh, heat and moisture weathered samples of wheat flour and powder river basin coal.

For PRB dust, the kinetic parameters are substantially higher in phase 2 for the fresh sample. Only in this phase, there are significant differences in the values of E_a and A between the fresh, heat weathered and moisture weathered samples. Furthermore, the reactivities of the both the weathered samples are only comparable to that of fresh one (Fig. 44) in other phases (1, 3 and 4). Therefore, the weathered samples do not pose a serious issue with the onset of ignition in this case as seen in PSC case.

4.5 CLOSURE

Weathering of fugitive dust layers in process industries can occur due to the process of wetting and subsequent drying or by exposure to temperatures higher than ambient for extended periods. The influences of both moisture-induced and heat-induced weathering on three types of dusts, the wheat flour, the Pittsburgh seam coal and the powder river seam coal, are analyzed. The tests, similar to the standard hot surface ignition test (ASTM E-2021), have been performed to study the influence of weathering on the critical ignition temperature. It is found that weathering does not change the ignition temperature in case of both the coal dusts, whereas heat weathering of wheat flour influenced a 10 K reduction in the minimum ignition temperature.

The results are substantiated by conducting thermogravetimetric tests with all the fresh and weathered dust samples, to determine the kinetic parameters those can be related to the ignition characteristics. Using the kinetic parameters such as the pre-exponential constant (A, s^{-1}) and the activation energy (E, kJ/mol), the reactivity of the samples at various temperature ranges are determined. Increase in the reactivity of wheat flour due to heat weathering has been demonstrated, which explains why this sample recorded a lower hot surface ignition temperature. For coal dusts, the reactivities are seen to be lowered due to both types of weathering, therefore, the ignition tests indicated no change in minimum hot surface layer ignition temperature. The simplicity of the present analysis can be an important component for ease of adoption by industrial dust testing practices for checking the significance of weathering on the dust.

Chapter 5. CONCLUSION AND FUTURE WORK

5.1 CONCLUDING REMARKS

The study of factors governing spontaneous ignition of combustible dusts has three main outcomes:

Detailed understanding of spontaneous ignition of dust problem in two-dimensional systems:

Experimental work done by devising a test set-up having two hot surfaces to provide a wedge like confinement for combustible dust revealed that the ignition behavior depends on the angle of the wedge. Acute angle geometry (60° wedge) resulted in ignition taking place close to the surface exposed to atmosphere. This is a striking result as the trivial expectations would be to have cooler temperatures in the dust that is immediate to surface bounded by convective heat loss conditions. In addition, experiments with 90° wedge showed that ignition occurred in the middle region. Only in case of flat plate tests was the ignition location close to the hot surface. Scaling analysis of heat flux through the dust and heat generation provided reasoning behind the geometrical dependence of ignition behavior.

Further, numerical simulation of the experiments, based on conjugate heat transfer model, was implemented to study the influence the geometry had on the heat loss from the dust surface exposed to ambient air. The validated model was extended to simulate wedge angles of 120° and 150°.

Mathematical approach to handle complex dust deposit geometry:

A mathematical method was developed and applied to two dimensional system of dust deposit subjected to high temperature on a surface at an angle and convective cooling on the horizontal top surface exposed to ambient conditions. The assumed temperature profile approach was proved to provide satisfactory results for complex geometries and asymmetrical boundary conditions. Therefore, the method can be used to analyze two- and three-dimensional dust deposit systems under complex confinements having various types of boundary conditions.

Recommendations to the industrial test standard:

The safety of dust layers accumulated on hot surfaces is prescribed by the determination of minimum layer ignition temperature using standard test method – ASTM E-2021. Two problems were identified and recommendations were made to the ASTM E-27 committee.

The first problem is the loss of one-dimensionality of the setup. This was caused by the use of highly conductive metal ring to contain the dust. A ring material that roughly matches the thermal properties of the dust was recommended in order to maintain the desired one-dimensional nature of heat transfer from hot plate to dust layer to air.

The second problem was identified as weathering of dusts. A method to quantify the change in hazard level of dust due to prolonged exposure to high temperatures or wetting-drying cycle was proposed. Organic dust (wheat flour) was found to be susceptible to heat weathering as its hazard level increased with weathering - the minimum ignition temperature decreased.

5.2 PLAN FOR FUTURE WORK

There is a vast amount of experimental data available for combustible dusts in one-dimensional geometrical configurations such as infinite slab, cube and cylinder, and about the minimum ignition temperature on hot surface or in an oven. The dust samples include metallic, organic and coal dusts. There is a scarcity of experimental data for two and three dimensional geometries with asymmetrical boundary conditions. Therefore, data should be added to literature for two-dimensional wedge like configurations as well as three-dimensional room corner configurations as shown in Fig.45. If a sample is found to ignite at lower temperature than prescribed by the flat plate test, the safe temperature should be redefined as geometry dependent. Similarly, data should be developed for the effect of heat and moisture weathering.

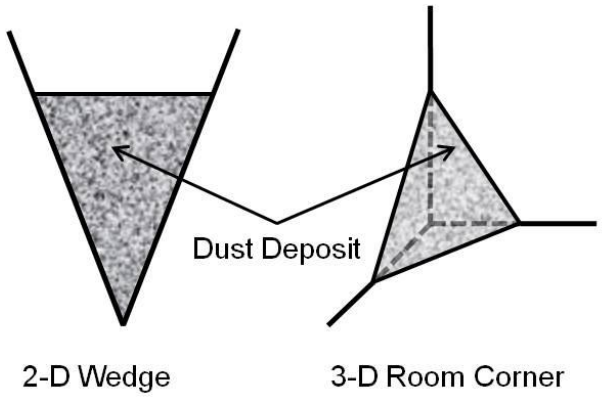

Figure45 Proposed geometrical configurations for experimental study of spontaneous ignition of combustible dusts in two and three dimensional configurations with asymmetrical boundary conditions.

The present study provided the insight about spontaneous ignition of dust deposited in complex surface geometries. This study can be extended to development of a tool that can predict critical boundary conditions for any geometry, based upon the assumed temperature profile method.

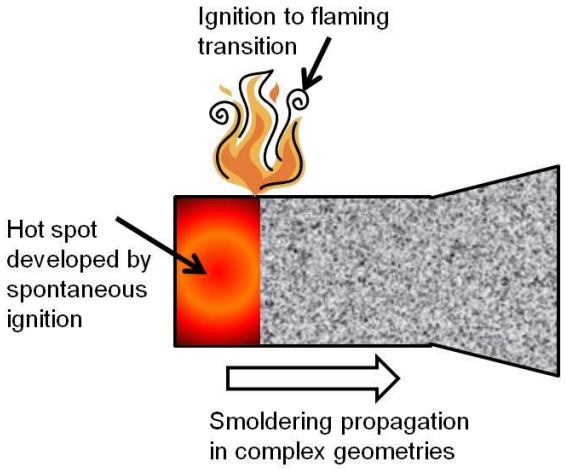

Figure46. Illustration showing hot spot developed that can lead to flames or propogate as a smoldering fire in complex geometries.

It is extremely tedious to detect, control or extinguish smoldering combustion. The mechanism of extinction can be represented mathematically with similar analysis done for spontaneous ignition. The dangers related to spontaneous ignition are higher, if the developed hot spot would sustain flames (as

shown in Fig. 46). Also, experimental research related to smoldering propagation in multi-dimensional systems is scarce. Therefore, this work should be extended towards three main areas:

1) Extinction mechanism: the effect of reduce oxygen concentration environment [47]
2) Ignition to flaming combustion transition mechanism
3) Smoldering propagation in complex geometries

In order to consider the oxygen concentration, enclosed experimental setup with gas analyzer could be used. Heterogeneous reaction mechanisms could be considered to simulate extinction conditions. Insight of extinction mechanism will help two areas: safe storage and controlling underground coal fires. The study of smoldering to flame transition mechanism is carried out in the past [62, 63]. This work is limited to transition due to increase in the oxygen concentration. Study of other factors such as evolution of light hydrocarbons, CO and temperature at the transition would provide crucial information to understand this phenomenon completely.

Extensive work is done on multi-dimensional smoldering spread in the past [46, 64]. Yet, the research is limited to uniform ignition fronts and simple geometries [65]. In order to understand, the behavior of smoldering front under complex geometries experimental study should be carried out. Smoldering front detection can be achieved through a combination of visual observation, center of gravity change due to weight loss, and gas and temperature monitoring. The study would not only provide a comprehensive method of determining two and three dimensional smoldering front, but will also provide data for validation of numerical simulations of smoldering in complex geometries.

References

1. *Investigation Report Combustible Dust Hazard Study*, 2006.
2. Eastern Research Group, I., *Combustible Dust Expert Forum*, 2011, U.S. Department of Labor Occupational Safety and Health Administration Directorate of Standards and Guidance. p. 46.
3. *NFPA 654, Standard for the Prevention of Fire and DustExplosions from the Manufacturing, Processing, and Handling of Combustible Particulate Solids*, in *Definitions*2006.
4. Hazards, N.R.C.C.o.E.o.I. and N.M.A. Board, *Classification of dusts relative to electrical equipment in class II hazardous locations: report of the Committee on Evaluation of Industrial Hazards, National Materials Advisory Board, Commission on Engineering and Technical Systems, National Research Council, National Academy of Sciences*. 1982: National Academies.
5. Regulations, I.s., *IEC 61241-2-1: Electrical Apparatus for Use in the Presence of Combustible Dust - Part 2: Test Methods - Section 1: Methods for Determining the Minimum Ignition Temperatures of Dust First Edition*, 1994.
6. ASTM, E., *2021, Standard Test Method for Hot-Surface Ignition of Dust Layers.* A. International, Editor, 2001.
7. European Standard, *EN 50281, Electrical apparatus for use in the presence of combustible dust part 2 1 test methods of determining minimum ignition temperatures*, 1999.
8. *NFPA 484, Standard for Combustible Metals*, in *Fire Prevention, Fire Protection, and Emergency Response* 2012: Quincy, MA.
9. NFPA 69, *Standard on Explosion Prevention Systems,* Quincy, MA: National Fire Protection Association, 2008.

10. ASTM, *WK1680 - New Test Method for Standard Test Method for Limiting Oxygen (Oxidant) Concentration of Combustible Dust Clouds*, 2003.
11. Reddy, P.D., P.R. Amyotte, and M.J. Pegg, *Effect of inerts on layer ignition temperatures of coal dust.* Combustion and flame, 1998. **114**(1-2): p. 41-53.
12. Joshi, K.A., *Factors governing spontaneous ignition of combustible dusts testFactors governing spontaneous ignition of combustible dusts test*, in *ASTM Committee E27 Meeting*2011: Tampa, FL.
13. ASTM, *E 2021, Standard Test Method for Hot-Surface Ignition of Dust Layers*, 2001.
14. Verlag, B., *DIN EN 15188. Determination of the spontaneous ignition behaviour of dust accumulations*, 2007.
15. Jones, J.C., *On the role of times to ignition in the thermal safety of transportation of bituminous coals.* Fuel, 2000. **79**(12): p. 1561-1562.
16. Park, H., A.S. Rangwala, and N.A. Dembsey, *A means to estimate thermal and kinetic parameters of coal dust layer from hot surface ignition tests.* Journal of hazardous materials, 2009. **168**(1): p. 145-155.
17. Janes, A., D. Carson, A. Accorsi, J. Chaineaux, B. Tribouilloy, and D. Morainvillers, *Correlation between self-ignition of a dust layer on a hot surface and in baskets in an oven.* Journal of hazardous materials, 2008. **159**(2): p. 528-535.
18. Semenov, N.N., I.A.I. Frenkel , and I.A.R. Shm dt-Chernysheva, *Chemical kinetics and chain reactions*. 1935: The Clarendon Press.
19. Frank-Kamenetskii, D.A., *Diffusion and heat transfer in chemical kinetics*. 2d enl. and rev. ed. 1969, New York,: Plenum Press. xxvi, 574 p.
20. Clemmow, D. and J. Huffington, *An extension of the theory of thermal explosion and its application to the oscillatory burning of explosives.* Trans. Faraday Soc., 1956. **52**(0): p. 385-396.

21. Gray, P. and M. Harper, *Thermal explosions. Part 1.—Induction periods and temperature changes before spontaneous ignition.* Trans. Faraday Soc., 1959. **55**: p. 581-590.

22. Thomas, P. and P. Bowes, *Thermal ignition in a slab with one face at a constant high temperature.* Transactions of the Faraday Society, 1961. **57**: p. 2007-2017.

23. Shouman, A., A. Donaldson, and H. Tsao, *Exact solution to the one-dimensional stationary energy equation for a self-heating slab.* Combustion and Flame, 1974. **23**(1): p. 17-28.

24. Shouman, A. and A. Donaldson, *The stationary problem of thermal ignition in a reactive slab with unsymmetric boundary temperatures.* Combustion and Flame, 1975. **24**: p. 203-210.

25. Kordylewski, W., *Critical parameters of thermal explosion.* Combustion and Flame, 1979. **34**: p. 109-117.

26. Kordylewski, W. and Z. Krajewski, *Thermal ignition of self-heating porous slab.* Combustion and Flame, 1981. **41**: p. 113-122.

27. Gray, P. and P. Lee, Thermal explosion theory, in Oxidation and Combustion Reviews Vol. 2, C.F.H. Tipper, Editor. 1967, Elsevier, Amsterdam. p. 1-184.

28. Averson, A. and A. Merzhanov, *The present state of the thermal ignition theory/An invited review/(Thermal ignition theory review, discussing mathematical problem statement, ignition characteristics approximate calculation methods, heat transfer mechanisms, geometrical and critical conditions, experimental tests, etc).* Combustion and Flame, 1971. **16**: p. 89-124.

29. Bowes, P.C. and Building Research Establishment., *Self-heating : evaluating and controlling the hazards*. 1984, [Garston, Merseyside] Amsterdam ; New York: Dept. of the Environment Elsevier. vi, 500 p.

30. Boddington, T., P. Gray, and D. Harvey, *Thermal theory of spontaneous ignition: criticality in bodies of arbitrary shape.* Philosophical Transactions of the Royal Society of London. Series A, Mathematical and Physical Sciences, 1971. **270**(1207): p. 467-506.

31. Hardee, H.C., D.O. Lee, and A.B. Donaldson, *A new method of predicting the critical temperature of explosives for various geometries.* Combustion and Flame, 1972. **18**(3): p. 403-410.

32. Von Karman, T., *On laminar and turbulent friction*. 1946: National Advisory Commitee for Aeronautics.

33. Hardee, H., A. Donaldson, and D. Lee, *Predicting the critical boundary temperature of multidimensional explosives.* Combustion and Flame, 1972. **19**(3): p. 331-342.

34. Bowes, P. and S. Townshend, *Ignition of combustible dusts on hot surfaces.* British journal of applied physics, 1962. **13**: p. 105.

35. Miron, Y. and C.P. Lazzara, *Hot surface ignition temperatures of dust layers.* Fire and materials, 1988. **12**(3): p. 115-126.

36. Lebecki, K., Z. Dyduch, A. Fibich, and J. Śliż, *Ignition of a dust layer by a constant heat flux.* Journal of Loss Prevention in the Process Industries, 2003. **16**(4): p. 243-248.

37. Anthony, E. and P. Field, *An Apparatus and Method for Determining the Self-Ignition Temperature of Dust Layers.* Department of the Environment and Fire Offices' Committee Joint Fire Research Organisation, Fire Research Station, Borehamwood, UK, 1975.

38. Hensel, W., U. Krause, W. John, and K. Machnow, *Critical parameters for the ignition of dust layers at constant heat flux boundary conditions.* Process Safety Progress, 1994. **13**(4): p. 210-213.

39. Dyduch, Z. and B. Majcher, *Ignition of a dust layer by a constant heat flux-heat transport in the layer.* Journal of loss prevention in the process industries, 2006. **19**(2-3): p. 233-237.

40. Kim, H.M. and C. Hwang, *Heating and ignition of combustible dust layers on a hot surface: Influence of layer shrinkage.* Combustion and flame, 1996. **105**(4): p. 471-485.

41. Chen, X.D., *Safer estimates of time-to-ignition of reactive porous solid of regular shapes.* Chemical Engineering and Processing: Process Intensification, 1997. **36**(3): p. 195-200.

42. Thomas, P., *On the thermal conduction equation for self-heating materials with surface cooling.* Trans. Faraday Soc., 1958. **54**: p. 60-65.

43. Nelson, C.R., *Chemistry of coal weathering. Volume 14.* 1989.

44. Miron, Y. and C.P. Lazzara, *Hot Surface Ignition Temperatures of Dust Layers.* Fire Mater., 1988. **12**: p. 115-126.

45. Park, H., *Hot Surface Ignition Temperature of Dust Layers with and without Combustible Additives*, 2006, WORCESTER POLYTECHNIC INSTITUTE.

46. Ohlemiller, T.J., *Modeling of smoldering combustion propagation.* Progress in Energy and Combustion Science, 1985. **11**(4): p. 277-310.

47. Bowes, P. and P. Thomas, *Ignition and extinction phenomena accompanying oxygen-dependent self-heating of porous bodies.* Combustion and Flame, 1966. **10**(3): p. 221-230.

48. Joshi, K.A., V. Raghavan, and A.S. Rangwala, *An experimental study of coal dust ignition in wedge shaped hot plate configurations.* Combustion and Flame, 2011. **159**(1): p. 376-384.

49. Chen, X., *The effect of drying heat and moisture content on the maximum temperature rise during self-ignition of a moist coal pile.* Coal Preparation, 1994. **14**: p. 223–236.

50. Casal, M., M.V. Gil, C. Pevida, F. Rubiera, and J.J. Pis, *Influence of storage time on the quality and combustion behaviour of pine woodchips.* Energy, 2010. **35**(7): p. 3066-3071.

51. Mujumdar, A.S., *Handbook of industrial drying*. 2007: CRC.

52. ASTM, E., *1226,“ .* Standard Test Method for Pressure and Rate of Pressure Rise for Combustible Dusts, 2005.

53. ASTM, E., *1515, Standard Test Method for Minimum Explosible Concentration of Combustible Dusts.* A. International, Editor, 2007.

54. ASTM, E., *2019, Standard Test Method for Minimum Ignition Energy of a Dust Cloud in Air.* A. International, Editor, 2007.

55. Eckhoff, R.K., *Dust explosions in the process industries*. 2003: Gulf professional publishing.

56. Wu, N., G. Kolb, and J.L. Torero, *The effect of weathering on the flammability of a slick of crude oil on a waterbed.* Combustion Science and Technology, 2000. **161**: p. 269-308.

57. Ibarra, J. and J. Miranda, *Detection of weathering in stockpiled coals by Fourier transform infrared spectroscopy.* Vibrational spectroscopy, 1996. **10**(2): p. 311-318.

58. Levendis, Y.A., K. Joshi, R. Khatami and A.F. Sarofim, *Combustion behavior in air of single particles from three different coal ranks and from sugarcane bagasse.* Combustion and Flame, 2011. **158**(3): p. 452-465.

59. Leroy, V., D. Cancellieri, E. Leoni, and J.L. Rossi, *Kinetic study of forest fuels by TGA: Model-free kinetic approach for the prediction of phenomena.* Thermochimica Acta, 2010. **497**(1-2): p. 1-6.

60. Kissinger, H.E., *Reaction Kinetics in Differential Thermal Analysis.* Anal. Chem., 1957. **29**(11): p. 1702-1706.

61. Cancellieri, D., E. Leoni, and J.L. Rossi, *Kinetics of the thermal degradation of Erica arborea by DSC: Hybrid kinetic method.* Thermochimica acta, 2005. **438**(1-2): p. 41-50.

62. Tse, S.D. and A. Fernandez-Pello, *Some observations of two-dimensional smoldering and the transition to flaming.* Transport phenomena in combustion, 1996: p. 689-700.

63. Tse, S.D., A. Fernandez-Pello, and K. Miyaska, *Controlling mechanisms in the transition from smoldering to flaming of flexible polyurethane foam*. 1996. Elsevier.

64. Mukunda, H., J. Basani, H.M. Shravan, and B. Philip, *Smoldering combustion of "incense" sticks—experiments and modeling.* Combustion science and technology, 2007. **179**(6): p. 1113-1129.

65. Ohlemiller, T., *Smoldering combustion.* SFPE handbook of fire protection engineering, 1995: p. 2-171.

66. Enig, J., D. Shanks, and R. Southworth, *NAVORD Report 4377.* US Naval Ordinance Laboratory, Nov, 1956. **7**.

67. Parks, J.R., *Criticality Criteria for Various Configurations of a Self-Heating Chemical as Functions of Activation Energy and Temperature of Assembly.* The Journal of Chemical Physics, 1961. **34**: p. 46.

68. Takeno, T., *Ignition criterion by thermal explosion theory.* Combustion and Flame, 1977. **29**(2): p. 209-211.

69. Bazley, N. and G. Wake, *The dependence of criticality on activation energy when reactant consumption is neglected.* Combustion and Flame, 1978. **33**: p. 161-168.

70. Gill, W., A. Donaldson, and A. Shouman, *The Frank-Kamenetskii problem revisited. Part I. Boundary conditions of first kind.* Combustion and Flame, 1979. **36**: p. 217-232.

71. Tam, K., *On the disappearance of criticality in the theory of thermal ignition.* Zeitschrift für Angewandte Mathematik und Physik (ZAMP), 1980. **31**(6): p. 762-766.

72. Mittelmann, H.D. and H. Weber, eds. *Bifurcation problems and their numerical solution*. Vol. 54. 1980, Springer. 176.

73. Fenaughty, K., A. Lacey, and G. Wake, *The disappearance of criticality for small activation energy with arbitrary Biot number.* Combustion and Flame, 1982. **45**: p. 287-291.

74. Gustafson, K. and B. Eaton, *Exact solutions and ignition parameters in the Arrhenius conduction theory of gaseous thermal explosion.* Zeitschrift für Angewandte Mathematik und Physik (ZAMP), 1982. **33**(3): p. 392-405.

75. Spence, A. and B. Werner, *Non-simple turning points and cusps.* IMA Journal of Numerical analysis, 1982. **2**(4): p. 413-427.

76. Boddington, T., C.G. Feng, and P. Gray, *Thermal explosions, criticality and the disappearance of criticality in systems with distributed temperatures. I. Arbitrary Biot number and general reaction-rate laws.* Proceedings of the Royal Society of London. A. Mathematical and Physical Sciences, 1983. **390**(1799): p. 247-264.

77. Tognotti, L., L. Petarca, and S. Zanelli. *Spontaneous combustion in beds of coal particles*. 1989. Elsevier.

78. Duane, T. and E. Synnott, *Ignition characteristics of spray-dried milk product powders in oven tests.* Journal of food engineering, 1992. **17**(3): p. 163-176.

79. Vázquez-Espí, C. and A. Liñán, *The effect of square corners on the ignition of solids.* SIAM Journal on Applied Mathematics, 1993: p. 1567-1590.

80. Balakrishnan, E., A. Swift, and G. Wake, *Critical values for some non-class A geometries in thermal ignition theory.* Mathematical and Computer Modelling, 1996. **24**(8): p. 1-10.

Appendix A. TABULAR LITERATURE REVIEW

Reference	Geometry				Type of Research				Year
	Slab	Cylinder	Sphere	Other	Theoretical	Experimental		Numerical	
						Hot Plate	Oven		
Frank-Kamenetskii [19]	•	•	•		•				1939
Clemmow and Huffington [20]	•				•				1955
Enig et al. [66]	•				•				1956
Gray and Harper [21]	•	•	•		•				1958
P. H. Thomas [42]	•				•				1959
Thomas and Bowes [22]	•				•				1961
Parks [67]	•	•	•		•				1961
Bowes and Townshend [34]	•				•		•		1962
Boddington et al. [30]		•	•	Equi-cylinder, cube, regular tetrahedron and thin circular disk	•				1971
Hardee et al. [31, 33]	•	•	•	Rectangular parallelepipied, the finite right cylinder, and cone	•				1972
Shouman et al. [23, 24]	•				•				1974
Takeno [68]	•	•	•		•				1977
Bazley and Wake [69]	•	•	•		•				1978

Reference	Geometry				Type of Research				Year
	Slab	**Cylinder**	**Sphere**	**Other**	**Theoretical**	**Experimental**		**Numerical**	
						Hot Plate	**Oven**		
Kordylewski [25]	•	•	•		•				1978
Gill et al. [70]	•	•	•		•				1979
Tam [71]	•	•	•		•				1980
Voss [72]	•				•				1980
Fenaughty et al. [73]	•	•	•		•				1982
Gustafson and Eaton [74]	•	•	•		•				1982
Spence and Werner [75]	•				•				1982
Boddington et al. [76]	•	•	•		•				1983
Miron and Lazzara [35]	•						•		1988
Tognotti et al. [77]		•				•			1988
Duane and Synnott [78]				Cube		•			1992
Vazquez-Espi and Linan [79]				Infinite square corner and 2-D rectangular cross-section	•			•	1993
Kim and Hwang [40]	•				•		•	•	1996
Balakrishnan et al. [80]				Infinite square rod and cube				•	1996
Chen [41]	•	•	•	Infinite square rod, short cylinder and cube				•	1997

Reference	Geometry				Type of Research				Year
	Slab	**Cylinder**	**Sphere**	**Other**	**Theoretical**	**Experimental**		**Numerical**	
						Hot Plate	**Oven**		
Reddy et al. [11]	•					•			1998
Lebecki et al. [36]	•					•			2003
Dyduch and Majcher [39]	•					•			2006
Janes et al. [17]	•			Cube		•	•		2008
Park et al. [16]	•					•			2009
Current Study	•			2-D Wedge cross section	•	•		•	2012

Appendix B. THEORY OF DUST LAYER IGNITION (1-D GEOMETRY)

Solution Methods	**Thomas and Bowes [22]**	**Hardee et al. [31]**	**Current Work**
Governing Equation		$k\frac{d^2T}{dx^2} = -\rho QAe^{-E/RT}$	
Boundary Conditions	At $x = 0$, $T = T_p$ At $x = 2r$, $k\frac{dT}{dx} = -h(T_s - T_\infty)$	At $x = r$, $T = T_p$ At $x = 0$, $\frac{dT}{dx} = 0$	At $x = 0$, $T = T_p$ At $x = 2r$, $k\frac{dT}{dx} = -h(T_s - T_\infty)$
Approximation	$e^{(-E/RT)} \approx e^{(-E/RT_p)} e^{\frac{E(T-T_p)}{RT_p^2}}$	$\frac{d\theta_p}{d\theta_{L/2}} = \frac{dL}{d\theta_{L/2}} = 0$	$\frac{d\theta_P}{d\theta_{h/2}} \approx \frac{d\theta_s}{d\theta_{h/2}} \approx 0$
Non-dimensional Equation	$\frac{d^2\theta}{dz^2} = -\delta e^{\theta}$	$\frac{d^2\theta}{dz^2} = -e^{-1/\theta}$	$\frac{d^2\theta}{dz^2} = -e^{-1/\theta}$
Non-dimensional Parameters	$\theta = \frac{E}{RT_p^2}(T - T_p)$ $z = \frac{x}{r}$ $\delta = \frac{QAEr^2\rho}{kRT_p^2} e^{(-E/RT_p)}$ $\alpha = hr/k$	$\theta = \frac{RT}{E}$ $z = \left(\frac{\rho QAR}{kE}\right)^{1/2} x$	$\theta = \frac{RT}{E}$ $z = \left(\frac{\rho QAR}{kE}\right)^{1/2} x$ $h^* = h/\left(\frac{\rho QAkR}{E}\right)^{1/2}$
Non-dimensional Boundary Conditions	At, z = 0, $\theta = 0$ At, z = 2, $-\frac{d\theta}{dz} = \alpha(\theta_s - \theta_\infty)$	At, z = L, $\theta = \theta_p$ At, z = 0, $\frac{d\theta}{dz} = 0$	At z = 0, $\theta = \theta_p$ At z = 2r*, $-\frac{d\theta}{dz} = h^*(\theta_s - \theta_\infty)$
Temperature Profile	$\theta = \theta_m - 2\ln\cosh\left(\sqrt{\frac{\delta e^{\theta_m}}{2}}(z - z_m)\right)$ where, at $z = z_m$,. $\frac{d\theta}{dz} = 0$	$\theta = a + bz + cz^2 + dz^3$ $a = \theta_p - \frac{L^2}{6}\left(e^{-1/\theta_p} - e^{-1/\theta_{L/2}}\right)$ $b = 0$ $c = \frac{1}{2}\left(e^{-1/\theta_p} - e^{-1/\theta_{L/2}}\right)$ $d = -\frac{1}{3L}\left(e^{-1/\theta_p} - e^{-1/\theta_{L/2}}\right)$ where, at z = L/2, $\theta = \theta_{L/2}$	$\theta = a + bz + cz^2 + dz^3$ $a = \theta_p - \frac{+e^{-1/\theta_{r*/2}} 4r*f(f-1)}{(1-f)(1-2(1+f))} - \frac{+e^{-1/\theta_{r*/2}} 4r*(1-f^2)}{4r*(1-f)(1-2(1+f))} - \frac{+e^{-1/\theta_{r*/2}} 2r*(1-f)}{6r*^2(1-f)(2(1+f)-1)}$ $\frac{}{h^*(\theta_s - \theta_\infty)(2f^2 - f)}$ $b = \frac{}{h^*(\theta_s - \theta_\infty)}$ $c = \frac{}{h^*(\theta_s - \theta_\infty)}$ $d = \frac{}{h^*(\theta_s - \theta_\infty)}$ where, at z = r*/2, $\theta = \theta_{r*/2}$

Critical Condition	$\delta_c = \frac{1}{2}\left(\frac{\alpha}{1+2\alpha}\right)^2 (1.4-\theta_\infty)^2$	$\frac{L^2}{\theta_{L/2} e^{1/\theta_{L/2}}} = \frac{24}{11}$	and, at $z = f{\cdot}2r^*, \frac{d\theta}{dz} = 0$ $\frac{r^{*2}}{\theta_{r^*/2}^2 e^{1/\theta_{r^*/2}}} = \frac{3(2f+1)}{f^2(9-2f)}$

Appendix C. MATLAB CODE – DUST LAYER IGNITION

```
clear all

close all

clc


R = 8.3145;

QA = 1.8E12;

E = 88100;

rho = 580;

hc = 5.0;

kc = 0.2;

Tinf = 22+273.15;


lt = 25.4E-3*2; %Half thickness of the slab

H = hc/(rho*QA*kc*R/E)^0.5;


Tp = 411.15;

Ts = Tinf;

Xp = Tp*R/E;

Xs = Ts*R/E;

Xinf = Tinf*R/E;

XsNew = Xs;


%Varying Ts

%For 2 inch Tp = 430.15 Ts = 330.15 dc_Hardee = 3.2, dc_Bowes&Thomas=3.2
```

```
%For 1 inch Tp = 461.15 Ts = 350.15 dc_Hardee = 3.4, dc_Bowes&Thomas = 3.3
%For 0.5 inch Tp = 499.15 Ts = 370.15 dc_Hardee=3.5,dc_Bowes&Thomas=3.4
%For 0.25 inch Tp = 534.15 Ts = 410.15 hc = 32 dc_Hardee = 3.5

%Varying hc
%For 2 inch Tp = 436.65 K Ts = 375.15 K hc = 6 k = 0.2
%For 1 inch Tp = 463.15 K Ts = 375.15 K hc = 10 k = 0.2
%For 0.5 inch Tp = 498.15 K Ts = 375.15 K hc = 17 k = 0.2

L = (rho*QA*R/kc/E)^0.5*lt;
%for errcount = 1:10
for k = 0.01:0.01:0.99
a = 1;
b = -1;
c = Xp+(H*(Xs-Xinf)*k^2*(2*k-1)*L/(1-k)/(1-2*(1+k))...
    +H*(Xs-Xinf)*k^2*L/4/(1-k)/(1-2*(1+k))...
    +H*(Xs-Xinf)*k^3*L/6/(1-k)/(2*(1+k)-1));

Xm = (-b-sqrt(b^2-4*a*c))/2/a;

Xm*E/R; %Temperature at critical ignition condition
Xp*E/R; %Constant plate temperature

C3 = (H*(Xs-Xinf)+4*L*(1-k^2)*exp(-1/Xm))/(4*L*(1-k)*(1-2*(1+k)));
C4 = (H*(Xs-Xinf)+2*L*(1-k)*exp(-1/Xm))/(6*L^2*(1-k)*(2*(1+k)-1));
C2 = (H*(Xs-Xinf)*k*(2*k-1)+exp(-1/Xm)*4*L*k*(k-1))/(1-k)/(1-2*(1+k));
```

```
C1 = Xp;


for i = 1:100
    X(i) = 2*L*i/100;
    Xd(i) = 2*lt*i/100;
    T(i) = C1 + C2*X(i) + C3*X(i)^2 + C4*X(i)^3;
    Td(i) = T(i)*E/R;
end
if Td(100) > Ts
    break
end
plot(Xd,Td)


end
%Xs = (Xs + Td(100)*R/E)/2;
%end
%Hardee et al del_c calcs
L/Xm/exp(1/2/Xm) %should equal eq 1 and 2
sqrt(3*(2*k+1)/k^2/(9-2*k)) %eq 1
 %Bowes Book Eq. 3.56
%alpha = hc*lt/kc;
%0.5*(alpha/(1+2*alpha))^2*(1.4-E*(Tinf-Tp)/R/Tp^2)^2 %eq 2
```

Appendix D. EXPERIMENTAL DATA: WEDGE TESTS

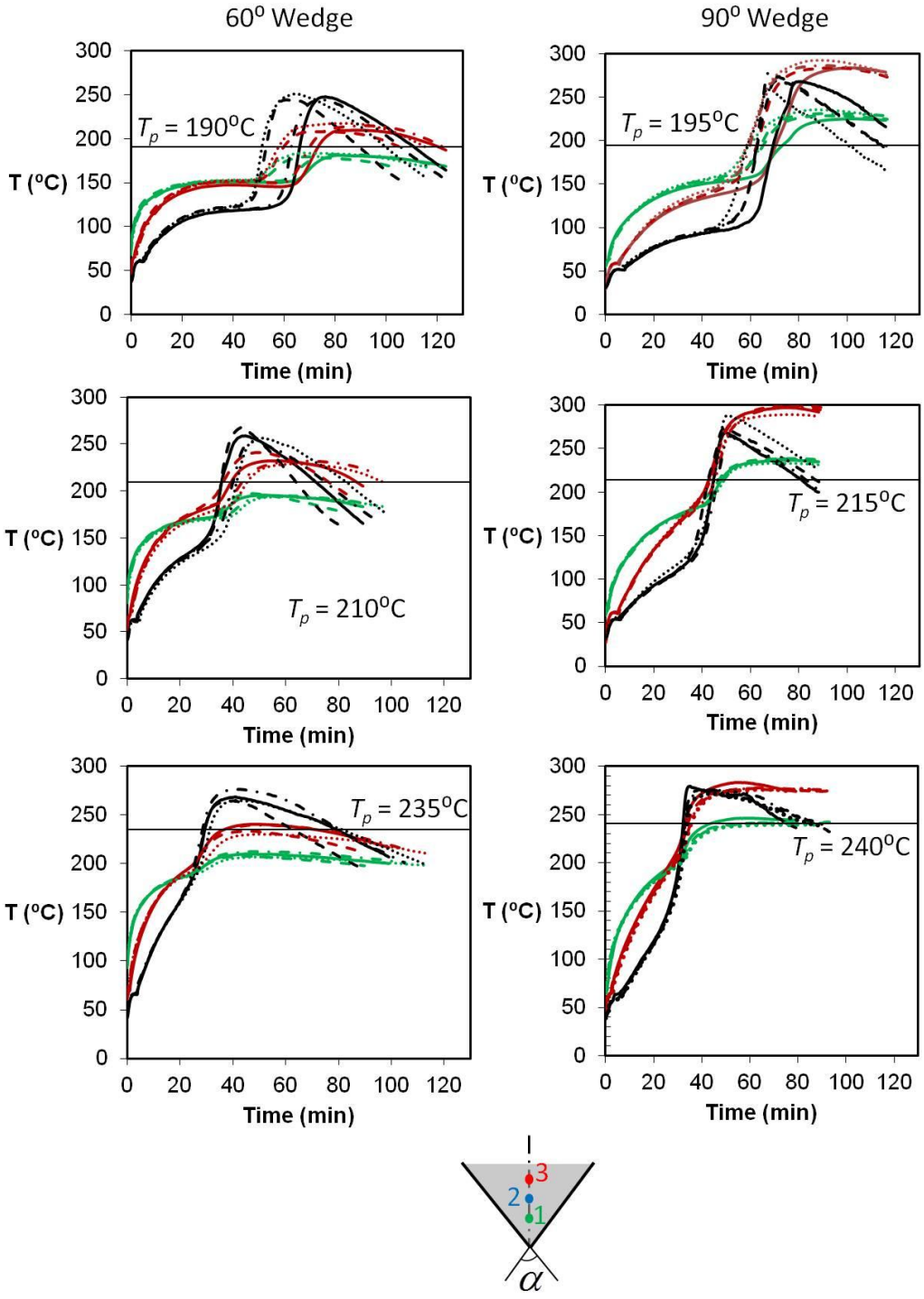

Figure47 Ignition tests done for wedge angles of 60° and 90° at critical and higher plate temperatures.

Appendix E. THEORY OF DUST DEPOSITS IGNITION (2-D GEOMETRY)

Solution Methods	**Hardee et al. [33]**	**Current Study**
Governing Equation	See non-dimensional equations below	$k\left(\frac{d^2T}{dX^2}+\frac{d^2T}{dY^2}\right)+\rho QAe^{-E/RT}=0$
Boundary Conditions	See non-dimensional boundary conditions below	$X = Y\frac{W}{H},\ \ T=T_p$, $X=0, \frac{dT}{dX}=0.$ $X=0,\ Y=H_m,\ \frac{dT}{dY}=0$ $\mathrm{X}=0, Y=H, -k\frac{dT}{dY}=h_c\left(T_s-T_\infty\right)$
Approximation	$\frac{\partial r_0}{\partial\theta_{h/2}}=\frac{\partial h}{\partial\theta_{h/2}}=\frac{\partial\theta_p}{\partial\theta_{h/2}}$	$\frac{\partial w_0}{\partial\theta_{h/2}}=\frac{\partial h}{\partial\theta_{h/2}}=\frac{\partial\theta_p}{\partial\theta_{h/2}}=\frac{\partial\theta_s}{\partial\theta_{h/2}}$
Non-dimensional Equation	$\frac{d^2\theta}{dr^2}+\frac{1}{r}\frac{d\theta}{dr}+\frac{d^2\theta}{dy^2}=-e^{1/\theta}$	$\frac{d^2\theta}{dx^2}+\frac{d^2\theta}{dy^2}=-e^{1/\theta}$
Non-dimensional Parameters	$\theta=\frac{RT}{E}$ $r=\left(\frac{\rho QAR}{kE}\right)^{1/2}R$ $z=\left(\frac{\rho QAR}{kE}\right)^{1/2}Z$	$\theta=\frac{RT}{E},\ \ h_c^*=\frac{h_c}{\left(\frac{\rho QAkR}{E}\right)^{1/2}}$ $x=\left(\frac{\rho QAR}{kE}\right)^{1/2}X$ and $w_o=\left(\frac{\rho QAR}{kE}\right)^{1/2}W,$ $y=\left(\frac{\rho QAR}{kE}\right)^{1/2}Y$ and $h=\left(\frac{\rho QAR}{kE}\right)^{1/2}H,$
Non-dimensional Boundary Conditions	$at\ r=\frac{r_0 z}{h}, \theta=\theta_p$ $at\ z=h, \theta=\theta_p$ $at\ r=0, \frac{\partial\theta}{\partial r}=0$	$at\ x=y\frac{w_o}{h}, \theta=\theta_p,$ $at\ x=0, \frac{d\theta}{dx}=0,$ $at\ x=0,\ y=h_m,\ \frac{d\theta}{dy}=0$ $at\ x=0, y=h, \frac{d\theta}{dy}=h_c^*\left(\theta_s-\theta_\infty\right)$ at $x=0$, $y=h/2, \theta=\theta_{h/2}$

Temperature Profile	$\theta - \theta_p =$ $A\left(r^2 - \frac{r_0^2 z^2}{h^2}\right)\left(z^2 - h^2\right)$ $+ B\left(r^2 - \frac{r_0^2 z^2}{h^2}\right)\left(z^3 - h^3\right)$ $+ C\left(r^3 - \frac{r_0^3 z^3}{h^3}\right)\left(z^2 - h^2\right)$	$\theta - \theta_s\left(\frac{y}{h}\right) - \theta_p\left(1 - \frac{y}{h}\right) =$ $A_w(x^2 \frac{h^2}{w_o^2} - y^2)(y^2 - h^2)\frac{w_o^2}{h^2} +$ $B_w(x^2 \frac{h^2}{w_o^2} - y^2)(y^3 - h^3)\frac{w_o^2}{h^2} +$ $C_w(x^3 \frac{h^3}{w_o^3} - y^3)(y^2 - h^2)\frac{w_o^3}{h^3}$
Critical Condition	$\frac{r_0^2}{\theta_{h/2}^2 \exp(1/\theta_{h/2})} = 28.8$	$\frac{r_0^2}{\theta_{h/2}^2 \exp(1/\theta_{h/2})} =$ $\frac{16 r_o^2 / h^2}{\left(\frac{\left(36h^2 + 14r_o^2\right)}{9h^4 + 19h^2 r_o^2 + 2r_o^4} - \frac{6}{9h^2 + r_o^2}\right)}$

Appendix F. MATLAB CODE – 2-D GEOMETRY

```
clear all

close all

clc


syms Xm Xp Xs Xinf k ro h


R = 8.3145; %Universal Gas Constant

QA = 6.6E9;%1.8E12; %Conjugate pair of Pre-exponential constant A and Heat of Combustion
Q

E = 66800;%89100; %Activation Energy

rho = 580; %Bulk density (kg/m^3)

hc = 8; %Convective heat transfer coefficient (W/m^2-K)

kc = 0.2; %Bulk thermal conductivity (W/m-K)

Tinf = 22+273.15; %Ambient temperature (K)


lt = 50.8E-3*0.5; %height of wedge from apex (m)

Tp = 190+273.15; %constant temperature of hot plates (K)

Ts = Tinf; %assumed constant surface temperature (K)


Xp = Tp*R/E; %non-dimensional hot plate temperature

Xinf = Tinf*R/E; %non-dimensional ambient temperature

Xs = Ts*R/E; %non-dimensional surface temperature

L = (rho*QA*R/kc/E)^0.5*lt; %non-dimensional height of wedge from apex

H = hc/(rho*QA*kc*R/E)^0.5; %non-dimensional convective heat transfer coefficient

j = 3; %angle counter
```

```
inew = 1; %flag counter (used if required)
tic %time start
M = 1000; %maximum divisions of the height done to find location of maximum temperature
while j < 18


    %hc = 11-j/2;
    %H = hc/(rho*QA*kc*R/E)^0.5; %non-dimensional convective heat transfer coefficient


  for ErrCnt = 1:100

  jj = j*5; %half angle of wedge
  alpha = jj; %half angle of wedge

  h = L; %non-dimensional height from appex
  ro = h*tan(alpha*pi/180); %half of maximum wedge width

  %k = 0.5;%Xm assumed to exist at k = 0.5

    %kk = 0.5;
    cc = ro/h;

    A1 = -(-3/2*h^4/ro^2-1/2*h^2)*cc^2;
    B1 = -(-7/4*h^5/ro^2+1/4*h^3)*cc^2;
    C1 = -(-9/4*h^5/ro^2+3/4*h^3)*cc^3;
```

```
    A2 = -(-3/2*h^4/ro^2-h^2)*cc^2;
    B2 = -(-7/4*h^5/ro^2-1/2*h^3)*cc^2;
    C2 = -(1/2*h^3)*cc^3;
    A3 = -(-2*h^3)*cc^2;
    B3 = -(-3*h^4)*cc^2;
    C3 = -(-2*h^4)*cc^3;


ABC = [A1,B1,C1;A2,B2,C2;A3,B3,C3];
%RHS = [exp(-1/Xp)-Xs/ro^2;exp(-1/Xm)-Xs*2*k/ro^2;H*(Xs-Xinf)+Xs/h-Xp/h];
RHS = [exp(-1/Xp);exp(-1/Xm);H*(Xs-Xinf)+Xs/h-Xp/h];

ABCinv = inv(ABC);

solABC = ABCinv*RHS;

A1112 = coeffs(solABC(1,1),exp(-1/Xm));
A12 = (eval(A1112(1)));
A11 = eval(A1112(2));
B1112 = coeffs(solABC(2,1),exp(-1/Xm));
B12 = (eval(B1112(1)));
B11 = eval(B1112(2));
C1112 = coeffs(solABC(3,1),exp(-1/Xm));
C12 = (eval(C1112(1)));
C11 = eval(C1112(2));
```

```
    A13 = 3*ro^2*h^2/16;
    B13 = 7*ro^2*h^3/32;
    C13 = 3*ro^3*h^2/32;

    c = Xs*0.5+Xp*0.5+(A12*A13+B12*B13+C12*C13);
    solXm = (1-sqrt(1-4*c))/2;
    %smaller root of the solution of quadratic equation chosen

maxXm(ErrCnt) = solXm;

solA11(ErrCnt) = A11;
solA12(ErrCnt) = A12;
solB11(ErrCnt) = B11;
solB12(ErrCnt) = B12;
solC11(ErrCnt) = C11;
solC12(ErrCnt) = C12;

%checking for Theta_S values

solA(ErrCnt) = solA11(ErrCnt)*exp(-1/maxXm(ErrCnt))+solA12(ErrCnt);
solB(ErrCnt) = solB11(ErrCnt)*exp(-1/maxXm(ErrCnt))+solB12(ErrCnt);
solC(ErrCnt) = solC11(ErrCnt)*exp(-1/maxXm(ErrCnt))+solC12(ErrCnt);

solXs(ErrCnt) = 2*(maxXm(ErrCnt)-Xp*0.5 ...
    - (solA(ErrCnt)*A13  ...
    + solB(ErrCnt)*B13  ...
```

```
    + solC(ErrCnt)*C13));

solTs(ErrCnt) = solXs(ErrCnt)*E/R;

ErrTs(ErrCnt) = abs(solTs(ErrCnt) - Ts)


% Convergence criteria
if ErrTs(ErrCnt) < 0.0001
    break
end

if ErrCnt > 1
    if ErrTs(ErrCnt)  > ErrTs(ErrCnt-1)
        if abs(ErrTs(ErrCnt) - ErrTs(ErrCnt)) > 10
        break %Solution not converging anymore!
        ErrCnt
        end
    end
end

Ts = (solTs(ErrCnt) + Ts)/2;
Xs = Ts*R/E;
if Xs < Xinf
    Xs = Xinf;
    Ts = Tinf;
```

```
    %break
end
    end

TsOpt(j) = Ts;
angles(j) = 2*jj;
ErrCnt = ErrCnt - 1;

for i = 1:M
    dist(i) = i*100/M;
    solXy(i) = solXs(ErrCnt)*(i/M)+Xp*(1-i/M) ...
        + solA(ErrCnt)*-(h*i/M)^2*((h*i/M)^2-h^2)*(ro^2/h^2)...
        + solB(ErrCnt)*-(h*i/M)^2*((h*i/M)^3-h^3)*(ro^2/h^2)...
        + solC(ErrCnt)*-(h*i/M)^3*((h*i/M)^2-h^2)*(ro^3/h^3);
    wedgedata(i,j) = solXy(i)*E/R;
end

Xign = max(solXy);
LocIgn(j) = find(Xign==solXy);
c3 = (j-1)/16;
c2 = 0;
c1 = 1-(j-1)/16;
figure1 = figure(1);
%axes('Parent',figure1,'FontSize',16,'FontName','Arial');
%box('on');
%hold('all');
```

```
plot(dist,solXy*E/R,'LineWidth',3,'Color',[c1 c2 c3])
xlabel('% Distance from apex','FontSize',16,'FontName','Arial');
ylabel('T (K)','FontSize',16,'FontName','Arial')
hold on

%ErrCnt = ErrCnt + 1;
figure2 = figure(2);
%axes('Parent',figure2,'FontSize',16,'FontName','Arial');
%box('on');
%hold('all');

plot(ErrTs,'LineWidth',3,'Color',[c1 c2 c3])
xlabel('Iterations','FontSize',16,'FontName','Arial');
ylabel('Error in Ts (K)','FontSize',16,'FontName','Arial');
hold on
 j = j+3;
 end
figure3 = figure(3);
%axes('Parent',figure2,'FontSize',16,'FontName','Arial');
%box('on');
%hold('all');
plot(angles,LocIgn/M*100,'LineWidth',3,'Color',[0 0 0])
xlabel('Wedge Angle','FontSize',16,'FontName','Arial');
ylabel('Ignition Location (% distance from apex)','FontSize',16,'FontName','Arial');
hold on
```

```
%Experimental Results
angle60 = 60;
maxloc60 = 75;
angle90 = 90;
maxloc90 = (75+50)/2;
angle180 = 180;
maxloc180 = (25+50)/2;
%Num results
nangles = [60,90,120,150];
nignloc = [64.1732,46.063,42.126,36.6142];


plot(angle60,maxloc60,'MarkerEdgeColor',[0 0 0],'MarkerSize',15,'Marker','v',...
    'LineWidth',4,...
    'Color',[0 0 0])
hold on
plot(angle90,maxloc90,'MarkerEdgeColor',[0 0 0],'MarkerSize',15,'Marker','v',...
    'LineWidth',4,...
    'Color',[0 0 0])
hold on
plot(angle180,maxloc180,'MarkerEdgeColor',[0 0 0],'MarkerSize',15,'Marker','v',...
    'LineWidth',4,...
    'Color',[0 0 0])
hold on
plot(nangles,nignloc,'MarkerEdgeColor',[0 0 0],'MarkerSize',15,'Marker','o',...
    'LineWidth',4,...
    'Color',[0 0 0])
```